Gaia revisited: atmospheric carbon dioxide as a symptom of a vegetation ozone driven climate cycle

Isabel Van Waveren

NL Biodiversity and Society, Naturalis Biodiversity Centre, Leiden, The Netherlands

Corresponding author

Isabel.VanWaveren@gmail.com

List of abbreviations

AMOC: Atlantic midocean circulation.

BCA: Black carbon aerosol.

CCN: Cloud condensation nuclei.

CFC: Chlorofluorocarbon.

CESM2: Atmospheric chemistry model over time with a focus on secondary organic aerosols.

E_{FOS}: Global emission of CO_2 from the burning of fossil energy sources.

E_{LUC}: Global emission of CO_2 related to land use change.

E_{SLGHG}: Increase in northern Pacific ocean CO_2 emission caused by short lived greenhouse gas accumulation.

E_{SOD}: Global ocean CO_2 emission caused by stratospheric ozone depletion

E_{SOW}: Ocean CO_2 emission following from a decrease in the solubility of ocean water due to seasonal ocean warming related to the inclination of the Earth axis.

G_{ATM}: Global atmospheric increment in atmospheric CO_2.

$G_{ATM\text{-}Here}$: Global atmospheric growth in CO_2 concentration, calculated here as ML_{YI} - ML_{YD}.

$G_{ATM\text{-}WCRP}$: Global atmospheric growth in CO_2 concentration as calculated by the World Climate Research Program.

GCB: Global Carbon Budget.

GCE: Global Carbon Equation.

IE: $E_{FOS} + E_{LUC}$.

INP: Ice Nucleating Particles.

IPCC: International Panel on Climate Change.

MCB: Marine Cloud Brightening.

ML_{YD}: Yearly decrease in atmospheric CO_2 concentration as measured by the NOAA at Mauna Loa and calculated herein.

ML_{YI}: Yearly increase in atmospheric CO_2 concentration as measured by the NOAA at Mauna Loa and calculated herein.

NOAA: National Ocean and Atmospheric Administration.

NPCE: Northern Pacific Carbon Equation.

O_{SE}: Global seasonal ocean CO_2 emission as hypothesized by the WCRP.

O_{SU}: Global seasonal ocean CO_2 uptake as hypothesized by the WCRP.

SCHWAB: Self-lofting chemically reactive arctic winter generated air bubble.

SCHWOM: Self-lofting chemically reactive warm ocean generated air mass.

S_{LAND}: Global uptake of atmospheric CO_2 through land sinks.

S_{LUC}: Surface area of land use change.

SOA: Secondary organic aerosols.

S_{OCEAN}: Global uptake of atmospheric CO_2 through ocean sinks.

S_{TOTAL}: $S_{LAND} + S_{OCEAN}$.

U_{BDD}: Ocean uptake in atmospheric CO_2 related biological drawdown.

UKESM1: Atmospheric chemistry model over time

U_{SIM}: Ocean uptake in atmospheric CO_2 caused by the seasonal melt increasing ocean water solubility due to the inclination of the Earth axis.

U_{SLGHG}: Increase in northern Pacific ocean CO_2 uptake caused by short lived greenhouse gas accumulation.

VOC: Volatile Organic Carbon.

WCRP: World Climate Research Program.

Abstract

A synoptic analysis of the history of climate science introduces all potential climate drivers. It is demonstrated that the Keeling curve can be seen to reflect yearly ocean CO_2 emission minus yearly ocean CO_2 uptake. It is also shown that the global carbon equation (GCE), at the foundation of present day climate models is not an equilibrium. This disequilibrium pertains to the neglect of the influence of industrial pollutants on the seasonal behaviour of the Northern Pacific. It is also demonstrated that the errors for carbon emission and uptake on land are too important to allow for the construction of the GCE.

Statistics are used to demonstrate that the increase in atmospheric CO_2 is determined by industrial pollutant emission. A significant determination coefficient between ocean behaviour and pollutants emission is interpreted as caused by ozone accumulation in the Arctic night. With the return of light, in spring, the short lived GreenHouse Gas (GHG) is envisioned to become relatively warm and self-lofting. The trajectory of this slowly ascending mixture is influenced by,

and influencing the existing pressure systems. Part of its heat is incorporated in the Northern Pacific Ocean that releases its gasses. This mixture enriched with the ocean emitted gasses ascends to the stratosphere at the equator where it causes stratospheric ozone depletion, which in turn results in global warming. This new interpretation of the climate cycle through ozone accretion in in the tropospheric arctic night and ozone depletion by ocean emitted gasses in the stratosphere of the low latitudes is substantiated by a reconstruction of the Keeling curve. This reconstruction consists of the superposition of six functions that determine the uptake and emission of CO_2 by the Northern Pacific Ocean. A regression analysis between the monthly Keeling curve and present reconstruction indicates that the two are identical.

Finally, it is explained that the climate cycle in the Pleistocene represents a response system between vegetation composition and stratospheric ozone driven by natural pollutants and stemming from the Mesozoic era when flowering plants made their appearance.

The present aberrantly high atmospheric CO_2 concentrations recorded at Moana Loa are interpreted as resulting from the reiteration of the natural warming phase of the Pleistocene climate cycle through industrial pollutants.

Key words: ozone, ocean degassing, emission, uptake, particulates, aerosols, global warming, Mauna Loa, Keeling, self-lofting.

Introduction

Efforts at describing what drives temperature on Earth date from the era of enlightenment when Herschel [1] counted sunspots to become ”acquainted with certain symptoms or indications … of the temperature of the seasons we are likely to have”. These early scientists are presented

today as giants on who's shoulders we are standing, but science history tends, in retrospective, to narrow down earlier discoveries to a path validating present day views.

As our new model requires multidisciplinary insights, this introduction will also serve to familiarize the reader with earlier neglected concepts, now newly braided into a pollutant driven climate model for system Earth. This historical review cannot be done without remarking upfront that the vigilance the CO_2 driven model required, generated information of immeasurable value, on which the present study leans heavily, indeed.

Early considerations

The work of Foote [2] represents such an early discovery, as she is suggested to have been first at demonstrating the warming effect of atmospheric CO_2. Foote [2] referring to carbonic acid gas did conclude that "an atmosphere of that gas would give our Earth a high temperature". This is incontestably true, but a rapid evaluation of her early work (Appendix 1, Fig 1) demonstrates that identical rates of temperature change are obtained for both the carbonic acid and her damp air.

Fig 1. Examples of erroneous historical validation of the CO_2 driven climate model for system earth. Visualization of the table of Foote [2] where her error margin is highlighted as two colours because she measured temperature after 2 or 3 minutes. Some experiments were shorter than other ones and this analysis gives the rates of change for identical duration and identical measuring intervals. It is not possible to evaluate how damp her damp air was. Moreover, it seems difficult to obtain 100% pure carbonic acid gas as it is very unstable.

While the *in vitro* reproduction of a theoretical atmosphere with water vapour and "acids" certainly was revolutionary, the experiment itself had proven that damp air (78% N_2 ± 20% O_2 ±

1% H_2O, and 1% of other gasses, at the time comprising 0.028% CO_2) is as sensitive to solar irradiance as pure carbonic acid gas (100% CO_2). Tyndall [3] repeated Foote's experiments and found that the most important greenhouse gas was water vapour [4].

Arrhenius [5] who tried to quantify how much of infrared (heat) radiation is captured by carbonic acid gas and water vapour in Earth's atmosphere, did not really rule out water vapour as a GreenHouse Gas (GHG), but found CO_2 to be a more effective one. A quick clustering analysis of the data from his table II illustrates the difference in absorption coefficients for carbonic acid gas and water vapour (Appendix 2). It indicates, however, that the two compounds investigated by Arrhenius in his experiment did not differ significantly in absorption effectivity.

Arrhenius [5] dispatched De Marchi's [6] conclusion that water vapour is the main climate driver on Earth, because he had calculated that the water vapour variability in the atmosphere in De Marchi's hypothesis required values beyond 100% saturation. We know now that condensation or crystallisation clouds form at a saturation beyond 100 % humidity for which they require particulates as condensation cloud nuclei (CCN) or ice nucleating particles (INP).

Such particulates (CCN's or INP's) had made their spectacular appearance in the scientific perception when the Krakatau explosion of 1883 caused blue suns, twilight glow, and a wide global atmospheric belt of sky haze in the lower latitudes [7, plate XXXV] at altitudes well beyond the tropopause [8, p. 348]. The Krakatau emissions had caused unmistakable global cooling. Abbot and Fowle [9] assigned it to the worldwide volcanic haze, which they simply found to have been reducing solar irradiation.

Croll's [10] early hypothesis about the occurrence of glacial epochs resulting from the obliquity of the earth's axis, its precession, and the eccentricity of the earth's orbit around the sun was also dispatched by Arrhenius [5] who argued that a certain degree of obliquity causes identical warming on both hemispheres. Arrhenius had neglected the asymmetrical continent distribution which play a role in the global heat distribution.

While sunspots, greenhouse gasses (GHG), including water vapour, particulates and the Milankovitch cycles, all were found to contribute in different proportions to our daily weather, it is relevant here to analyse further how carbon dioxide was found to represent the chief global temperature driver.

Recent developments

Circumstantial evidence with respect to the warming effect of GHG was brought to stage by Sagan and Mullen [11] with the "faint sun paradox". These authors required nitrogen compounds to explain the high temperatures allowing H_2O to be liquid under the low solar radiation that a young sun would represent. Later, these GHG were preferred to be CO_2 as "CO_2 at high concentrations could have performed a similar function as could other polyatomic gasses" [12]. Please note that, for these authors, any other polyatomic gas could perform a similar function, so why not water vapour or ozone?

In 1940, thanks to the work of John Shaw at Oxford University, it was already known that water vapour, carbon dioxide and ozone play an important part in the heat balance of the Earth, because they absorb radiation in the critical part of the spectrum. By 1965, this had even become textbook knowledge, see for instance in the Handbook of Geophysics [13, fig. 10.2].

In spite of the three above mentioned compounds identified as the potential cause for global warming, it wasn't water vapour, nor ozone but CO_2 that was found to be responsible for global warming. This may be explained by the scientific approach followed by the "U.S. Standard Atmosphere of 1962". This work defines atmospheric composition as obeying the perfect gas law requiring ideal air to be devoid of water vapour and dust.

Nonetheless, instruments continuously registering particle concentrations at high altitude were already in use since 1955 and testify to a scientific interest under less ideal conditions. This

interest did have consequences as when air transport moved to stratospheric altitude, it caused concern. Indeed, ozone depletion through pollutant emission in the stratosphere was expected to have a climatic effect [14]. A considerable gap in academic knowledge on pollutants and aerosols had developed. This was possibly due to the cold war [15].

The National Report of the Carbon Dioxide Assessment Committee of 1983 [16] already depicted an increase in temperature of 3 °C associated with a doubling of the atmospheric CO_2 concentration, without any reference to aerosols, thus echoing the earlier Charney report [17].

The 1983 report [16] dealt with the impact of anthropogenic aerosols in the following way: "Although anthropogenic aerosols are particularly noticeable in regions near and downwind of their sources, there does not appear to have been a significant long-term increase in the aerosol level in remote regions of the globe **other than possibly the Arctic**. The climatic impact of changes in anthropogenic aerosols, if they occur, cannot currently be determined. One cannot even conclude that possible future anthropogenic changes in aerosol loading would produce worldwide heating or cooling, **although carbon-containing arctic aerosols definitely causes local atmospheric heating**."

The increase of the tropospheric ozone concentration in the northern hemisphere was found to stem from photochemical reactions of nitrogen oxides and hydrocarbons emitted by high-flying jet aircraft [18] and little was said about the properties of ozone as a greenhouse gas, while in the 1983 report [16, table 4.1] tropospheric ozone was found influence surface temperature change stronger than other constituents.

In this same table water vapour was also found to have a strong effect on surface temperature.

The use of water has tripled since the 1960s and the industrial use has at least quadrupled [19] but water isn't considered in terms of global temperature. Presently, agricultural irrigation raises serious concern because the daytime cooling from irrigation is overshadowed by nocturnal

warming from cloud cover [20]. These studies relate to agriculture only, but industrial cooling causes water to leave earth surface as hot damp polluted air that rises rapidly to stratospheric altitudes. These emissions form and pollute both, condensation and the crystallisation clouds (cirrus), but are not mentioned anywhere in terms of climate drivers.

So, in spite of the broad spectrum of potential greenhouse gas mentioned above, earliest efforts, as we will see below, focussed immediately on CO_2.

Modern situation

As early as 1966, the oil industry appointed Lovelock to study a geotechnically enhanced biological pump that would naturally draw down CO_2 back into the oceans. This early symptom-control-driven science led to the first steps at improving our understanding of System Earth [21] but it left us with the expectation that the oceans are CO_2 sinks, or rather bins taking up CO_2 at any temperature.

By 1974, Lovelock and Margulis [12] had introduced “life” (photosynthesis) as a geological force capable of stabilizing the early atmospheric temperature and composition to the levels we experience today. This is the well-known Gaia hypothesis, requiring the seeding of condensation clouds with dimethyl sulphides to dim or brighten the ocean surface [21]. Ayers and Cainey [22] tried to corroborate this Gaia hypothesis by quantifying how algal blooms would provide a feedback loop between life, marine cloud seeding, temperature, and carbon dioxide concentrations, but they concluded that the modelling of climate change in this way was incomplete. Nonetheless the search for what constitutes condensation cloud nuclei (CCN) continued and half a decade ago Zheng et al. [23] summarized that, apart from the sulphides envisioned by Lovelock et al. [21] numerous other particulates, organic particles, sea salts, volatile organic carbon (VOC) compounds and their mixtures, all could play a role in condensation cloud

growth. The unique relation between algal blooms and dimethyl sulphide or rather the unique degradation product that they provide to the troposphere as sea spray, was not required to create a response system between the carbon and the climate cycle.

However innovative through the introduction of feedback loops, the Gaia hypothesis has turned out to be inadequate in that it did not address the formation of the carbon sinks that permanently withdraw carbon from land, ocean and atmosphere. Moreover, the feedback loop envisioned in the Gaia hypothesis resulted in a constant cloud cover, temperature and atmospheric CO_2 concentration, while the Pleistocene climate cycle is characterized by an Antarctic temperature fluctuating regularly between -8 and 2 ˚C and a CO_2 concentration fluctuating between 200 and 300 ppm. These cannot be explained by the Gaia hypothesis, but the present new hypothesis will explain them.

The role of ozone

When the first hole in the ozone layer above Antarctica was discovered [24, 25], the focus of the scientific community shifted to the short-term health implications of ultraviolet radiation while neglecting the climate issues related to the ozone layer in the stratosphere [26]. In 1990 Yung [27] already explained that sulphates and other aerosols react with ozone and it was clear to him that the CO_2 concentration in the atmosphere is regulated by the oceans and their temperature. Later, it was demonstrated that black carbon aerosol (BCA) can carry nitric acid (HNO_3) and nitrogen dioxide (NO_2) and will react with stratospheric ozone converting it to oxygen [28]. Depletion of the stratospheric ozone layer had already been mentioned as having a climatic impact in 1970 [14]. These insights became more or less forgotten but were ‘rediscovered’ later on [29, 30, 31, 32, 33] and they are the foundation for the present contribution.

From a broad set of possibilities to CO_2

By the end of the last century, from sunspots, via orbital forcing, to particulates, GHG and ozone depletion, all hypotheses had been brought to the scientific arena, but in spite of the ongoing scientific debate concerning the relative role of each of the various processes at hand, the first (authorless) 1990 International Panel on Climate Change (IPCC) report [34] introduced its request to the United Nations for funding international research by stating upfront:

"We are certain of the following: there is a natural greenhouse effect which already keeps the Earth warmer than it would otherwise be; emissions resulting from human activities are substantially increasing the atmospheric concentrations of the greenhouse gasses: carbon dioxide, methane, chlorofluorocarbons (CFCs) and nitrous oxide. These increases will enhance the greenhouse effect, resulting on average in an additional warming of the Earth's surface. The main greenhouse gas, water vapour, will increase in response to global warming and further enhance it. The size of this warming is broadly consistent with predictions of climate models, but it is also of the same magnitude as natural climate variability".

In granting this proposal, admirable in its multinationalism, the UN deepened the gap between an objective but slow, and a biased but rapid development of our insights in System Earth. The UN funding revived the circumstantial evidence of Sagan and Mullen [11] and reinforced the homeostatic Gaia hypothesis. Simultaneously a NASA research team [35] found that aerosols from smoke and the simultaneous enhancement of solar ultraviolet radiation due to ozone depletion, fitted in the scenario of a nuclear winter, thus fully changing the context of the ozone-hole hype from a climate issue to a short-term health or peace issue. Ozone had, in spite of the earlier insights [27, 28] left the scientific arena as a potential climate driver.

The role of CO_2

The 2007 Nobel Peace Prize, honouring the multinational cooperation of the UN-sponsored IPCC, without settling the science, had given renewed credibility to a CO_2-driven

System Earth and by 2021, the Nobel Prize for Physics, awarded "for the physical modelling of Earth's climate, quantifying variability and reliably predicting global warming" implicitly reinforced the CO_2 driven climate model again. This award had anchored climate modelling (implicitly atmospheric CO_2 driven climate modelling) deep in time as it honoured a more than 50 year old paper [36]. Manabe and Wetherald had focussed on the influence of CO_2, cloudiness, O3 and albedo on Earth's thermodynamics at fixed relative and absolute atmospheric humidity, but this focus wasn't at the core of the award. They did find that a doubling of CO_2 at a fixed relative humidity gave a temperature increase of 2 ˚C, but also that less than a doubling in O_3 gave about the same type of result (table 7), while changes in albedo affected temperature even more (table 8).

The other recipient of the 2021 Nobel Prize for Physics was Hasselmann for his 1976 paper [37]. Hasselmann did not prove that CO_2 was driving global climate, but he had managed to separated weather from climate as the two represent different time scales.

A first attempt at a hypothetical backbone of a fully CO_2-driven System Earth had made its public appearance in 2007 as the Global Carbon Budget (GCB) where the atmospheric accumulation of CO_2 consisted of anthropogenic emission minus ocean uptake and an unidentified sink [38, fig 4]. While the atmospheric increase in CO_2 concentration was recorded in the Keeling curve, the industrial emission was known and the required ocean sink had been established [39], in order for this GCB to be in balance an unidentified sink needed to be discovered. This unidentified sink was provided two years later [40] and by 2016, the Global Carbon Budget had fully developed into the Global Carbon Equation (GCE) [41]. This GCE is still in practice and still states that the atmospheric increase in CO_2 (G_{ATM}), as recorded in the Keeling curve based on measurements by the National Ocean and Atmospheric Administration (NOAA) at Mauna Loa reflects what CO_2 concentration remains in the atmosphere after ocean (S_{OCEAN}) and land sinks (S_{LAND}) took up the bulk of the industrially (E_{FOS}) and agriculturally (E_{LUC}) emitted CO_2.

It is expressed in the following way

$$(E_{FOS}) + (E_{LUC}) = (S_{OCEAN}) + (S_{LAND}) + (G_{ATM}) \quad (0)$$

This equation, developed by the World Climate Research Program (WCRP) is endorsed by the IPCC and is the backbone of most climate models like the 2023 one [42].

Simultaneously, ozone depletion was considered by another UN funded organization, the UN Environment program that developed the Montreal protocol, in order to gain control over the industrial production of chlorofluorocarbon (CFC) and its consequences for human health. The focus on chlorofluorocarbons, and since 2016 hydrofluorocarbons, is worrisome as the radical molecules, which destroy ozone [43] in the tropo- and the stratosphere are ubiquitously present because they come with industrial pollutants [44].

The present contribution aims at alleviating a dangerous division of labour between the IPCC and the UN environmental program. It is dangerous in the sense that it results in blind spots for both groups. The potential climatic consequences of ozone accumulation and depletion seem to be safely salvaged with the Montreal protocol team but its focus is on health. The health issues of high atmospheric CO_2 concentrations, other GHG or pollutants the atmosphere seem to be safely salvaged with the IPCC but its focus is on climate.

Activities of the IPCC

The IPCC appears exhaustive in all its potential climate drivers, but their model, following the UN environmental program, underestimates both the causes and the consequences of ozone depletion. In this context, it is the role of H_2O in all its phases that requires more insight.

The intertwining of H_2O and aerosols

In the IPCC model of 2022 [45, chapter 7, fig 6], clouds are presented as a diffuse and continuous shield. This representation does not do justice to water, which, at the pressures and temperatures related to the mass of our planet, is near its triple point. This means that small pressure and temperature changes result in shifts in phase. So, instead of considering the cloud shield as a single diffuse water droplet blanket, one should conceive Earth as protected by a thermos-troposphere. This troposphere has indeed a double shield or, rather, a double sieve: an inner liquid cloud sieve and an outer solid ice sieve. While a single blanket may be capable of reflecting solar radiation back into space, the pathway of solar radiation between these two sieves can be envisioned as that of heat in a double walled thermos-bottle, keeping the Earth warm. The external solid sieve of the sphere at the boundary of the tropo- and the stratosphere is composed of featherlike ice clouds (cirrus clouds). The internal sieve, consisting of condensation clouds (stratus, stratocumulus or cumulonimbus clouds), that occupy the troposphere. Both cloud layers behave differently. While the ice clouds are part of the lower current of the stratospheric Brewer Dobson circulation cell [46] and flow toward the poles of the hemispheric winter [47], the condensation clouds are confined to three conspicuous climate cells (the Hadley, Ferell and Polar cells) and play a more regional role.

Both cloud type densities are determined by the availability of both water and particulates. Water vapour, comprising 1-3% of the tropospheric gasses, isn't limiting the formation of clouds. It is the specific weight of particulates, their emission frequency and intensity that are a limiting factor to cloud formation. The altitudinal distribution of the particulate density determines wat cloud type will be formed: at low altitudes condensation clouds will be formed through Cloud Condensation Nuclei (CCN) and higher up, ice clouds through Ice Nucleating Particles (INP). These particulates affect Earth's kinetics through their various properties: their albedo, their chemical composition or their role at slowing down solar irradiation through the greenhouse gas (GHG) that they generate. The balance between these physical and chemical processes is difficult

to establish, especially as they can be influenced by seasonality and light availability at the poles because such pollutants can be sensitive to photolysis.

Aerosols and earth's albedo

The role of particulates as CCN's and INP's affecting the Earth's albedo continued to get attention from the IPCC. This is exemplified by their 1997 view [48] that "Tropospheric aerosols (microscopic airborne particles) resulting from combustion of fossil fuels, biomass burning and other sources have led to a negative direct forcing" by which they meant cooling. This view is maintained in their latest report 2023 [49], endorsing the freshly published view that direct negative forcing of aerosols can even be considered to mask part of the GHG global warming [50]. However, in 2023, actual climate models are still found to fail at adequately accounting for the role of the dust concentration [51]. Indeed, it appears that aerosol emissions that seed condensation clouds have caused regional dimming, but cannot explain the subsequent brightening trends [52]. Similar types of uncertainties were found for aerosol/ice cloud (cirrus) interactions, where positive or negative albedo effects can be established regionally but these effects fail to be reproducible in global climate models [53].

Aerosol's chemical role

It is surprising in this respect that the IPCC only considered aerosols to brighten or dim solar radiation, because Liss and Lovelock [54] had already pointed at a climate driven by a cocktail of gasses and aerosols where the latter were expected to react with ozone. This is highly relevant as it has been found that ozone depletion cools the stratosphere [31] but warms the troposphere [33, 55] and that the photolysis of ozone often is exothermic [56] while winter accumulation of ozone in the Arctic can cause the short lived GHG ozone to give seasonal warming [57]. It must therefore be deduced that the IPCC, did – and does - not pay due attention

to the influence that aerosols and pollutants have on the short lived greenhouse gas ozone and its implication for Earth's energy budget.

Aerosols in the past

An aerosol-driven System Earth is nonetheless supported by our knowledge from earth history. Patterns between aerosols/dust and climate have been pointed out for the not too far geological past. Indeed, dust (loess) typically characterizes arid glacial phases of the Pleistocene [58] Antarctic whereas glacial maxima in the tropics are characterized by higher concentrations of charcoal [59]. Moreover, areas at midlatitudes, such as the Chinese Loess Plateau, display the proof of enhanced wildfires during the past eight glacial/interglacial cycles, the intensity of which has been found to be inversely correlated with global atmospheric CO_2 concentrations [60]. This indicates that glacial maxima are arid and fire prone and vis versa interglacial maxima are humid and fire frequency is relatively low.

Natural fire as a source of pollutants

Forest fires do not only produce large quantities of pollutants such as SO_2 [61] and NO_x [62], but these high-temperature fires also carry small particulates (products of incomplete combustion being chemically reactice) to the tropopause and beyond [63]. It is therefore conceivable that, under natural circumstances, fire-generated INP form ice clouds in the tropopause. These ice clouds are part of the lower current of the stratospheric Brewer Dobson cell [46] which current transports the cirrus clouds with their potentially reactive pollutants to the poles of each hemispheric winter.

Tropospheric ozone accumulation and stratospheric ozone depletion

Ozone accumulates in the troposphere during the polar winter night [57, 64] and starts getting depleted with the return of the light in spring. But ozone also gets depleted in the lower stratosphere [31, 65]. The cycle of ozone, consequently, requires further scrutiny as ozone accumulation in the troposphere and its depletion in the stratosphere can cause tropospheric warming and stratospheric cooling, which stratospheric cooling in turn has been reported to result in tropospheric warming again [33].

A crucial role for the arctic heat anomaly

The short lived GHG ozone has been reported to give heat accumulation in the troposphere and to result in aberrant polar vortex behaviour [55] the outer rim of these vortices forms the jet stream. Lower atmospheric warming, the northern jet-stream intensity and sea-ice cover in the Arctic correlate [66]. This relation between northern Pacific weather, jet streams and polar vortices is confirmed by past warming phase of the last Pleistocene climate cycle because there is evidence for the dry trade wind and wet storm periods on Hawaii to be related to the intensity of this same northern jet stream [67]. Reconstructions of the climate in the past provide therefore evidence that aerosols can force the arctic heat anomaly through the accumulation of short lived GHG like ozone and in their wake all the equilibrium shifts, including storm intensity and frequency, that determine the climate in the Northern Pacific Ocean. Even the frequency of the El Niño events in South (!) America could thus be explained [68].

A second hole in the stratospheric ozone layer

Despite the 1987 Montreal Protocol that globally stopped the industrial use of ozone depleting substances and appeared to restore the ozone hole above the Antarctic, a second hole appeared in the ozone layer above the Arctic in 2020 [65]. Moreover, the annual mean arctic temperature amplification [69] has become increasingly clear. So time has come to determine

whether the sum of all emitted pollutants (aerosols, dust, charcoal, sea spray) rather than dimming solar radiation through "negative forcing'' induces global warming through ozone accumulation in the Arctic and its depletion in the stratosphere.

Falsifying the Global Carbon Equation

In the following the Global Carbon Equation will be scrutinized. First it will be demonstrated that the increase in atmospheric CO_2 (G_{ATM}) as recorded in the Keeling curve is equal to the yearly increase in atmospheric CO_2 concentration as measured at Mauna Loa (ML_{YI}) minus decrease in atmospheric CO_2 concentration as measured at Mauna Loa (ML_{YD}). Knowing the total industrial emission and total natural uptake from the literature employed by the WCRP, ocean emission (O_{SE}) and uptake (O_{SU}), as defined by the GCE, can be calculated and, in contradiction to the existing assumptions [70], the two are shown to be significantly different. Also, because the error margins for the land sinks (S_{LAND}) and the emission from land use change (E_{LUC}) are important, these errors will be argued to be too large to build on to. Moreover their relation with the global atmospheric growth, analysed statistically, will be demonstrated to either be insignificant or to have been inverted. Having established reasonable doubt, a new hypothesis is presented where the atmospheric CO_2 growth (G_{ATM}) is fully generated by the Northern Pacific Ocean and expressed in the Northern Pacific Carbon Equation (NPCE).

Although these data-based considerations might appear to have a flavour of "climate denialism'', the conclusion will be supported by demonstrating that, instead of industrial CO_2, industrial pollutants seasonally cause both an increase in ocean CO_2 emission and a minor increase in ocean CO_2 uptake, resulting in the extreme yet symptomatic atmospheric CO_2 growth (G_{ATM}) that has alarmed us.

A new carbon equation for the Northern Pacific Ocean

This new hypothesis will be substantiated by reconstructing the Keeling curve as the sum of six functions that determine the uptake and emission of CO_2 by the Northern Pacific Ocean. Five of the functions are seasonal and reflect heat flows between the tropo- and the hydrosphere for which heat flows the uptake and emission of CO_2 are considered a proxy. One function, following from the stratospheric ozone depletion, is global and reflects the heat flow from the strato- to the hydrosphere, causing global CO_2 emission. Two of the five functions pertaining to the heat flows between the tropo- and the hydrosphere, reflect the natural seasonal ocean CO_2 uptake and emission. Two other functions reflect how this heat flow is enhanced by pollutant emission. A fifth function reflects the biological pump taking up tropospheric CO_2 and transferring it to the ocean sinks. The sum of these six functions has a convincingly high probability ($p = 0$) and determination coefficient (0.99896) in correlation with the CO_2 (Keeling) curve constructed with the monthly data of NOAA since 1961.

This new interpretation of the Keeling curve will be shown to be consistent with a stratospheric ozone and natural fire driven Pleistocene climate cycle and it will be argued that the conditions triggering the transition from a glacial to an interglacial maximum are presently reiterated by industrial pollutant emission at the top of an interglacial maximum.

Material and Methods

Fact checking the interpretation of science history

The data of Foote [2] and Arrhenius [5, table 2] were (Appendices 1 and 2) used respectively for a histogram and a principle components analysis in PAST as offered in Hammer et al. [71].

Data sets

Analysis of hourly daily and monthly averages of atmospheric CO_2 concentrations from 1960 to 2019, are made freely available online by the NOAA Observatory on Mauna Loa and the South Pole [72] (Appendices 3, 4, 5, 6). The yearly industrial emissions from fossil fuels (E_{FOS}) are based on Liu et al. [33, fig 1]. The yearly change in the emission caused by land use (E_{LUC}) is also available online on the website of the Carbon Brief [73]. The yearly uptake in atmospheric CO_2 by land sinks (S_{LAND}) was taken from Gasser et al. [74]. The surface of land use change was found in Winkler et al. [75, fig. 3]. The yearly ocean sink (S_{OCEAN}) values were found in Bennington et al. [76, fig 3, blue line]. Friedlingstein et al. [42, table 1] was used to transfer all data from ppm to Gigaton (Gt) carbon. These various data sets are provided in Appendix 7. Pollutant concentrations in the atmosphere over time were found in Griffiths et al. [77, fig 13, red line] and represent various atmospheric chemistry models (Appendix 8). These models reflect various studies on anthropogenic activities having a burden on ozone formation in the troposphere. Such anthropogenic activities like industrial emission, transport and biomass burning produce numerous particulates like aerosols, sulphate, NO_x, sea salt, organic and black carbon and soil dust. Two models were considered for the analysis of the probabilities and determination coefficients they displayed in comparison with what Friedlingstein et al. [42] consider industrial emission ($IE = E_{FOS} + E_{LUC}$). The two models are the UKESM1-0-LL model that focuses more on volatile organic carbons (VOC), and the CESM2-WACCM model having more focus on

secondary organic aerosols (SOA) [77]. The compilation of these regression analyses are summarized in Table 1.

Table 1. Comparison between O_3 production and industrial CO_2 emission

X axis	Y axis	R^2:	p:	Equation
IE	UKESM1	0.97837	$1.6444E^{-42}$	$Y= -11.36\ x^2 + 227.5x - 262.8$
UKESM1	CESM2	0.95461	$1.1631E^{-33}$	$Y= 0.0003063\ x^2 + 1.173\ x\ -226.8$
IE	CESM2	0.9511	$9.0534E^{-37}$	$Y= -9.12\ x^2 + 179.2\ x - 310.6$

Two functions modelling the net chemical production minus loss of O_3, UKESM1-0-LL with a focus on volatile organic carbons (VOC), and CESM2-WACCM with a focus on secondary organic aerosols as shown in Griffiths et al. [77, fig. 13], are compared to the sum of fossils fuels (E_{FOS}) [33, fig 1] plus the emission caused by land use (E_{LUC}) [73] considered in the GCE to reflect industrial emission [73] (IE = (E_{FOS}) + (E_{LUC})).

The highest determination coefficient (R^2) and the lowest probabilities (p), under the assumption that industrial emission (IE = E_{FOS} + E_{LUC}) determines the modelled atmospheric chemistry, were used to determine which model (UKESM1 or CESM2) is best to study of the effects of aerosols and pollutants on the Northern Pacific Ocean behaviour (Table 1). UKESM1, giving slightly better determination and probabilities, was chosen for the present demonstration.

The impact of pollutants and industrial CO_2 compared

The polynomial regression analyses of Hammer et al. [71] were used to compare the determination coefficients (R^2) and probabilities (p) between the pollutants and the yearly ocean

519 behaviour at Moana Loa, viz. yearly atmospheric CO_2 increase (ML_{YI}), yearly atmospheric CO_2
520 decrease (ML_{YD}) and their difference, being the yearly growth of the atmospheric CO_2 (G_{ATM}).
521 For each regression analysis between ocean behaviour and pollutants or emitted volumes of
522 industrial CO_2, identical orders of polynomial functions were used. The data set with all
523 probabilities and determination coefficients of all examined polynomial regression analyses was
524 reduced to the 50 most relevant ones and presented in Appendix 7.
525
526 **Two methods to calculate atmospheric CO_2 growth**
527
528 Two calculation methods for atmospheric increase in CO_2 concentration are compared, viz.
529 the method followed by the World Climate Research Program [42] and our own method
530 (Appendix 3, Fig 2). The WCRP evened out seasonality in the atmospheric growth in CO_2
531 concentration ($G_{ATM\text{-}WCRP}$) curve following Ballantyne et al. [70]. In their method, the difference
532 in atmospheric CO_2 concentration between several consecutive years ΔC is divided by that
533 number of years (Δ t) and looks as follows: ($G_{ATM\text{-}WCRP}$) = (Δ Concentration/ Δ t) (Appendix 9).
534 In the present contribution, the atmospheric increase in CO_2 concentration is calculated by
535 subtracting the yearly atmospheric CO_2 decrease/ocean uptake (ML_{YD}) from the yearly
536 atmospheric CO_2 increase/ocean emission (ML_{YI}) from the consecutive period ($G_{ATM\text{-}Here}$). This
537 was done on the basis of the selection of highest and lowest emission month of each year between
538 1961 and 2019 as offered by the NOAA (Appendix 3).
539 The value of the yearly atmospheric decrease/ocean uptake in CO_2 (ML_{YD}) was calculated by
540 subtracting the lowest monthly atmospheric CO_2 concentration from that year from the value of
541 the highest monthly CO_2 concentration preceding it. The yearly atmospheric CO_2 increase/ocean
542 emission (ML_{YI}) was obtained by subtracting the lowest monthly values in atmospheric CO_2
543 concentration from the highest monthly concentration following it.

Fig 2. Details of the Keeling illustrating two ways to calculate the yearly atmospheric growth (G_{ATM}).

A. Method used herein : $G_{ATM} = ML_{YI} - ML_{YD}$. B. Method used by the WCRP $G_{ATM} = \Delta C / \Delta t$.

The difference between the two values ($ML_{YI} - ML_{YD}$) constitutes the yearly $G_{ATM\text{-}Here}$.
It was calculated here for both the yearly difference and its 3-year average (Appendix 3 and 9).
Box plots of $G_{ATM\text{-}WCRP}$ and $G_{ATM\text{-}Here}$ were compared with the statistical PAST program [71] to establish whether they were identical or not.
The difference between the various calculations of G_{ATM} was also evaluated by calculating the percentage error between the various calculation methods:
Percentage error = averaged G_{ATM} – actual G_{ATM} (being one or three years, as calculated by the carbon group or as calculated here)/actual G_{ATM} x 100.

Reconstruction of the Keeling curve

Regional seasonality

Hakkarainen et al. [78] showed that seasonality approaches symmetry in the high latitudes of the southern hemisphere, unlike the northern hemisphere that is clearly asymmetrical. This was hypothesized here to reflect the near absence of industrial bias to seasonal warming or cooling in the Antarctic. We reproduced such a yearly emission diagram here for the randomly chosen period of 1990 to 1996 (Fig 3) using the monthly data sets provided by NOAA, for both Mauna Loa and The South Pole [79].

Fig 3. Visualization of the difference in timing and yearly amplitude between the atmospheric CO_2 concentrations in different geographical localities for the randomly chosen 1992-1996 period. (a) Mauna Loa (red line), (b) the South Pole (black line). The data are from NOAA [79] (Appendix 5).

Approximating true seasonality

A second-order regression analysis of the monthly atmospheric CO_2 as recorded by the NOAA on Antarctica [79] (Appendix 5) served to establish the global ocean emission, expected to be free of seasonality (Fig 4). This gave a function of $y = 8.784*x^2E\text{-}07 + 102*x + 331.9$.

Fig 4. Polynomial function drawn through the monthly atmospheric CO_2 concentrations as recorded by NOAA on the South Pole between 1980 and 2022 [79]. This function serves to establish the average seasonal amplitude in atmospheric CO_2 emission of the south pole by subtracting the monthly average from the mean determined by the function $y = 8.784*E^{-05}\ x^2 + 102*x + 331.9$.

The maximum amplitude of these monthly excursions from the regression line for the month of weakest (March) and strongest atmospheric CO_2 concentrations (December) were summed up, averaged and divided by two. This gave an approximation of the seasonal southern hemispheric positive and negative atmospheric CO_2 excursions from the global ocean emission. It was varying between of 0.25 to -0.25 ppm (see Appendix 6). This amplitude was considered to represent seasonal fluctuations free of industrial enhancement.

Industrial impact on ocean uptake

The function of yearly industrial pollutants enhanced ocean CO_2 uptake (the solubility pump) for the northern hemisphere was made inversely proportional to the sea ice extant as found in Yulin et al. [98, fig 6 line 2] and also proportional to the UKESM1 [77] (Appendix 10).

Industrial impact on ocean emission

The yearly seasonal Northern Pacific Ocean CO_2 emission was calculated based on the southern hemisphere as explained above for the yearly seasonal uptake; in order to spread this function over the correct number of months with the correct intensity, it was expressed in percentages made proportional to the average day length between 20° and 55° NL (see Appendix 9 and 10) and made to reach the maximum of 0.25 ppm approximated above for the southern hemisphere.

The function of yearly industrial pollutants enhanced ocean CO_2 emission for the northern hemisphere was constructed with the expectation that the pollutant function applied here (UKESM1) is proportional to the heat produced by pollutants in the Arctic, which heat is taken up by the oceans resulting in the zone of CO_2 emission in the northern hemisphere as depicted by Hakkarainen et al. [81, fig 2]. This extra emission was spread in a yearly returning series of percentages over time established in comparison to the monthly Keeling curve (Appendix 10). It is stressed here that these percentages were made identical for each seasonal cycle and that they were made proportional to the UKESM1 function [77].

Stationary and cumulative functions

These two functions of seasonal and industrially driven hydrosphere warming and cooling were made stationary. For the seasonality of the CO_2 emission and uptake, this is self-explanatory, as driven by recurrent temperatures, but for the effects of industrial pollutants this is less straightforward but explained through thermal energy being fully transformed to chemical energy.

616

617 **Global warming proportional to pollutant emission**

618 Also part of the solar irradiance energy warming a particular air mass will cause the
619 airmass to be ascending in the troposphere like a droplet in a lava lamp. This ascending energy
620 turns again into chemically energy in the stratosphere when the ozone layer gets depleted. The
621 increase in solar radiation following from the stratospheric ozone depletion was made cumulative
622 as the thickness of the ozone layer is transformed permanently, it was also made proportional to
623 the pollutant emission over time as described for the UKESM1 cocktail [77] (Appendix 10).

624

625 **Estimating the biological pump**

626 The biological pump is estimated to reach 0.3 ppm/year, based on the increase in
627 atmospheric CO_2 concentration during El Niño years when the ocean CO_2 emission is not
628 functioning as a biological pump [80, fig 6]. The intensity of El Niño events were spread mildly
629 over three months from November to January (Appendix 10). In the absence of discrete and
630 multidisciplinary data on the increase in El Niño events, the biological pump was made to reduce
631 linearly from 100% in 1961 to 98% in 2019.

632

633

634 **Summing it up and comparing to the Keeling curve**

635 The sum of all six functions (two seasonal, two seasonal-industrial, one biological and one
636 stratospheric) represents the monthly atmospheric CO_2 concentration from 1961 to 2019 (684
637 month), which was added to the atmospheric CO_2 concentration of January 1961. This result was
638 compared with the Keeling curve (Appendix 8, column S) using a polynomial regression analysis.
639 The detailed explanation of the calculation employed in Appendix 10 is detailed further on in the
640 interpretations or in Appendix 10.

641

642

643 **Results**

644

645 **The atmospheric increase in CO_2 concentration**

646

647 The atmospheric increase in CO_2 concentration was calculated as by the World Climate
648 Research Program [42] ($G_{ATM\text{-}WCRP}$) for the months of strongest emission (from May to May) and
649 lowest emission (from September to September) and were compared with box plots to the
650 atmospheric increase in CO_2 concentration calculated in the present contribution ($G_{ATM\text{-}Here}$). This
651 was done for a period of one year, as well as for the average over three years (Appendix 9, Fig 5).
652 Although this seems just a simple difference in methodology, it reflects a fundamental difference
653 in interpretation. While the $G_{ATM\text{-}Here}$ is considered to fully reflect ocean behaviour being
654 seasonally influenced by industrial emission, $G_{ATM\text{-}WCRP}$ is believed to represent the yearly carbon
655 equation, where seasonality is evened out because seasonal ocean CO_2 uptake is expected to be
656 equal to seasonal CO_2 emission.

657

658 **Fig 5. Box plots allowing for the comparison of six potential methods to calculate the**
659 **atmospheric increase in CO_2 concentration**.
660 $G_{ATM\text{-}Here\ 1y}$: method used herein ($G_{ATM\text{-}Here\ 1y} = ML_{YI} - ML_{YD}$) for one year; $G_{ATM\text{-}Here\ 3y}$: method
661 used here in for the average of 3 years; $G_{ATM\text{-}WCRP\ May\ 1y}$: method used by the WCRP ($G_{ATM\text{-}WCRP\ 1y} = \Delta C/\Delta t$), from May to May of the former year; (d) $G_{ATM\text{-}WCRP\ Sept\ 1y}$: method used by the
663 WCRP from September to September from the former year; $G_{ATM\text{-}WCRP\ May\ 3y}$: method used from
664 May to May of three years before; $G_{ATM\text{-}WCRP\ Sept\ 3y}$: method used by the WCRP from September

665 to September from the three years before. Black dashed rectangle: largest spread; blue dashed
666 rectangle: largest interquartile; red dashed rectangle: lowest and highest medians.
667
668 The box plots allowing for the comparison of the six methods to calculate G_{ATM} indicate that the
669 method employed here ($G_{ATM\text{-}Here}$) gives the same results as for the methods used by the WCRP.
670 Indeed:
671 a. The median of $G_{ATM\text{-}here}$ as calculated here for a single year is slightly inferior to $G_{ATM\text{-}WCRP}$ for
672 May and September (May 1y, Sept. 1y), while the median of $G_{ATM\text{-}Here}$ for three years is slightly
673 larger than the $G_{ATM\text{-}WCRP}$ for September for three years but equal to the other calculations of
674 $G_{ATM\text{-}WCRP}$ for May and September.
675 b. The interquartile range of $G_{ATM\text{-}WCRP}$ September 1 year is larger than all others, including both
676 calculation methods for $G_{ATM\text{-}Here}$.
677 c. The same is the case for the spreading of $G_{ATM\text{-}WCRP}$ September 1 year.
678
679 Moreover, the errors between the averages of all 6 calculation methods for the increase in
680 atmospheric CO_2 concentration were also considered (Table 2). The largest error (-1.56 %) was
681 obtained for the 3-year calculation of our $G_{ATM\text{-}Here}$, and the smallest (0,09 %) for the $G_{ATM\text{-}WCRP}$
682 from the World Climate Research Program for September for 1 year.
683
684 **Table 2. Comparison between the six calculation methods for atmospheric CO_2 growth**

G_{ATM}	Error margin
$G_{ATM\text{-}WCRP\ Sept\ 3y}$	1.33
$G_{ATM\text{-}Here\ 1y}$	0.78
$G_{ATM\text{-}WCRP\ May\ 3y}$	0.38

$G_{ATM\text{-}WCRP\ Sept\ 1y}$	0.09
$G_{ATM\text{-}WCRP\ May\ 1y}$	-0.97
$G_{ATM\text{-}Here\ 3y}$	-1.56

Error margin for the average value for the atmospheric increase in CO_2 concentration (G_{ATM}) between 1963 and 2018 calculated as $G_{ATM\ Here} = ML_{YI} - ML_{YD}$ for one or three years or as $G_{ATM\text{-}WCRP} = \Delta C/\Delta t$, when considering the month of strongest emission (May) and the month of weakest emission (September) for a period of one year and a period of 3 years.

It can consequently safely be said that the $G_{ATM\text{-}Here}$ calculated here as yearly ocean CO_2 emission minus yearly ocean CO_2 uptake reproduces the $G_{ATM\text{-}WCRP}$ as calculated by the World Climate Research Program (WCRP) [42]. This means that the following is true.

$$G_{ATM\text{-}Here} = G_{ATM\text{-}WCRP} \quad (1)$$

Implications for the Global Carbon Equation

The global carbon equation (GCE) states that the total industrially emitted CO_2 ($IE = E_{FOS} + E_{LUC}$) minus total up taken CO_2 ($S_{TOT} = S_{OCEAN} + S_{LAND}$) is equal to the atmospheric increase in CO_2 concentration (G_{ATM}), or:

$$IE - S_{TOT} = G_{ATM} \quad (2)$$

As demonstrated above, $G_{ATM} = ML_{YI} - ML_{YD}$, so that the GCE can also be expressed as follows:

$$IE - S_{TOT} = ML_{YI} - ML_{YD} \quad (3)$$

or

$$(IE - S_{TOT}) - (ML_{YI} - ML_{YD}) = X \quad (4)$$

If the Global Carbon Equation is true, than X = 0.

This is tested bellow with the box plots of the averages of this equation over time (Fig 6).

Fig 6. Superimposed box and jitter plots for equation (2). G_{ATM} calculated as IE-$S_{TOT,}$ as $G_{ATM\text{-}Here}$ (= ML_{YI}-ML_{YD}) for one and three year, measured as $G_{ATM\text{-}WCRP} = \Delta C/\Delta t$, for the month of May and September for one and three years, respectively; the difference X between the six calculations methods for G_{ATM} based on the measurements at Mauna Loa and G_{ATM} calculated as IE-$S_{TOT;}$ red dashes line: Median of G_{ATM} as calculated here for one year.

In this box plot we see that X, being the difference between G_{ATM} calculated as in the GCE, as industrial emission (IE) minus global sinks (S_{TOT}), and G_{ATM} established with the monthly atmospheric CO_2 record at Mauna Loa, remains positive.

Furthermore when comparing X, for instance, to the diurnal fluctuation recorded on the 28-th of July 2024, being more than 8 ppm CO_2 (>16 Gt C), these differences appear to be insignificant.

But when taking the averages of all calculation methods of X (0,395 Gt C) and comparing it to the averages of the various parameters of the GCE (Table 3), it is clear that the imbalance X represents a high percentage of the sinks and sources.

Table 3. Analysis of average imbalance X in the GCE and the average value of the different members of the GCE.

Sinks & sources of CO_2	**Average (in Gt C/year) from 1963 to 2018**	**% of the average X (0.395 Gt/year) of the various sinks and sources**
S_{LAND}	2.18	18%

S_{OCEAN}	1.91	20%
E_{FOS}	5.97	6%
E_{LUC}	1.27	31%

The averaged values of all sinks and sources were calculated with Appendix 7. The average imbalance in the GCE of X was calculated as ((100 /Average of sinks & sources) * Average X).

This demonstrates that the data for the sinks and sources of atmospheric CO_2 are still too tentative to allow for the modelling of the GCE.

In search of X

According to the WCRP [42] seasonal ocean CO_2 emission (O_{SE}) and seasonal ocean CO_2 uptake (O_{SU}) are equal and even out. Also according to the WCRP the yearly CO_2 emission (ML_{YI}) is the industrial CO_2 emission ($IE = E_{FOS} + E_{LUC}$) plus the seasonal ocean CO_2 emission (O_{SE}). This can also be expressed as:

$$ML_{YI} = IE + O_{SE} \quad (5)$$

Still according to the WCRP [42], the yearly CO_2 uptake (ML_{YD}) is the total of the CO_2 sinks ($S_{TOT} = S_{OCEAN} + S_{LAND}$) plus the seasonal ocean CO_2 uptake (O_{SU}). This can be expressed as:

$$ML_{YD} = S_{TOT} + O_{SU} \quad (6)$$

As IE, ML_{YI}, $ML_{YD,}$ and S_{TOT} are known, O_{SU} and O_{SE} can be can calculated for each year (Appendix 12).

$$O_{SE} = ML_{YI} - IE \quad (7)$$

$$O_{SU} = ML_{YD} - S_{TOT} \quad (8)$$

749 The box plots of these yearly calculations (Fig 7) indicate that the difference between the seasonal
750 ocean emission (O_{SE}) and the seasonal ocean uptake (O_{SU}) is positive, significant and equal to X
751 for a calculation using $G_{ATM\text{-}Here}$ 1y. All other five calculation methods of X and G_{ATM} based on
752 the data at Mauna Loa give similar results but are not shown here for practical reasons. This
753 indicates that the basal paradigm of Ballantyne et al. [70] stating that, within the approach to the
754 GCE of the WCRP, O_{SE} and O_{SU} are equal, is not true.
755
756 **Fig 7. Box plots illustrating that X, the imbalance in the GCE, is positive and reflects the**
757 **difference between seasonal ocean CO_2 emission and seasonal CO_2 uptake.**
758 ML_{YI}: yearly atmospheric increase in CO_2 (Fig 2), ML_{YD} yearly atmospheric decrease in CO_2 (Fig
759 2), IE: Total of the industrial emission (E_{FOS} + E_{LUC}), S_{TOT}: total of the CO_2 sinks (S_{OCEAN} +
760 S_{LAND}), O_{SE}: seasonal ocean emission, O_{SU} :seasonal ocean CO_2 uptake, G_{ATM}: $G_{ATM\text{-}Here}$ 1y.
761
762 **X compared to land sinks and land use change over time**
763 Quite obviously, the disbalance X, in the GCE is mild, but nonetheless about 18 % of the
764 average yearly atmospheric CO_2 uptake through land sinks [74] and even 31 % of the emission
765 through land use change as newly calibrated by the carbon brief [73].
766 The imbalance in the GCE not only represents a high percentage of the yearly land sinks and
767 sources, but large error margins also exist in the data sets from the original registrations [74, 75,
768 76]. It is therefore relevant here to analyse the true relation between atmospheric CO_2 growth
769 (G_{ATM}) and land use change (E_{LUC}) or land sinks (S_{LAND}) (Fig 8).
770
771 **Fig 8. Counterintuitive trend between atmospheric CO_2 growth (G_{ATM}) and land CO_2 sinks**
772 **and sources.**

A. Correlation between atmospheric growth (G_{ATM}) and land use change emission in CO_2 (E_{LUC}). B. Correlation between atmospheric growth (G_{ATM}) and CO_2 land sinks (S_{LAND}). C. Correlation between atmospheric growth (G_{ATM}) and the surface area of land use change (S_{LUC}).

A clear correlation between the development of the sinks and source over time and the G_{ATM} was not expected, but the statistical analysis between the three should have confirm the nature of the correlation hypothesized by the WCRP. This is not the case. The CO_2 emission from land use change (E_{LUC}) correlates negatively with the atmospheric CO_2 growth (G_{ATM}). This is confirmed by the positive correlation between CO_2 land sink uptake (S_{LAND}) and the same atmospheric CO_2 growth (G_{ATM}). The determination coefficients are weak, but the probabilities are relevant. Consequently the initial hypothesis that agriculture causes CO_2 emission and that land sinks result in CO_2 uptake is either unproven or incorrect. This potential paradox will be explained below and in the discussion section, but here we focus on the mathematical implications indicating that land use change rather reflects CO_2 uptake, while land sinks rather reflect CO_2 emission.

The relation distilled from GCE stating that industrial CO_2 emission minus ocean and land CO_2 sinks uptake represent the atmospheric CO_2 growth, as expressed in (9):

$$(E_{FOS} + E_{LUC}) - (S_{OCEAN} + S_{LAND}) = G_{ATM} \quad (9)$$

is debatable because in our statistical analysis E_{LUC} decreases as G_{ATM} increases, while S_{LAND} decrease as G_{ATM} increases, while in the original GCE, E_{LUC} had been expected to increase similarly to E_{FOS} while S_{LAND} had been expected to decrease together with S_{OCEAN}, the statistics from Figure 8 rather reflects an equation as expressed in (10):

$$(E_{FOS} - E_{LUC}) - (S_{OCEAN} - S_{LAND}) = G_{ATM} \quad (10)$$

This paradox is elucidated when considering the comparison between the surface of land use change and atmospheric CO_2 emission that still correlate positively (Fig 8 C). This indicates that

798 something other than CO_2 emission from land use change (E_{LUC}) has caused atmospheric CO_2
799 growth (G_{ATM}) and that this new factor contributing to atmospheric growth correlates to the
800 surface of land use change (S_{LUC}).
801 As was explained in the introduction, volatile organic carbon, water vapour, black carbon, aerosols
802 and pollutants played a part in the mitigation of cooling at the glacial maximum; here we
803 hypothesise that the surface of land use change is a proxy for the emission of such pollutants,
804 which explains the positive correlation between agriculture (E_{LUC}) and global atmospheric growth
805 (G_{ATM}).
806
807 **A new hypothesis**
808 Thus we can deduce that the Global Carbon Equation stating that atmospheric CO_2 growth (G_{ATM})
809 represents the difference between industrial emission (IE) and natural sinks (S_{TOT}) is debatable
810 because it
811 (1) leans too heavily on tentative estimates of land sinks (S_{LAND}) and land use change emission
812 (E_{LUC}),
813 (2) represents a debatable hypothesis on the relation between land sinks and sources of CO_2 to
814 atmospheric CO_2 growth,
815 (3) and requires that seasonality is evened out which is not the case.
816
817 From here on, the GCE, finding its roots in the 1979 Charney report [17], is abandoned and a new
818 interpretation of atmospheric growth in CO_2 (G_{ATM}) as yearly ocean emission in CO_2 (ML_{YI})
819 minus the yearly ocean uptake in CO_2 (ML_{YD}) will be explored.
820
821 **Implications of the new hypothesis**
822

The chief implication of this new interpretation of G_{ATM} as ocean generated is that, if ocean emission (ML_{YI}) is superior to ocean uptake (ML_{YD}), this imbalance represents the full G_{ATM} (which is positive) which can only be explained by the oceans releasing more CO_2, than that they take up. This means that the oceans are not taking up industrial CO_2 and we have to conclude that industrial CO_2 emission is not perceived in the troposphere. As industrial CO_2 isn't perceived in the troposphere it doesn't accumulate there and consequently industrial CO_2 can't cause global warming. In the absence of CO_2 as the chief driver for global warming and taking into account that the surface of land use change, being a proxy for pollutant emission, plays a part in the atmospheric CO_2 increase (Fig 8), it will be investigated in the following if such pollutants can, indeed, be demonstrated to drive the warming that causes oceans to release their gasses.

Having reviewed, in the introduction, the historically mentioned diversity in potential climate drivers, we now build on the predictions of Liss and Lovelock [54] who concluded in the foremost last paragraph in their paper on climate change that it was "… perhaps naïve to think that one gas acting alone (e.g. Dimethyl Sulphide) is responsible for particle formation; it is much more likely that a cocktail is involved. Many of these gases also play potentially important roles in air quality, particularly halogens in ozone destruction".

Comparing pollutant emission and ocean behaviour

As shown in the methodology section, UKESM1 is the pollutant emission that compares best with industrial emission ($IE = E_{FOS} + E_{LUC}$) (Table 1). Here we show how the yearly ocean emission (ML_{YI}), the yearly ocean uptake (ML_{YD}) and their difference (G_{ATM}) correlate with the UKESM1 pollutant emission values over time (Table 4).

Table 4. Comparison between pollutant emission and Northern Pacific Ocean behaviour.

X-axis	Y-axis	R^2	p:	Equation
UKESM1	ML_{YI}	0.5442	3.96 E^{-11}	0.0116 x + 7.537
UKESM1	G_{ATM}	0.40494	7.94 E^{-08}	0.00835 x - 2.982
UKESM1	ML_{YD}	0.09629	1.78 E^{-02}	0.002422 x + 10.52

The determination coefficients (R^2) and probabilities of not being correlated (p) from a polynomial regression analysis between of pollutants (UKESM1) to the yearly ocean CO_2 emission (ML_{YI}), yearly ocean uptake (ML_{YD}) and their difference (G_{ATM}) are shown here.

The R^2 values in Table 4 indicate that the pollutants determine 54% of the yearly ocean CO_2 emission (ML_{YI}), only 9 % of the yearly ocean CO_2 uptake (ML_{YD}) and 40 % of the tropospheric increase in CO2 concentration (G_{ATM}). This indicates that the pollutants have a strong impact on ML_{YI}, and a weak impact on ML_{YD}. In other words industrial pollutant emission influences both ocean CO_2 uptake as ocean CO_2 emission but the emission more than the uptake.

Ocean behaviour over time

When comparing monthly and yearly ocean uptake and emission over time it appears that both their intensities increased over time. While ocean uptake, on a monthly base, is more intense than ocean emission, the duration of ocean emission is longer than the duration of ocean uptake (Fig 9). A near systematic dominance of yearly ocean CO_2 emission over uptake follows from this emission duration. It also becomes clear from this intensity and duration analysis that for the period of 1961 to 2019, the duration in month of ocean uptake decreased in favour of ocean emission that increased in duration.

Fig 9. Ocean CO_2 uptake and emission.

A. Duration of ocean CO_2 uptake (red) and CO_2 emission (black) compared. B. Monthly ocean CO_2 uptake (red) and monthly ocean CO_2 emission (black) compared. C. Yearly ocean CO_2 uptake (red) and yearly ocean CO_2 emission (black) compared.

Interpretation

Modern situation

Pollutants

It has been found above (results section) that it is defendable that industrial CO_2 accumulation is not perceived in the troposphere and that the oceans are not taking up CO_2, but are emitting it. As seen in the methods, the pollutants cocktail holding more Volatile Organic Carbon (UKESM1) gives better results in comparison to industrial emission than the cocktail holding more Secondary Organic Aerosols (CESM2) by giving the best determination coefficients (R^2) and probabilities (p), so UKESM1 has been considered above (Table 4) and will also be used in the following for the following for a reconstruction of the Keeling curve.

Temperature driving yearly ocean behaviour

Seasonal CO_2 ocean emission, impacted by the pollutant emission, appears in earliest spring in the highest latitudes of the Northern Pacific, moves gradually towards the low latitudes until June, after which it disperses in southern direction [81, fig.2]. This emission wave is interpreted here to results from the heat anomaly for which we invoke the Le Chatelier principle,

894 stating that changes in temperature, pressure, volume, or internal concentration of a solute, each
895 and all can shift the equilibrium state of the solute [82]. The oceans are a chemical solute with a
896 constant pressure and volume. Hence, only temperature will shift the internal concentration of its
897 solutes and it is temperature that drives the ocean CO_2 emission wave recorded in Hakkarainen et
898 al [81, fig 2].
899
900 **Pollutants enhancing seasonal CO_2 emission**
901 This emission wave is interpreted here as induced by a temperature anomaly stemming
902 from the Arctic because it appears in the high latitudes in spring, at polar sunrise [78, fig. 2]. The
903 temperature anomaly is considered to following from pollution when for instance nitrogen
904 compounds in the presence of lightening [83] cause the accumulation of the short lived
905 greenhouse gas ozone [57]. Ozone has a clear reaction with volatile organic carbons, which
906 reaction can be both photochemical and exothermic [84]. Because the reactions are
907 photochemical, ozone accumulates in the arctic winter night and only starts getting depleted when
908 the light returns in spring. The ozone enriched airmass is considered to become self-lofting in
909 early spring, as solar irradiation makes it relatively warm, which heat causes it to ascends slowly
910 over the Northern Pacific Ocean [85, fig. 3], while intensifying its large pressure systems. This
911 Self-lofting CHemically reactive arctic Winter accumulated Air Bubble (SCHWAB) incorporates
912 in its stormy course part of its heat into the ocean [86] that releases its gasses, amongst other CO_2.
913 These gasses come to enrich and react with the ascending airmass, which we can follow thanks to
914 the science community's focus on CO_2 . This air mass appears in the arctic high latitudes/ low
915 altitudes and escapes to the stratosphere in the low latitudes/high altitudes [85]. The amount of
916 pollutants reaching the high latitudes is expected to determine the importance of the arctic heat
917 anomaly, how much heat is incorporated in the ocean, how much gas the ocean releases and how
918 much ozone is depleted in the stratosphere.

919

920 **Natural and industrial pollutants in the Arctic**

921 As explained in the introduction, natural forest fires produce massive quantities of SO_2
922 [61] and other pollutants like NOx or NH_3 [62]. Both forest fires and the burning of coals generate
923 soot particles found in the atmosphere [87]. Smoke from wild fires also contributes to particulates
924 in the stratosphere [88] as recent wild fires are reported to have brought smoke into the
925 stratosphere of Canada [89], United States [90] and Australia [91].

926 All these fires reflect complete and incomplete combustion of organic molecules forming
927 pollutants as alkenes [84] that occur in the natural system in cuticular waxes of plants [91]. Such
928 molecules also contribute to (green) fossils fuels, rubbers (natural and industrial), and to plastics
929 [93] that form pollutants. Hence, fire (natural and industrial) injects substantial amounts of partly
930 and fully combusted pollutants in the troposphere through heat. Elevated temperatures or simple
931 air transport [94] bring the particulates to the tropopause where they form INP to the cirrus clouds.
932 Such aerosols are indeed reported from cirrus clouds [95]. Polluted cirrus clouds concentrate
933 yearly in each hemispheric winter pole [47], driven by the lower current of the Brewer Dobson
934 stratospheric circulation cell [46].

935

936 **Arctic tropospheric chemistry rather than albedo**

937 This interpretation of the seasonal polar enrichment of pollutants in the Arctic results in,
938 both, the accumulation of the short lived GHG ozone and a changing polar albedo. This duality
939 explains the uncertainties reported for the predictability of aerosol-ice cloud (cirrus) interactions
940 [53], because these uncertainties are only albedo based. But aerosols do not only dim solar
941 irradiance, they are also responsible for chemical polar ozone accumulation causing the SCHWAB
942 to form. The accumulation initiates the formation of a localized heterogenic tropospheric airmass
943 containing relative high concentrations of the short lived GHG ozone. This localized and short

944 lived GHG air mass becomes relatively warm as soon as it receives the first light beams in spring.
945 Part of the heat generated by the ascending air mass gets incorporated in the ocean through storms
946 and results in the emission of a broader spectrum of ocean gasses as suggested earlier by Liss and
947 Lovelock [54] and illustrated here in Table 5.
948
949 **Table 5. Solubility indicators for pure gasses**.

Gas type	Concentration in water at 0˚C	Concentration in water at 60˚C	Solubility indicator ((concentration at 0˚C - concentration at 60˚C)/60)
H_2	0 .0019	0 .00115	0 .0000125
N_2	0 .029	0 .01	0 .000316667
CH_4	0 .04	0 .012	0 .000466667
CO	0 .045	0 .01	0 .000583333
He	0 .04	0 .0013	0 .000645
O_2	0 .07	0 .0225	0 .000791667
Ar	0 .1	0 .03	0 .001166667
C_2H_6	0 .13	0 .02	0 .001833333
C_2H_4	0 .28	0 .12	0 .002666667
CO_2	3 .45	0 .6	0 .0475
H_2S_2	7	1 .5	0 .091666667
Cl_2	10	3 .2	0 .113333333
SO_2	225	25	3 .333333333
NH_3	900	180	12

950

951 The solubility indicator was calculated by subtracting a gas's concentration in water
952 arbitrarily chosen at 60 °C, from its equally arbitrarily chosen concentration at 0 °C and
953 dividing it by 60 ((concentration in g gas/ kg water at 0 °C) - (concentration in g gas/ kg
954 water at 60 °C)/60). It is summarized here for gasses at one atmosphere under air with a
955 normal composition. Data were found in the Engineering toolbox [96]. This indicates what
956 gasses are more soluble than CO_2, and consequently have already escaped the ocean when
957 CO_2 has escaped; such data are not readily available for SF6.
958
959 This ocean gas emission explains the divergence between ocean CO_2 uptake and emission
960 (Fig.10): the ocean gas emission adds to the temporary GHG effect of the SCHWAB. The
961 statistical analysis of the monthly ocean emission for the Northern Pacific Ocean by year (Fig.
962 10), indeed, objectivizes the trend already observed in Figure 9 and shows that both monthly
963 emission and monthly uptake increased over time, but that monthly ocean emission increased
964 faster than monthly ocean uptake.
965
966 **Fig 10. Trends in monthly increase in CO_2 emission and uptake over time compared.**
967 Here we see that monthly emission increases faster than monthly uptake.
968
969 Such ocean emitted gasses, water vapour included, ascend to the stratosphere where they cause
970 ozone depletion. Global stratospheric ozone anomalies were indeed described by Hassler et al.
971 [31, fig.6] as related to aerosol emissions and they depicted a clear decrease in stratospheric O_3
972 percentages over time, for which there are numerous recent confirmations [32, 33, 55]. The figure
973 6 of Hassler et al. [31] is even reminiscent of warming stripes of Hawkins [97].
974
975 **Pollutants enhancing seasonal CO_2 uptake.**

Yearly ocean CO_2 uptake (ML_{YD}) is interpreted here as related to a growing volume of cold arctic water forming each year [98], because of a larger amount of industrial pollutant emission results in more heat generated each year and a larger volume of melted ice. Atmospheric CO_2 uptake can be seen as related to the sea-ice melting processes [99]. As the melted ice is also polluted it is expected to cause some eutrophication thus intensifying the biological pump taking atmospheric CO_2 down into ocean sediments sinks.

Atmospheric increase in CO_2 concentration

The atmospheric increase in CO_2 concentration (G_{ATM}) results from the difference between yearly CO_2 ocean emission and its uptake. It has a R^2 in correlation to UKESM1 that is 9 % higher than the average of emission and uptake. This suggests that some of the atmospheric growth in CO_2 concentration cannot be explained by the UKESM1 pollutant emission alone. First of all UKESM1 does not cover all the pollutants as Secondary Organic Aerosols having an albedo effect are less represented in that cocktail [77]. Also some of the atmospheric growth in CO_2 concentration can also be explained by the greenhouse effect of all the gasses escaping from the warming northern Pacific sea surface. In this way they contribute to further emission while they travel up to the stratosphere, as for instance water vapour, but also other gasses more soluble than CO_2 (Table 5). Finally this difference can also be explained by the pollutants brought directly into the stratosphere during air transport [94] and depleting the stratospheric ozone directly or depleting the stratospheric ozone directly by being produced at such high temperatures (for instance cement [100]) that the pollutants end up directly in the stratosphere. Each and all of these processes together in various ratios can be seen to contribute to the faster amplification of the Northern Pacific Ocean CO_2 emission over its uptake.

Duration of CO_2 emission versus CO_2 uptake in the northern Pacific Ocean

Starting 1980 (Fig 11), the duration of yearly ocean emission increased. Yulin et al, [98, fig.4] show that changes in the rate of decrease in sea ice extent occurred by the end of the nineties of the former century. In recording the moment of highest CO_2 uptake each year, the start of the uptake season is seen to shift very mildly from April to May while yearly ocean emission starts earlier in August instead of September (Appendix 13). This results in a slightly shorter uptake period.

Fig 11. Analysis of how the emission season became longer than the uptake season, for 60 years, each time considering 2 decades.

A. transition from emission to uptake moves to a later period. B. transition from uptake to emission moves to an earlier period.

A liquid and a solid shield for the Earth surface

Solid Earth's infra-red emission [101] increases the temperature from the stratosphere to the troposphere where solar radiation accumulates because it is briefly slowed down by solid, liquid and gaseous particulates. The infra-red emission is caused primarily by the solid Earth surface, but also by all dust, aerosols, particulates and GHG, as a function of their absorption potential.

The Earth is shielded by two zones of water suspended in the troposphere thanks to particulates, the outer solid zone of feathery ice clouds called cirrus formed by INP, and an inner liquid zone consisting of condensation clouds formed by CCN. The ice shield determines how much radiation enters and leaves the troposphere [102] but also how much pollutants reach the poles, and the condensation cloud shield determines how much infra-red light bouncing back from solid earth is retained in the lower troposphere. Particulates, pollutants and gas concentration in the troposphere consequently play a crucial role in temperature on Earth. Natural and industrial modulation of the

concentration of these gasses and pollutants in the troposphere are considered here to determine the intensity, the geographical position and the composition of a gas flow between ocean and troposphere. This gas flow, in turn is expected to determine the thickness of the stratospheric ozone layer. The thickness of the stratospheric ozone layer determines the Pleistocene cyclicity to which present day interglacial maximum belongs.

Seasonal and pollutant driven ocean behaviour

As demonstrated above, the existing global carbon equation (GCE) is neither in balance nor does the statistical analysis of the relation between is components support its present formulation. As explained above pollutants can be seen to determine the Pleistocene cyclicity. There is consequently sufficient reason to present a new hypothesis for what determines the Keeling curve in the Northern Pacific Ocean. It can be expressed as follows:

"Pollutants cause tropospheric winter ozone accumulation resulting in a relatively warm self-lofting chemically reactive air bubble (SCHWAB) starting its ascend as soon as light returns to the high latitudes. The trajectory of the SCHWAB influences and is influenced by existing pressure systems which causes storm intensification. The storm intensifications results in the incorporation of part of the arctic heat anomaly into the Northern Pacific Ocean. The warmed Northern Pacific Ocean releases its gasses because the solubility of gasses depends on the temperature of the water they are in. With this evaporation the latent heat vaporization generated by the yearly arctic heat anomaly is fully consumed. The oceans do not warm up through the arctic heat anomaly but the ocean emitted gasses ascend to the stratosphere where they deplete ozone. The stratospheric ozone depletion results in stratospheric cooling and in turn global tropospheric warming and global CO_2 emission (land and oceans).

When expressing this new hypothesis in an equation, the Northern Pacific Carbon Equation (NPCE), the atmospheric increase in CO_2 concentration can be re-defined as:

$$G_{ATM} = (E_{SOW} + E_{SLGHG} + E_{SOD}) - (U_{SIM} + + U_{SLGHG} + U_{BDD}) \quad (11)$$

Where:

E_{SOW}: Ocean CO_2 emission following from seasonal ocean warming. This function is stationary as it relates to the inclination of the Earth axis.

$E_{SLGHG:}$ Increase in ocean CO_2 emission caused by the heat generated by the (Short Lived) greenhouse gas in the SCHWAB. This increase in ocean emission is made proportional to pollutant emission. It is stationary as with this evaporation the latent heat generated by the yearly arctic heat anomaly is fully consumed.

E_{SOD}: Ocean CO_2 emission caused by stratospheric ozone depletion. Stratospheric ozone depletion follows from ocean emitted GHG ascending to the stratosphere because of the warming ocean. This stratospheric ozone depletion gives tropospheric warming and is made proportional to pollutant emission,. This function is made cumulative as stratospheric ozone depletion is irreversible.

U_{SIM}: Ocean uptake in atmospheric CO_2 following from the seasonal ice melt increasing ocean water solubility (related to the inclination of the Earth axis). This function is stationary as it relates to the inclination of the Earth axis.

U_{SLGHG}: Increase in ocean uptake in atmospheric CO_2 following intensified ocean cooling caused by the short lived GHG in the arctic heat anomaly. This increase in ocean uptake is made proportional to pollutant emission. It is stationary as the ocean cooling and hence the CO_2 uptake stops as soon as the ice starts accreting again and cold water isn't added to the ocean anymore.

U_{BDD}: Ocean uptake in atmospheric CO_2 related to biological CO_2 draw down off the coast of Peru because of algal blooms. It is made to weaken slightly over time from 100 to 98% as presently too little data exist on the frequency of El Niño events. It is inferred from the ocean emission CO_2

taking place during El Niño years, assuming that during normal La Niña years, the ocean takes up what the El Niño CO_2 emission anomaly emits during El Niño events [80].

The best impression of how these functions intertwine can be obtained when zooming in on a shorter period. Here the earliest 1961-1964 period is shown as the cumulative, the stationary functions and their sum still fit into one readable diagram (Fig 12).

Fig 12. Details of the 6 functions that determine the uptake and emission of CO_2 by the northern Pacific Ocean and their sum.

(1) Black: ocean CO_2 uptake following from an increase in ocean water solubility due to ocean cooling related to seasonal ice melt (U_{SIM}). (2) Red: increase in ocean CO_2 uptake following from an increase in ocean water solubility due to ocean cooling related to seasonal melt driven by the short lived GHG (U_{SLGHG}). (3) Blue: ocean CO_2 uptake through biological draw down (U_{BDD}). (4) Dark green: ocean CO_2 emission following from a decrease in ocean water solubility due to seasonal ocean warming (E_{SOW}). (5) Turquoise: increase in ocean CO_2 emission following from a decrease in ocean water solubility due to ocean warming related to seasonal tropospheric heat anomaly stemming from the short lived GHG accumulation in the Arctic (E_{SLGHG}). (6) Purple: CO_2 emission from cumulative ocean heat uptake throughout the year because of ozone depletion in the stratosphere, (E_{SOD}). (7) Apple green: monthly sum of all these functions (Sum 1-6).

When adding the atmospheric CO_2 concentrations measured at Mauna Loa by the NOAA in May 1961 as in Equation 9 (Appendix 10) in the following way:

$$G_{ATM\ ML\text{-}MONTH} = ((E_{SOD} + E_{SLGHG} + E_{SOW}) - (U_{SLGHG} + U_{BDD} + U_{SM})) + 316{,}89\ ppm \quad (12)$$

and comparing the data set for each month as offered by the NOAA [72] to the function expressed with the above equation (Fig. 13) with a regression analysis generated by the statistical program

PAST [71], it is found that they are practically identical. Indeed the probability that the two are not identical is 0 (p = 0), and they have a determination coefficient of 0.99896.

Fig 13. Comparing the monthly reconstruction of the Northern Pacific Carbon Equation (NPCE) based on the assumption it is pollutant driven, and the monthly atmospheric CO2 concentrations recorded by NOAA at Mauna Loa.

A. Function (black) expressing the reconstructed pollutant driven north Pacific CO_2 emission behaviour ($G_{ATM\ ML\text{-}MONTH}$) compared to (red) the monthly recording of the CO_2 concentration at Moana Loa as placed online by the NOAA [72]. B. The regression analysis comparing both functions. Details of the functions are given in Appendix 10.

The various components of the Northern Pacific Carbon Equation are presented in detail as macro's in Appendix 10 and are explained in the following.

Seasonally versus industrially driven ocean behaviour

Seasonality manifests itself nearly identically in both hemispheres. True seasonal ocean emission through warming (E_{SOW}) and seasonal ocean uptake through seasonal arctic melting and hence ocean cooling (U_{SIM}), determined by inclination of the earth's axis, are approximately comparable on both hemispheres. These are "approximately comparable" as differences in continent configuration on both hemispheres may give minor differences. As explained in the methods this seasonality accounts for approximately 0,25 ppm of yearly seasonal CO_2 emission and -0,25 ppm of yearly seasonal CO_2 uptake.

Industrialisation manifests itself chiefly on the northern hemisphere through the accumulation of pollutants during the polar night when photolysis is impeded. In the northern hemisphere

industrial pollutant emission first causes an increase in CO_2 uptake (and other gasses, many being more soluble than CO_2, see Table 5). This uptake follows from a mild intensification of the solubility pump due to extra ocean cooling related to extra seasonal arctic ice melt initiated by the winter night accumulation of the short lived GHG (U_{SLGHG}) and possibly other pollutants also behaving like GHG. On the northern hemisphere industrial pollutant emission also manifests itself later on as a decrease in ocean water solubility resulting in ocean CO_2 emission. This emission follows from slow incorporation in the northern Pacific of the heat generated by the ascending SCHWAB (E_{SLGHG}).

The ascend of ozone depleting substances to the stratosphere

The above considerations explain how, yearly, industrial pollutants form a self-lofting chemically reactive arctic winter night generated air bubble (SCHWAB) enriched with ocean emitted GHG-pollutant cocktail, ascend through the troposphere.. CO_2 and CH_4, being the focus of climate scientists are participating in the SCHWAB and reveal how the SCHWAB escapes to the stratosphere through the Hadley cell at the equator [85, fig 3].

El Niño events are also accompanied by an increase in atmospheric CO_2 concentration half way to the troposphere [80, fig. 6]. This indicates that the arctic heat anomaly can also induce accidental variations in atmospheric interconnectivity [68] that do not only result in an ascending SCHWAB but also a Self-lofting CHemically reactive warm Ocean generated air Mass (SCHWOM) ascending through the troposphere.

The solubility of gasses at various temperatures (Table 5) indicates that when CO_2 is emitted, H_2S_2, Cl_2, SO_2 and NH_3 are also emitted. In this respect sulphur dioxide (SO_2) and chlorine (Cl_2) are extremely relevant as their emissions into the stratosphere cause ozone loss when the chlorine (Cl_2) loading of the stratosphere is high [103]. Sulphur hexafluoride (SF_6) also needs mentioning, in spite of not having been able to insert it in the solubility table (Table 5), as it is both a very

potent GHG and it is reacting with stratospheric ozone [104]. Atmospheric SF_6 has been increasing since 1997 and the asymmetrical distribution pattern between the northern and the southern hemisphere [105, fig. 1 red or blue circles] indicates it reflects the same type of processes as those described here for CO_2. These temporary chemical ocean warming effects are considered here to cause the global stratospheric ozone depletion that give stratospheric cooling and global tropospheric warming [33]. This tropospheric warming explains the gradual increase in global ocean CO_2 emission (E_{SOD}) and was made proportional to the UKESM1 function [77].

The solubility and the biological pump (U_{BDD})

The relation between the ocean sinks (S_{OCEAN}) [76] and the yearly atmospheric growth (G_{ATM}) at Mauna Loa as conceived herein (Fig 14) shows that the two are co-varying as expected by the WCRP. This would indicate that as the northern hemisphere gets warmer the ocean CO_2 sinks become larger. This echoes the WCRP hypothesis that industrial CO_2 is taken up by the oceans, but as we have seen above and as will be developped in the discussion, industrially emitted CO_2 escapes to the stratosphere and presently the Northern Pacific Ocean emit more CO_2 than that it takes up.

Nonetheless, in the present temperature driven model more industrial CO_2 emission does means that more cold water gets produced at the poles which colder water is expected to take up more CO_2. This effect is feeding both, the chemical CO_2 sollubility pump and the biological pump because cold water simply contains more disolved gasses which will serve the biological CO_2 drawn down. Moreover the ice has accumulated pollutants, and as the ice melts it causes eutrophication which can also be expected to induce a stronger biological draw down of CO_2. The sollubility and the biological pump are consequently impossible to disentangle.

Nonetheless, considering the late scientific focus on the weakening of the Atlantic MidOcean Circulation [106] and knowing that the El Niño southern Oscillation [107] is part of the general

ocean ventilation process, the biological pump was treated separately as the biological draw down (U_{BDD}) taking place in upwellings areas. As explained in the Methods [80] it was made to reached 0,3 ppm of CO_2 yearly starting in november and ending in january and to decrease slightly over time from a 100% to 98 % to acknowledge the potential slowing down of the AMOC.

Fig 14. Ocean CO2 Sinks (S_{OCEAN}) and yearly northern Pacific G_{ATM} compared.
Regression analysis comparing the ocean sinks (S_{OCEAN}) [76] and yearly atmospheric growth G_{ATM} as measured at Mauna Loa.

Fitting the NPCE in the Pleistocene climate cycle

During a Pleistocene cooling phase outgoing heat is larger than incoming heat and during a Pleistocene warming phase incoming heat is larger than outgoing heat. Ozone depletion in the stratosphere is known to cause cooling in the stratosphere and warming at the earth surface [55]. When projecting a sawtooth pattern as suggested by Maslin and Brierly [108] on the four last Pleistocene climate cycles [109], each cycle can be typified by slow cooling (approximately 100,000 years) and rapid warming (approximately 10,000 years), inversely accompanied by a slow increase and a rapid decrease in dust concentration (Fig 15). When introducing the of the stratospheric ozone cycle in a Pleistocene climate cycle, slow cooling represents slow stratospheric ozone accumulation (more accretion than depletion), causing earth surface cooling while rapid warming represents rapid stratospheric ozone depletion (more depletion than accretion) causing surface warming. The CO_2 concentration in the ocean being directly linked by the Le Chatelier principle to water temperature, this means that stratospheric ozone accumulation causes oceans to take up more CO_2 than they release, while stratospheric ozone depletion causes oceans to release more CO_2 to the atmosphere. For the Pleistocene the focus is on dust and

charcoal (aerosols/ particulates), as both are inversely proportional to CO_2 and temperature [59]. We examine here how organic compounds (VOC'S) and pollutants that forest emanate or produce through (partial) combustion [110] play a part in these shifting ozone balances.

Fig 15. Sawtooth pattern projected on the four last climate cycles.
Blue lines: temperature anomaly (Δ t in C^o), green lines: CO_2 atmospheric concentration (in ppm), red lines: dust concentration(in ppm), grey vertical bar: glacial maximum (after Maslin and Bierly [108] and Petit et al. [109]).

Earth, in the absence of all its shields, is considered to be cooling. This means that it emits heat, which is a heat flow coming from its core [111]. So, in order for the troposphere to momentarily have a constant temperature during a glacial maximum or an interglacial maximum, incoming temperature has to be slightly higher than the outgoing temperature. This is not detailed any further here, because the cooling of the earth is expected to be undetectably slow at the very high time resolution we are considering here, but it is added *pro memori*.

The Pleistocene cooling phase

Starting at an interglacial maximum and going toward the next glacial maximum, the global kinetic imbalance (OUT > IN) is interpreted as driven by photosynthesis taking H_2O and CO_2 out of the troposphere into vegetation and sinks, but leaving O_2 behind ($CO_2 + H_2O$ => $C_6H_{12}O_6$ (organic molecule) + O_2). This leads to an ever more oxygen rich and inflammable troposphere. In the early cooling phase, the air is warm and very damp, and forms condensation clouds rather than ice clouds, fire is rare. During the early cooling phase, the tropopause, which altitude can be seen as thermally defined [112], has just expanded, forest fires have approached their minimum and cirrus cover is minimal. This allows for the heat reflected by both the

condensation clouds and the earth surface during the early cooling phase to escape rapidly from the troposphere. Because forest fires are scarce, the SCHWAB is weak and little ocean emitted gasses accompanied it to the stratosphere. Water, CO_2 and potentially reactive molecules like VOC, NO and CO [113, 114] are incorporated in the vegetation and its sinks and the stratospheric ozone accumulation at the tropic is faster than its break down at the stratospheric poles. The stratospheric ozone layer is thickening, it is warming and the troposphere is cooling.

The glacial maximum: mitigation of cooling

As the climate cools, vegetation adapts and concentrates in the low latitudes and altitudes where gymnosperms occupy a larger proportion of the vegetation cover. While gymnosperms have a regeneration cycle through fire, evergreen angiosperms like *Lithocarpus,* peaking in the tropics during the glacial maximum, not only have a co-evolution with fire [115] but also distinguish themselves by having relatively high concentrations of inflammable alkanes. So as the climate cools fire frequency increases due to increasing O_2 concentrations related to the ongoing photosynthesis, but also increases due to the intensification of the aridity related to the colder climate. CO_2 and H_2O are have been buried as organic molecules in sinks. The self-lofting forest fires inject incompletely combusted organic molecules and other pollutants into the tropopause [116] where they form IPN to the cirrus clouds. The cooling to warming threshold is attained when the SCHWAB fed by the pollutants from the forest fires, is large enough to cause the storms that will incorporate heat into the oceans that will release their gasses. This is when the ocean starts degassing, a.o. CO_2, but much more importantly chlorine (Cl_2), sulphur dioxide (SO_2) or ammoniac (NH_3) being much more soluble and reactive with ozone than CO_2. The spectacular reactivity with ozone of gasses like C_2H_2/Ar/O_2, being slightly less soluble in water than CO_2, do need mention in this context. Indeed warming conditions just beyond those allowing for the

present ocean CO_2 emission conditions can result in C2H2/Ar/O2 degassing which deplete ozone very rapidly [117].

The glacial maximum threshold can consequently be seen to be related to the accumulation of gymnosperm and *Lithocarpus* generated volatile organic carbon at the high latitudes during the arctic winter causing winter ozone accumulation [57], and in it wake strong ocean gas emissions. The intense ocean gas emission results in a slower ozone accretion at the equatorial stratosphere then its depletion at the polar stratosphere, this stratospheric ozone thinning introduces the Pleistocene warming phase.

The interglacial maximum: mitigation of warming

As the climate becomes warm and more humid, the vegetation dominated by the fire prone gymnosperms and *Lithocarpus* retreats to high altitudes and latitudes giving way to the chiefly deciduous angiosperms forests. Natural fire is less frequent in these deciduous forests and produces the fewer ice nucleating particle transported to the poles by the lower current of the stratospheric Brewer Dobson circulation cell. The troposphere is at its warmest, so it is at its highest and as surface expansion is the square of the altitude increase, the tropopause expansion, comprising the cirrus clouds expansion has also contributed in a less dense cirrus cloud deck allowing solar radiation (heat) to escape the troposphere again. During this phase less ozone accumulates in the high latitudes, the SCHWAB is smaller and less ocean gasses reach the stratosphere. Stratospheric ozone accretion at the equator is more important and frequent than it depletion at the poles. The stratospheric ozone layer becomes thicker and Earth grows back to its natural cooling state where vegetation captures and sequestrates the water and carbon dioxide that had partly warmed Earth.

A vegetation/stratospheric-ozone response system

In the natural Pleistocene climate cycle, fire frequency determines the quantity and the quality of the pollutants. These pollutants are envisioned to have these pollutants determine the size and temperature of the SCHWAB, which determines the degree of the storm intensification which determines the nature and the quantity of the ocean released gasses that are reacting with ozone as they ascend into the stratosphere. Various papers [84, 117, 118 fig. 1, 119] testify to this process.

Two CO_2 air masses at two different altitudes and two different latitudes, indicate that it takes about one year for the SCHWAB to migrate from the Arctic get to the top of the Hadley cell [85, fig.6]. Under natural climatic stasis circumstances, as the interglacial maximum we have reached presently should have been, one would not expect the new air mass to already presents itself while the old one is still escaping the troposphere.

As explained in the paragraphs on mitigation of cooling and mitigation of warming, the pollutant formation in the natural Pleistocene climate cycle reflects a response system with the vegetation composition. Cooling circumstances reduce the area of the chiefly deciduous angiosperms while favouring the expansion of the conifer forests having a regenerative cycle through fire and thus forming the pollutants driving the ozone cycle.

This interpretation of the Keeling curve echoes the response system of Lovelock [12] between algal blooms and cloudiness, known as the Gaia theory, but here the drivers are pollutants from fires and the response system is between the stratospheric ozone and the vegetation composition.

A complex stacked function in the Pleistocene

It is argued here that vegetation has been driving the climatic feedback mechanisms. This model is partly complementary to the model of Ellis and Palmer [120] leaning on the albedo of the polluted ice intensifying Milankovitch eccentricity cycles. But during the Pleistocene the climate

cycles become slightly longer each time and do not really match the eccentricity cycles but can be seen as modulating them (Fig 16).

Quite clearly, when comparing the Milankovitch cycles of Berger and Yin [121] to the past four Pleistocene climate cycles [109], obliquity does modulates temperature, as a high obliquity gives warming and a low obliquity gives cooling, whereas precession does the contrary but again these cycles have periods being divergent from the vegetation driven ones and are superimposed on the latter.

Three sunspot related cycles (unnamed ~9.7-ka; 'Heinrich-Bond' ~6.0-ka; Hallstatt ~2.5-ka), have also been demonstrated to play a minor but periodic role in Earth's climate forcing during the Pleistocene [122], these reflect functions that are also superimposed on the other ones.

Fig 16. Comparison between the four last climate cycles and the Milankovitch cycles.

A. Blue: temperature, Green: CO_2, red: dust. Red shading: high obliquity, blue shading: low obliquity (after Petit et al. [109]). B. Milankovitch cyclicities after Berger et al. [121].

The Pleistocene temperature curve, composed of numerous superimposed functions is strongly serrated and also requires events of higher and more irregular frequencies to explain the observed patterns. Historical evidence of volcanism, being irregular can also be seen to determine the temperature and CO_2 patterns from the Pleistocene. Indeed eruptions are known to have an impact on climate [9]. Insight in volcanic intensity and frequency supports this [123].

Meteorites produce high concentrations of dust in the stratosphere as was measured with the Chelyabinsk meteorite [124]. Meteorites strike Earth's atmosphere annually, but bigger impacts occur at century or millennium frequency [125]. Meteorites consequently, can cause unexpected serration to the Pleistocene temperature curve and in its wake, the atmospheric CO_2 concentration.

Finally, grazers may have impacted the length of the cooling period by rapidly promoting the fire prone grasslands over forested areas [126]. This complex co-evolutionary process offers an explanation for the lengthening of the cooling period. Thus grazing known to supress forest growth can be considered to have resulted in the lengthening of the cooling period of each Pleistocene climate cycle.

Industry mimicking the Pleistocene warming phase

What was sketched above is a natural Pleistocene climate cycle, but industrial emissions producing pollutants can have the same effect [14]. Considering the influence that the Brewer Dobson Cell has on stratospheric gas mixing [127], industrially emitted gasses are considered here to either impact ozone indirectly through transport to the poles [46] or through direct hot injection in the stratosphere. A relation between ozone depletion and climate is not contested in the IPCC reports, but since 2007, the causality of relation has often been inverted in the scientific literature, in spite of earlier work [31] demonstrating the covariance between aerosols and lower stratospheric ozone depletion.

Where are we now within the Pleistocene climate cycle?

In the past 140 000 years, there were 110,000 years of cooling and 20,000 years of warming [128] while the interglacial maximum had a duration of approximately 10,000 years, comprising about 5000 years of climatic stasis and 5000 years probably representing a slow start of cooling. The amplitude of the temperature during the Pleistocene has been of 10 to 12 °C, and the amplitude of the CO_2 concentration was in the range of 100 to 120 ppm. This indicates that (on average!) cooling took place by 0.1 degree Celsius and 1 ppm CO2 every 1000 years, while warming was of approx. 0.5 °C and 5 ppm /1000 years. Warming in the natural cycle was

consequently about 5 times faster than its cooling. During the long Pleistocene cooling phase minor uptake imbalance events were only required to occur once every 1000 years. Similarly, during the short warming phase ocean CO_2 emission only requires a modest imbalance every 200 years.

In the past 60 years, ocean emission as measured at Moana Loa by the NOAA was of approximately 100 ppm CO_2. As the recent excursion of the atmospheric CO_2 has the amplitude of a glacial cycle, and considering that it took place more than 300 x faster than during a natural warming phase, it cannot be said that it is accidental.

In considering the Pleistocene climate cycles (Fig 15), it is clear that we are at the top of an interglacial, and in scrutinizing numerous glacial records of oxygen isotope data and pollen records at both high and low latitudes [128] there is good reason to consider that the interglacial maximum has been passed and the cooling cycle was on its way. It is therefore defendable that present aberrantly high atmospheric CO_2 concentrations indicate that anthropogenic industriousness has reiterated the mitigation of cooling conditions from the glacial maximum of the Pleistocene climate cycle, but now on top of an interglacial maximum, thus bringing us in a climatic no-mans land, at a rate of change never experienced before.

Discussion

Because the above findings are in several aspects in contrast to commonly believed hypotheses, it is essential to discuss here the various seemingly inconsistent aspects, viz. the fate of industrially emitted CO_2, the role of light-absorbing particles, the role of GHG, the oceanic pH, the role of volcanic material and sea spray, the ozone cycle, the limits of the global carbon pump,

the presently highlighted thermos conditions of planet Earth, the role of the southern hemisphere and the fragility of our insights on carbon dioxide emission due to land use change.

Where did the industrially emitted CO_2 go?

The present analysis demonstrates that oceans are emitting CO_2 and not taking it up. While the G_{ATM}, as it is envisioned in the present paper, records the difference between ocean CO_2 emission and ocean CO_2 uptake, the IPCC considered it to reflect the Industrial Emission (IE) minus the Total Sinks. Within the IPCC hypothesis expressed by the Global Carbon Equation, seasonal ocean emission (O_{SE}) and uptake (O_{SU}) were expected be equal and hence neglectable. In Figure 9 we have seen that the duration of ocean CO_2 uptake decreases, which, in the light of a paradigm that states that ocean uptake follows directly from increased industrial emission is difficult to conceive. Increased yearly uptake for a shorter seasonal period of time is explained here, as modelled, as following from an increase in melting speed related to the yearly arctic heat anomaly. We also see in Figure 9 that the period of emission increases in duration, this is explained here, by higher temperatures of ocean surface water related to the SCHWAB becoming larger. When explaining the atmospheric increase in CO_2 concentration, as argued in this paper, merely through first a tropospheric local and then a stratospheric global heat anomaly, the question arises why is the industrial CO_2 emission not perceived in the Keeling curve?
This can be explained by the study of El Niño events that cause a CO_2 concentration anomaly in the mid troposphere at 6 km altitude [79]. This indicates that the CO_2 produced at sea surface and relatively high sea surface temperature, rises rapidly to 6 km. This relatively high sea surface temperature represents a anomaly of *less than 1 C°* [129]. Knowing that El Niño years are accompanied with a CO_2 increase of 1 ppm four months after the event, and knowing the CO_2

rises to the mid troposphere, estimated at 6 km, the ascending speed of that CO_2 holding air mass is 2 m/ hour.

At 0,7 m from a domestic chimney employing coal, lowest temperatures are 178 C° [130]. The exhaust temperature of gas vehicle varies between 150 and 600 C° [131] while the analysis of the European waste heat potential summarizes industrial categories that start a 100 C° and end at > 1000 C° [132]. Industrial and domestic CO_2, are consequently entering the troposphere at "temperature anomalies" of minimally 60 C° and can be expected to rise at 120 m/hour.

Consequently, while the primary condition for the global carbon equation (being that land, ocean and atmosphere form a closed system) is incontestably true, this does not necessarily imply that land, ocean and troposphere are also a closed system. Indeed, CO_2 at low temperatures anomalies already escapes from the troposphere to the stratosphere [85], which means that gasses entering the troposphere at minimally 60 x that temperature cannot be expected to accumulate in the troposphere, but reach into the stratosphere, while the cirrus clouds sieve out the coarser ozone sensitive particulates.

This corroborates the NPCE and indicates that what is measured at Moana Loa is not industrial CO_2 accumulation, but a flow of gasses escaping the warming Northern Pacific Ocean. This yearly flow of relatively warm air mass is denounced by the daily CO_2 measurements at Mauna Loa. It must consequently be concluded that the Keeling curve reflects the acceleration of ocean warming, which we showed in our model is proportional to industrial pollutant emission. This means that oceans are presently degassing at a speed and acceleration higher than at a glacial/interglacial transition, and, in the wake of this acceleration, so does the stratospheric ozone depletion causing the ocean emission to accelerate.

Where are the ocean gasses coming from?

The formation of coastal and oceanic carbon sinks [133] gives an imbalance in the global carbon budget calculated in this way, by sequestration the carbon into shelf and ocean sediments. This imbalance can be solved by considering that the mid-ocean ridges have heightened nutrient flows when active [134] and constantly feed the oceans with gasses. The gasses are transferred at each transition from a glacial to an interglacial maximum from the oceans to the atmosphere when natural ozone formation at the poles and it depletion in the stratosphere causes the ocean surface to warm and emit the gasses that have been accumulating in the ocean during a Pleistocene cooling phase.

Polyatomic molecules and other light-absorbing aggregates

The words of Lovelock and Margulis [12]: "CO_2 at high concentrations could have performed a similar function as could other polyatomic gasses" refer to the fully hypothetical models developed for the early Archean, when it was assumed that the young Sun was faint. By now the faint Sun paradox is found to be questionable for the early Archean period [135]. The higher rotation velocity of the early Earth could have caused Earth to be warmer [136]. These decisions, rather than results, pertain to a hypothesized the deep past. We are now focussing on the past 2.5 million years where the troposphere is chiefly composed of N_2 and O_2, and where of all trace elements, H_2O, with an average concentration of 0.4% is the most frequently occurring polyatomic molecule in the atmosphere after which CO_2 follows far behind, as it is measured in parts per million, and CH_4 is even more scarce as it is measured in parts per billion. Without any doubt all electrons within all atoms of these molecules when excited by light and when falling back to a lower energy level will, depending on it atomic composition, emit more or less infra red light and as such participate to the earth's kinetic budget, but the most frequent more than other compounds. Water vapour is the most frequent and the width of the absorption spectrum of water

vapour clearly encompasses that of other polyatomic molecules in the troposphere. Furthermore pollutants also occur frequently in the troposphere, alkenes, for instance, represent an important fraction of the particulate matter [137] and they are present in higher concentrations than methane. Particulate matter, for instance, displaying high concentrations in the Ganges valley can be expected to cause radiative absorption [138]. As explained in the introduction: all solid particulates, all gasses, and all liquids cause radiative absorption. The hypothetical choice of CO_2 for a debatable problem in the Archean, should be treated with a correct sense of proportionality, instead of elevating CO_2 to the chief kinetic driver for System Earth.

Ocean pH

Given that the oceans, on a yearly basis, take up less CO_2 than that they are releasing, CO_2 uptake cannot be causing the oceans to decrease in pH, and consequently the cause for this changing pH must be sought for elsewhere. Indeed, the alkalinity changes measured lately in the ocean [139] appear to be in contradiction with the present ocean degassing model. To understand this change in pH of the oceans, it is important to return to the theoretical basis of the alkalinity of solutes. The Le Chatelier principle states that changes in temperature, pressure, volume, or internal concentration of a solute, each and all can shift the equilibrium state. The oceans are a chemical solute, and neither the pressure nor the volume of the surface water are changing considerably. This leaves temperature to determine the pCO_2 and its pH in ocean surface water.

Hawaii as an atypical upwelling area

The focus on the temperature dependency of pH and pCO_2 in ocean systems, requires a new interpretation for the covariance between the atmospheric CO_2 recorded at Mauna Loa

Observatory and the nearby ocean station ALOHA for which the study of Dore et al. [140] set the tone. In analysing how the conclusion that "Increasing concentration of atmospheric carbon dioxide leads to higher dissolution of carbon dioxide in the ocean, thus lowering the ocean pH" [141] came about, we return to the early study [140] that showed atmospheric CO_2, (G_{ATM}) and pCO_2 in ocean water are inversely proportional but increase both, while the pH is proportional to the G_{ATM} but decreases [140, fig. 1]. This decreasing pH is interpreted as caused by the uptake of atmospheric CO_2 , but can also be assigned to the intensification of seasonal storms carrying cold nutrient rich water to the ocean surface and thus stimulating the calcium carbonate production ($CaCO_3$) which drives the ocean water pH down [142]. When considering the pH at in situ temperature [140, fig. 3], we see it decrease from spring equinox to autumn equinox, thus clearly reflecting a temperature signal. It consequently is what happens in between autumn equinox and spring equinox that is relevant to understand the pH and the pCO_2 registered at the ALOHA ocean site. In this context Calil and Richards [143] show that Hawaii is an atypical situation for the whole Northern Pacific as it is influenced by upwelling and that starting September the ocean is cooling again. The increasing intensity of such cooling upwelling settings over time has been associated to the recent climate conditions [144]. The sea water temperature, the pCO_2 and the pH at the ALOHA ocean site, consequently reflect upwelling intensification while the overall atmospheric CO_2 signal is determined by the Northern Pacific as a whole.

Volcanic particulates and sea spray

When the Krakatau explosion of 1883 caused global cooling, Abbot and Fowle [9] highlighted volcanic glass and sulphur as potential components of the haze that obstructed solar radiation through "volcanic glass and sulphur". The petrology of dust that fell upon the mirror of their telescope had indicated the presence of "volcanic glass, quartz, feldspar and kaolin" but this

composition raised some doubt at the time as to its origin, which sulphur did not. By now [e.g., 145] such particulates are known to be normal volcanic products and excellent ice nucleating particles [146], which again, considering the altitude of the event, does not mean that the temporary cooling came from those particulates. There is consequently no reason to associate cooling to sulphur clouds, neither in the tropo- or the stratosphere as has since then been propagated. Sea spray containing sulphur [23] is typical of the storm of a Pleistocene warming phase, while sulphur in the natural stratospheric presence of hydrochloric acid will deplete ozone [103].

Volcanoes are all different, depending on their genesis and their position relative to the oceans. Pering et al. [147], for instance, demonstrate that, for the La Fossa crater, Vulcano Island, and the North East Crater of Mt. Etna, the sulphur production varied between 4% and 1% of their water production. Volcanoes are also producing ash clouds, the composition of which is primarily siliceous [148]. Volcanoes, injecting both water and ash in the atmosphere, are the way, par excellence, to form ice nucleating particles (INP) [149]. In the light of water as a source of free radicals or chlorine hydrates, it is crucial not to be tempted to jump to the conclusion that water vapour will result in our long awaited high tech solution to the mitigation of warming, on the contrary.

In a comparable way marine cloud brightening (MCB) through dimethyl sulphides from sea spray will only dim or brighten Earth's surface as cloud condensation nuclei (CCN), but have no chemical cooling effect. In fact effort have even been made at reducing sulphur emission [150]. So, it cannot really be the dimethyl sulphides that will be dimming solar radiation, but rather it is the altitude at which such particle resides, given their density and origin, that will determine its role in our climate cycle. All particulates will come to increase the density of either of the walls of our thermos-sphere (the condensation cloud or the ice cloud wall) and dimethyl sulphides can be

seen as depleting ozone [27], while our knowledge of the stratosphere composition, its chemical behaviour and its vertical circulation patterns are insufficient to try chemical experiments with it.

The ozone cycle

Despite the 1987 Montreal protocol aiming at the global reduction of the infamous CFCs, a global increase in atmospheric concentrations of CFC-11 or CF6 was observed in the last decade [151]. Moreover, there is convincing evidence for the direct participation of polar stratospheric cirrus in the polar stratospheric ozone depletion via sunlight-giving photochemical reactions in spring, for which notably hydrogen oxide radicals (HO_x), nitrogen oxides (NO_x) and sulphur are responsible [152]. This is in strong support of satellite-observed warming pattern that resembles closely the atmospheric distribution of chlorofluorocarbons (CFCs), as highlighted in a review on climate models and radiative forcing [153]. Finally as mentioned above, ozone reacts with free radicals and water in the damp phase can dissociate into H and OH, both being very reactive free radicals (Pers. Comms. Prof. Wijbrans, July 11-th 2024). Considering the importance such free radicals have for our climate, and seeing how faithfully the emission over time of for instance SF6 follows the fluctuations we also observe for the ocean emitted CO_2, it is of crucial importance that we learn to separate between natural and industrial occurrences of free radicals.

Asymmetric ozone distribution patterns comparable to those for CO_2 or CH_4 [84, fig.6] in the troposphere can be witnessed in Bednarz et al. [118, fig. 2]. In analysing the tropospheric behaviour of ozone [118, fig. 1], we see it appears in the winter in the northern high latitudes, expand in spring and retrieve in summer. Ozone even react with water vapour [112], thus supporting our new model where a self-lofting chemically reactive arctic winter night generated air bubble (SCHWAB) appears early in the year in the northern high latitudes, and comes to intensify the existing atmospheric interconnectivity, by lowering the Aleutian Low and

heightening the Hawaiian High. The SCHWAB is influenced by, and influencing the existing pressure systems, to finally escape to the stratosphere at the equator with the ascending currents of the Hadley cell.

Lightning frequency has increased drastically in the Arctic over the past decade [154]. This increase follows from higher aerosol concentrations in the atmosphere [155]. The predominant mechanism of ozone formation in the upper troposphere is lightning-induced precursors such as oxides or pollutants like nitrogen (NO_x), carbon monoxide (CO), and hydrocarbons (HC) [82]. While lightening frequency is highest in the arctic summer [156], one should keep in mind that ozone depletion requires bromides, which only become available as soon as (sea) ice starts melting [157]. Lightening in the absence of bromides can explain the winter accumulation of the short lasting GHG ozone in the arctic winter night, as it is sensitive to photolysis requiring light.

The intensification of industrial and agricultural dust and pollutants like for instance the volatile organic carbons, or isoprene produced by the palm oil industry [158] can be expected to intensify the formation of the SCHWAB over time. It explains why the period of ocean CO_2 emission became longer than the period of ocean CO_2 uptake, starting a month earlier, and ending a month later, thus indicating that the SCHWAB became larger and more sensitive to light, with time.

Funnel shaped hemisphere

The lower current of the stratospheric Brewer Dobson circulations concentrates cirrus clouds each year at the pole of the hemispheric winter [46]. These cirrus clouds are formed by ice nucleating particles of diverse industrial origin [47] and can be envisioned to get transported in this way to the high latitudes. This lower current functions like a funnel, each time occupying a smaller latitudinal circumference. This means that it concentrates all pollutants that reached freezing altitudes towards the poles, which poles being the coldest heaviest atmospheric point on earth will

attract these pollutant laden ice clouds . This explains why the UKESM1 emission [77], reflecting industrial activities distributed randomly over the northern hemisphere are giving good results in correlation with the G_{ATM} measured at Mauna Loa.

The limits of the biological carbon pump

The modelling of an algal bloom driven System Earth, as is the Gaia hypothesis, was unsuccessful [22]. Nonetheless phytoplankton is still considered as a means for the restoration of the natural carbon cycle by drawing atmospheric carbon down to the ocean sinks through the biological pump [e.g., 159]. Many authors still expect that boosting phytoplankton production through Fe seeding will draw down the CO_2 concentration in the atmosphere and mitigate warming, but it has often been tried to validate this hypothesis, though without success [e.g., 160]. The Banda Sea upwelling area sheds light on this vexing situation [161]. Parts of these phytoplankton blooms do reach the ocean bottom as faecal pellets holding both inorganic $CaCO_3$ [162] and organic carbon of zooplanktonic origin. The Banda Sea is such an upwelling area where cold and nutrient-rich upwelling water causes organic carbon drawdown through a more elaborate food chain favouring the sedimentation of the refractory (= resistant to decay) zooplankton exoskeletons and eggs. These upwelling waters are feeding each consecutive trophic level with a specific speed and duration adapted to the life cycle of these species. Any imbalance in these equilibria developed over time will have a so-called harmonica effect. Nutrient supply and the intercorrelated pH and temperature of marine systems are even responsible for the Harmful Algal Blooms (HAB) [163] inducing the CO_2 transport into the troposphere.

Albedo or chemically driven global warming

In 2023, direct negative forcing through aerosols raised alarm. Aerosols from aviation were even considered to mask part of the GHG global warming [50]. This suggested that the air transport industry could mitigate global warming in a similar way as Marine Cloud Brightening (MCB) would do. But clouds reflect on both sides and most infrared radiation comes from the earth surface which means that the denser the clouds, the more intense the reflection. Moreover, pollutants from (air transport) industry participate in both lightening intensification and in the shedding of molecules participating in the chemical formation of the winter ozone accumulation. In its latest report [49] the IPCC supported the view that particulates induced albedo could mask the effect of GHG [50] and prepared to lean towards geoengineering, but, in contrast with studies from the 1970 [14], they only focussed on clouds albedo and neglected the chemically induced arctic heat anomaly.

Southern hemisphere

The southern hemisphere displays the same atmospheric increase in CO_2 concentration as the northern hemisphere but only experiences mild seasonal CO_2 emission fluctuations. This is explained here because industrialisation is less prolific in the southern hemisphere and has less influence on tropospheric ozone. Furthermore, the Antarctic consists of a continent which, with its low thermal mass, is slow at warming up. The heat anomaly from the winter ozone accumulation is consequently chiefly occurring in the northern hemisphere, while the heat anomaly following from ozone depletion in the stratosphere is experienced globally.

Land use change emission, land use change surface

The relation between G_{ATM} and land use change was established above in the results through the new hypothesis that land use change surface (S_{LUC}) increase is responsible for an increase in the production of aerosols and pollutants. Here we see (Fig 17) that land sinks (E_{LUC}) increase with increasing land use change surface. E_{LUC} instead of emitting CO_2 to the troposphere, is found here to form a sink, which is explained here as being transported to hydrosphere through consumption and thus disappearing from the troposphere. This explains, for instance, the extreme eutrophication of the North Sea [e.g. 164] .

Fig 17. Trend analyses between land sinks (S_{LAND}) and land use change emission (E_{LUC}) or surface of land use change (S_{LUC}).

The difficulties at separating between land CO_2 sinks (S_{LAND}) and land use change CO_2 emission (E_{LUC}) have been reported by their developers [74, 75]. The evaluation of these two parameters is more complex than commonly believed. Indeed, Hakkarainen et al. [80, fig. 3] show that the tropical rainforests belts are emitting CO_2. In the most recent publications of June 2024 of a the European Centre for Medium-Range Weather Forecasts [165] we also see very clearly that, on land, in the summer there is CO_2 emission in the southern hemisphere. This is also true when looking at the areas where the Brazil tropical forest did not undergo burning and cutting [166] and this holds also for Africa [167]. The response of tropical trees to rising temperatures is a key uncertainty limiting our ability to predict CO_2 biosphere-to-atmosphere feedbacks in a warming world. Indeed tropical trees show that the ratio between photosynthesis and respiration intensity is affected by high temperatures for some taxa more than for others [168]. These considerations can explain the paradoxical correlations observed in our statistical analysis of the relation between carbon sinks and sources on land. Alternatively, the CO_2 emission of tropical forests [80, fig.3]

can also be explained by fungi in soils because fungal respiration rates also increase at increasing temperatures [169].

Present paradoxical considerations are mentioned here to urge a reassessment of the impact of agriculture on CO_2 but even more so on organic aerosols. Indeed, agriculture according to present analysis is expected to result in more aerosols, volatile organic carbons (pollutants), and as demonstrated here, more ocean CO_2 emission. The use of natural land sinks to store CO_2 is welcomed of course, but it is advised to pay attention to the taxa used to these purposes and the latitudes where this is done. Also respiration of forest soils requires further study.

Stratospheric ozone depletion reflected in ocean CO_2 emission only

In the present reconstruction of Keeling curve (Fig 12, 13, Appendix 10) the influence of stratospheric ozone depletion was only made to influence ocean CO_2 emission (E_{SOD}) but not the increase in uptake through the solubility pump. It is therefore highlighted here that present study reflects the northern hemisphere until 2019 where the Arctic was hardly affected by stratospheric ozone depletion, in mild contrast to the Northern Pacific Ocean at Maua Loa [170, fig. 11 a] which was affected by it. Recent results even indicate that stratospheric ozone depletion is most conspicuous in the tropics [171, fig. 4 e] while it is absent in the high northern and moderate in the high southern latitudes. This negative ozone accumulation anomaly in the stratospheric tropics is in support of present Pleistocene climate model where the ozone cycle starts in the high tropospheric latitudes, comes to feed the low latitude stratospheric ozone layer and gets depleted in the high stratospheric latitudes.

Angiosperms taking the floor

Since their diversification in the Cretaceous, the angiosperms are considered to have outcompeted the gymnosperms that retrieved to colder areas [172]. This overtaking is accompanied with cooling [172]. The cooling from the Mesozoic to the Cenozoic is typically associated with a decrease in atmospheric CO_2 concentrations, accompanied by an increase in amplitude and possibly periodicity [173, fig1]. It is suggested here that our Pleistocene vegetation driven cyclicity in temperature and atmospheric CO_2 concentration, reflects the end member of co-evolution between vegetation composition and the troposphere that started in the Mesozoic. This would imply that the very fast and even accelerating capacity of angiosperms at drawing down both carbon dioxide and water from the troposphere has had bearings on the stratospheric ozone cycle, allowing for more ozone accretion at the stratospheric low latitudes than depletion at the stratospheric high latitudes.

Limitations of this study

The present study demonstrates that the Keeling curve is a symptom of temperature driven System Earth, which temperature is determined by a cocktail of industrial pollutants injected in the tropopause. The pollutant values taken from Griffiths et al. [77] had a very low resolution which required that the monthly values were made linear between two consecutive years (Appendix 10), such important parameters should be more detailed and provided by industry on a regular base. Also, in spite of Griffiths et al. [77] looking far into the future, predictions aren't developed in the present study, as pollutant production depends on a Montreal protocol type of regulations which feasibility belongs to the political domain which is far beyond the scope of this paper. Also the bulk chemical transformation taking place in the arctic winter night was only touched upon, but requires further investigation.

In the present study the contribution of the biological pump to the solubility pump is potentially underestimated and deserves further scrutiny.

With respect to the stratospheric ozone depletion, the turnover speed of the polluted Brewer Dobson Cell will also contribute to the thickness of the stratospheric ozone layer and influence earth surface irradiance, but this was not considered here either.

So while this study is supported by good statistical results, it is far from perfect and its chief quality is that it brings our knowledge on the strato-, tropo-, hydro- and biosphere together in one model for the Northern Pacific Ocean. The Atlantic ocean, the southern Pacific , the southern hemisphere, the Canadian Rockies, New Zeeland, all function differently as in these divergent sites vegetation and lithosphere contribute differently to the atmospheric CO_2 concentration. The only thing that all these localities share is the global warming following from the stratospheric ozone depletion.

The ideal study consists of a full kinetic global budget for System Earth. In such a kinetic study, the turnover speed of the conveyer belt and all its tributaries is required. Estimates in the contribution of the formation of Pacific mid and deep water to the global kinetic ocean budget are still tentative and divergent. Also, complex functions describing the statistical presence and absence of clouds reflecting the solar radiation allowed by the thickness of the stratospheric ozone layer are required to make a more detailed kinetic model, but this has not been developed for System Earth yet.

Conclusions

Our introduction aimed at being exhaustive with respect to all the hypothesis brought to the scientific arena until now and has made it plausible that a CO_2 driven climate model has been

favoured prematurely over other models, like the pollutant-stratospheric ozone driven climate model highlighted here. Independently, these early decisions initiated the international UN scientific co-operation that enabled the present study through the wealth of data on which this paper leans heavily.

The atmospheric increase in CO_2 concentration (G_{ATM}), commonly believed to reflect the tropospheric accumulation of industrial CO_2 that was not taken up by the oceans and land sinks as expressed in the Global Carbon Equation of the WCRP [42] is demonstrated here to reflect the difference between the Northern Pacific Ocean CO_2 emission and its uptake. By replacing G_{ATM} with the difference between the northern Pacific CO_2 emission and uptake, the Global Carbon Equation proves to be out of balance by 0.395 Gt C. The further analysis of this imbalance indicates that it reflects the difference between Northern Pacific Ocean seasonal emission and its uptake, as interpreted by the World Climate Research Program. Although minimal, it does represent 25% of the average emission CO_2 through land use change and 15 % of the average CO_2 uptake of land sinks. This imbalance chiefly reflects the difficulties at estimating the CO_2 land sinks and land sources. The complexities in establishing the CO_2 emission through land use change (E_{LUC}) and land sinks (S_{LAND}) are shown to be of fundamental nature and are significant enough to urge new studies.

Because the increase in atmospheric CO_2 as recorded in the Keeling curve is fully explained by the northern Pacific emission and uptake in CO_2, industrial CO_2 emission is not detected in the troposphere. This absence is explained by the heat of industrial emission causing CO_2 to self-loft out of the troposphere. In the absence of CO_2 as the GHG causing global warming, industrial pollution is considered as a driver for it, because pollutants are expected to be sieved out of the self-lofting industrial emission by forming ice clouds (cirrus) in the tropopause. The pollutants forming the ice clouds are brought to the Arctic by the lower current of the stratospheric Brewer Dobson cell. In the arctic winter night, these chemically diverse particulates often transform into

the short lived GHG ozone, which in the absence of light allowing for photolysis, accumulates. This ozone rich chemically reactive mixture becomes self-lofting as soon as it gets illuminated in early spring.

The Keeling curve was hypothesized here to reflect the yearly ascend of the self-lofting chemically reactive arctic winter generated air bubble (SCHWAB) at Mauna Loa , but also its ozone depleting consequences in the stratosphere. To help the readers imaging, we envision a lava lamp principle where the trajectory of the SCHWAB is influenced by, and influencing the existing pressure systems, to finally escape to the stratosphere at the equator.

This was tested by modelling, under the following assumptions: (1) CO_2 uptake depends on seasonal melting, (2) CO_2 uptake also results from enhanced melting through ozone accumulation in the arctic winter night, (3) seasonal CO_2 uptake is also related to the intensity of La Niña (biological pump), (4) seasonal ocean CO_2 emission takes place in the Northern Pacific Ocean, (5) the Northern Pacific Ocean CO_2 emission is also influenced by the incorporation arctic heat anomaly into the Northern Pacific, and (6) CO_2 emission is also caused by the buffering of the SCHWAB by the ozone in the stratosphere, resulting in global stratospheric cooling and global tropospheric warming. The cumulative result of this modelling exercise was found to reproduce the Keeling curve.

The present societal focus on industrial CO_2 emission is an attempt to deal with a symptom. While aerosols are being presented lately as causing cooling and thus masking the true GHG warming, it is demonstrated here that the chemical warming effect of these aerosols widely surpasses their effect as cloud brightening seeds. This is especially true as the troposphere with an outer solid ice cloud shield and an inner condensation cloud shield functions as a thermos-troposphere.

Present new hypothesis, where climate change is driven by industrial pollutant emission, is corroborated by a fire dust-driven Pleistocene response system between vegetation composition

and the stratospheric ozone layer, thus reminiscent of the Gaia hypothesis of Lovelock [12]. The cooling phase of the Pleistocene climate cycle, going from the interglacial to the glacial maximum, is mitigated by the increasing frequency of (gymnospermous) forest fires producing natural pollutants that result in a natural SCHWAB unleashing a broad spectrum of ocean emitted gasses depleting the ozone that accumulated in the lower stratosphere during the Pleistocene cooling phase. This causes the stratospheric ozone layer to become thinner, and results in stratospheric cooling and tropospheric warming. The warming phase, from the glacial to the interglacial maximum, is mitigated by the return to warm and humid circumstances reducing the fire frequency by restoring the dominance of the vegetations rich in deciduous (chiefly angiosperm) trees over the vegetations having a fire regenerating cycle (chiefly gymnosperms). This shift in vegetation type ratios allows for the SCHWAB to ascend to the stratosphere without unleashing a broad spectrum of ocean emitted gasses, thus resulting in more ozone accumulation in the stratospheric tropics than ozone depletion in the stratospheric poles. This causes the ozone layer to become thicker, and results in stratospheric warming and tropospheric cooling.

The present study can be seen to build onto the introductory sentence of the first (1990) IPCC report [34] in the following way:

"We are certain of the following: there is a natural greenhouse effect which already keeps the Earth warmer than it would otherwise be; pollutant, volatile organic carbons in particular, (organic) dust, black carbon and particulate matter emissions resulting from human activities are substantially causing a yearly arctic heat anomaly increasing the atmospheric concentrations of the greenhouse gasses: carbon dioxide, methane, chlorofluorocarbons (CFCs), nitrous oxide, water vapour, and others gasses which solubility at increasing water temperature is higher than that of CO_2. These increases reduce the greenhouse effect in the lower stratosphere resulting on average in an additional warming of the Earth's surface."

Acknowledgements

I am indebted to Dr S. Kaptein for having helped with the understanding of the method of the World Climate Research Program at evening out the seasonality in the Keeling curve and for correcting my transfer functions from ppm CO_2 to Gt Carbon. I am grateful for the editing and proof reading of the experienced editor and research geologist Prof. Dr. T. Van Loon. I am very grateful for the critical proofreading by Prof. Dr. Ing. JW Erisman, Chair of the Netherlands Scientific Climate Council, who sent me five incisive questions which I managed to resolve herein. I thank Dr. WJE van de Graaff (editor and geologist), Drs M. van Dongen and Drs F. Mrozek (geologists) for their proof reading and I am thankful for the English corrections by Drs SP Maas (geoscientist). I kindly thank Henk Caspers, Martine Hermsen and Eric Jan Bosch for their help with the illustrations.

Literature references

1. Herschel W. Observations tending to investigate the nature of the sun, in order to find the causes or symptoms of its variable emission of light and heat; with remarks on the use that may possibly be drawn from solar observations. Philos. Trans. Royal Soc. 1801; 91: 265-318. doi.org/10.1098/rstl.1801.0015
2. Foote E. Circumstances affecting the heat of the Sun's rays. Am. J. of Sc. Arts, 1856; XXII (LXVI): 382-383.

3. Tyndall J, 1861. On the absorption and radiation of heat by gasses and vapours, and on the physical connexion of radiation, absorption, and conduction. Philos. Trans. Royal Soc.1861; 151: 1-36
4. Held I, Soden BJ. Water vapour feedback and global warming. Annu. Rev. Energy Environ. 2000; 25: 441–75.
5. Arrhenius S. On the influence of carbonic acid in the air upon the temperature on the ground. Philos. Mag. 1896; 41: 237-276.
6. De Marchi L. Le cause dell'era glaciale, Pavia, Fratelli Fusi. 1895.
7. Russell FAR. Spread of the phenomena round the world, with maps illustrative thereof. In: Symons GJ, editor. The eruption of Krakatoa and subsequent phenomena. London, UK, Trübner & Co; 1888. pp. 334-339.
8. Archibald D. Diurnal and secular variation in the duration and brilliancy of the twilight glows of 1883-1884 and the height above Earth of the stratum that caused them. In: Symons GJ, editor. The eruption of Krakatoa and subsequent phenomena. London, UK: Trübner & Co; 1888. pp. 340-381.
9. Abbot CG, Fowle FE. Volcanoes and climate. Smithsonian Miscellaneous Collections 1913; 60 (29): 1-24.
10. Croll, J. On the physical cause of the change of climate during geological epochs. Phil. Mag.1864; 28:121–137.
11. Sagan C, Mullen G. Earth and Mars: evolution of atmospheres and surface temperatures Science, New Series, 1972; 177 (4043): 52-56.
12. Lovelock JE, Margulis L. Atmospheric homeostasis by and for the biosphere: the Gaia hypothesis. Tellus. 1974; XXVI: 1-2.
13. Valley SL. Handbook of Geophysics, A. F. C. R. L.1965.

14. Carter LJ. The Global Environment: M.I.T. Study Looks for Danger Signs Science, 1970; 169 (3946): 660-662. doi: 10.1126/science.169.3946.660.

15. Mohnen VA, Hidy GH.. Chapt. 16. Atmospheric nanoparticles early metrology and observations (1875–1980) In: Ensor DS, editor, Aerosol science and technology: History and Reviews RTI press, 2011. P 411-457.

16. National Research Council. Changing Climate: Report of the Carbon Dioxide Assessment Committee. Washington, DC: The National Academies Press; 1983. doi.org/10.17226/18714.

17. National Research Council. *Carbon Dioxide and Climate: A Scientific Assessment*. 1979. Washington, DC: The National Academies Press. Available: https://doi.org/10.17226/12181.

18. Liu SC, Kley D, McParland M, Mahlman J, Levy H. On the origin of tropospheric ozone. J. Geophys. Res. 1980; 85:7546-7552.

19. Wada Y, Beek L, van Kempen C, Reckman J, Bierkens MFP. Global depletion of groundwater resources. Geophys. Res. Lett. 2010; 37: L20402. doi:10.1029/2010GL044571.

20. Chen X, Jeong S. Irrigation enhances local warming with greater nocturnal warming effects than daytime cooling effects. Environ Res. Lett. 2018; 13 024005. doi: org/10.1088/1748-9326/aa9dea

21. Lovelock JE, Mags RJ, Rasmussen RA, 1972. Atmospheric Dimethyl Sulphide and the Natural Sulphur Cycle. Nature. 1972; 237: 452-453.

22. Ayers GP, Cainey JM. The CLAW hypothesis: a review of the major development Environ. Chem. 2007; 4: 366–374. doi:10.1071/EN07080

23. Zheng G, Kuang C, Uin J, Watson T, Wang J. Large contribution of organics to condensational growth and formation of cloud condensation nuclei (CCN) in the remote

1865 marine boundary layer. Atmos. Chem. Phys. 2020; 20: 12515–12525. doi.org/10.5194/acp-
1866 20-12515-2020.
1867 24. Crutzen PJ. The influence of nitrogen oxides on atmosphere ozone content. Q. J. R.
1868 Meteorol. Soc.1970; 96: 320-325.
1869 25. Molina M, Rowland F. Stratospheric sink for chlorofluoromethanes: chlorine atom-
1870 catalysed destruction of ozone. Nature. 1974; 249: 810-812.
1871 26. Nielsen OJ, Bilde M. Reflection on two Ambio papers by P. J. Crutzen on ozone in the
1872 upper atmosphere : This article belongs to Ambio's 50th Anniversary Collection. Theme:
1873 Ozone Layer. Ambio. 2021; 50(1): 40-43. doi: 10.1007/s13280-020-01425-6.
1874 27. Yung YL. Chemical kinetics and modelling of planetary, NASA conference publications
1875 1990. 3077. In : First International conference on laboratory research for planetary
1876 atmospheres. Ed. Fox K, Allen JE, Quillen DT. Proceedings of a conference held at Bowie
1877 State University Bowie, Maryland October 25-27, 1989. p 181- 209.
1878 28. Strawa A, Pueschel R, Ferry G. The roles of aerosols in stratospheric ozone chemistry.
1879 Earth Science Enterprise, Atmospheric Physics. 1998; 171.
1880 29. Siegmund P, Sigmond M, Kelder H. The stratosphere as a puppeteer of European winter
1881 climate. Europhysics News. 2004; 35: 73-75. doi.org/10.1051/epn:2004303
1882 30. Hassler B, Bodeker GE, Dameris M. Technical Note: A new global database of trace
1883 gasses and aerosols from multiple sources of high vertical resolution measurements.
1884 Atmos. Chem. Phys. Discuss. 2008; 8: 7657–7702.
1885 31. Randel WJ, Polvani L, Wu F, Kinnison DE, Zou CZ , Mears C. Troposphere – stratosphere
1886 temperature trends derived from satellite data compared with ensemble simulations from
1887 WACCM. J. Geophys. Res. – Atmospheres 2017. doi:org/10.1002/2017JD027158.

32. Liu W, Hegglin M, Checa-Garcia R, Li S. Gillett N, Lyu K, Zhang X, Swart NC, 2022 a. Stratospheric ozone depletion and tropospheric ozone increases drive Southern Ocean interior warming. Nat. Clim. Change. 2022; 12. doi: 10.1038/s41558-022-01320-w.

33. Lin J, Emanuel K. Why the lower stratosphere cools when the troposphere warms. PNAS 2024; 121. e2319228121. 10.1073/pnas.2319228121.

34. IPCC, 1992. First Assessment Report Overview and Policymaker IPCC Supplement. Published with the support of Australia, Canada, Germany, The Netherlands, Spain, United States of America, Austria, France, Japan, Norway and United Kingdom. Printed in Canada 178 pp.

35. Turco RP, Toon OB, Ackerman TP, Pollack JB, Sagan C1983. Nuclear winter: global consequences of multiple nuclear explosions. Science. 1983; 222 (4630): 1283-1292. doi:10.1126/science.222.4630.1283.

36. Manabe S, Wetherald R. Thermal equilibrium of the atmosphere with a given distribution of relative humidity. J. Atmos. Sci. 1967; 24: 241-259. doi: 10.1175/1520-0469.

37. Hasselmann K. Stochastic climate models Part I. Tellus. 1976; XXVIII (6): 443-485.

38. Houghton RA. Balancing the Global Carbon Budget. Annu. Rev. Earth Planet. Sci. 2007; 35: 313-47.

39. McNeil BI, Matear RJ, Key RM, Bullister JL, Sarmiento JL. Anthropogenic CO2 uptake by the ocean based on the global chlorofluorocarbon data set. Science. 2003; 299: 235–239.

40. Le Quéré C, Raupach M, Canadell J, Marland G, Bopp L, Ciais, et al. Emissions of organic compounds from western US wildfires and their near-fire transformations. Atmosph. Chem. and Phys; 2022: 22. 9877-9893. 10.5194/acp-22-9877-2022.

41. Ciais P, Sabine C, Bala G, Bopp L, Brovkin V, Canadell JG, Chhabra A, DeFries R, Galloway J, Heimann M, Jones C, Le Quéré C, Myneni R, Piao S, Thornton P, Willem J,

1913 Friedlingstein P, Munhoven,G. Carbon and Other Biogeochemical Cycles. In:
1914 Intergovernmental Panel on Climate Change (editors). Climate Change: The Physical
1915 Science Basis, Contribution of Working Group I to the Fifth Assessment Report of the
1916 Intergovernmental Panel on Climate Change, Cambridge University Press, Cambridge,
1917 United Kingdom and New York, NY, USA. 2013.
1918 doi.org/10.1017/CBO9781107415324.015.
1919 42. Friedlingstein P, O'Sullivan M, Jones MW, Andrew RM, Bakker DCE, Hauck J, et al.
1920 Global Carbon Budget 2023. Earth Syst. Sci. Data 2023; 15; 5301–5369,
1921 doi.org/10.5194/essd-15-5301-2023.
1922 43. Denisov ET. Mechanisms of the Reactions of Radicals with Ozone. Rus J. Phys. Chem. B,
1923 2014; 2: 58-66.
1924 44. Harrison RM. Chapter 8: Chemistry of the Troposphere. In: Harrison RM. Pollution: cause
1925 effects and control, Royal Society of Chemistry, 2013; p.182-203.
1926 doi.org/10.1039/BK9781849736480-00182.
1927 45. IPCC, 2022. Impacts, Adaptation, and Vulnerability. Contribution of Working Group II to
1928 the Sixth Assessment Report of the Intergovernmental Panel on Climate Change. In:.
1929 Pörtner HO, Roberts D. Tignor M, Poloczanska ES, Mintenbeck K, Alegría A, Craig M,
1930 Langsdorf S, Löschke S, Möller V, Okem A, Rama B, editors. Cambridge University
1931 Press, Cambridge, UK and New York, USA. 2022. doi:10.1017/9781009325844.
1932 46. Noël S, Weigel K, Bramstedt K, Rozanov A, Weber M, Bovensmann H, Burrows J. Water
1933 Vapour and Methane Coupling in the Stratosphere observed with SCIAMACHY Solar
1934 Occultation Measurements. Atmos. Chem. Phys. 2018; 18: 4463- 4476.
1935 doi.org/10.5194/acp-18-4463.

1936 47. Zhao F, Tang C, Dai C, Wu X, Wei H. The Global Distribution of cirrus clouds reflectance
1937 based on MODIS Level-3 Data. Atmosphere 2020; 11(2): 219.
1938 doi.org/10.3390/atmos11020219
1939 48. IPCC 1997. Technical Report. Published with the support of Australia, Canada, Germany,
1940 The Netherlands, Spain, United States of America, Austria, France, Japan, Norway and
1941 United Kingdom. Printed in Canada 1997. 178 pp.
1942 49. IPCC, 2023: Sections. In: Climate Change 2023: Synthesis Report. Contribution of
1943 Working Groups I, II and III to the Sixth Assessment Report of the Intergovernmental
1944 Panel on Climate Change [Core Writing Team, H. Lee and J. Romero (eds.)]. IPCC,
1945 Geneva, Switzerland, pp. 35-115, doi: 10.59327/IPCC/AR6-9789291691647
1946 50. Quaas J, Jia H, Smith C, Albright A, Aas W, Bellouin N, Boucher O et al. Robust evidence
1947 for reversal of the trend in aerosol effective climate forcing. Atmos. Chem. Phys. 2022; 22:
1948 12221–12239. doi: org/10.5194/acp-22-12221-2022.
1949 51. Kok JF, Storelvmo T, Karydis VA,. Adebiyi AA , Mahowald NM,. Evan AT, He C,
1950 Leung DM. Mineral dust aerosol impacts on global climate and climate change Nature
1951 Reviews Earth & Environment. 2023; 4: 71-86.
1952 52. Julsrud I R, Storelvmo T., Schulz M, Moseid KO, Wild, M. (2022). Disentangling aerosol
1953 and cloud effects on dimming and brightening in observations and CMIP6. Journal of
1954 Geophysical Research: Atmos. 2022; 127. doi: org/10.1029/2021JD035476
1955 53. Zhao N, Dong X, Huang K, Fu JS, Lund MT, Sudo K, Henze D, Kucsera T, Lam YF, Chin
1956 M, Tilmes S. Responses of arctic black carbon and surface temperature to multi-region
1957 emission reductions: a hemispheric transport of air pollution phase 2 (HTAP2) ensemble
1958 modelling study , Atmos. Chem. Phys. 2021; 21: 8637–8654. doi.org/10.5194/acp-21-
1959 8637-2021.

54. Liss PS, Lovelock JE. Climate change: the effect of DMS emission Environ. Chem. 2007; 4: 377–378. doi:10.1071/EN07072.

55. Friedel M, Chiodo G, Stenke A, Domeisen D, Fueglistaler S, Anet J G, Peter T. Springtime arctic ozone depletion forces northern hemisphere climate anomalies. Nature Geosc. 2022; 15: 1-7.10.1038/s41561-022-00974-7.

56. Chartrand D, de Grandpre J, McConnell J. An introduction to stratospheric chemistry: Survey article. Atmosphere-Ocean. 1999; 37: 309-367.

57. Law KS, Hjorth JL, Pernov J B, Whaley C. Skov H, Collaud CM et al. Arctic tropospheric ozone trends. Geophysical Research Letters, 2023; 50: e2023GL103096.

58. Muhs D, Cattle S, Crouvi O, Rousseau D, Sun J, Zárate M. Loess Records. In: Knippertz P, Stuut JB, editors. Mineral Dust: A key player in the Earth System Springer Verlag, 2014. p 411-441. doi: 10.1007/978-94-017-8978-3.

59. Van der Kaars S, Wang X, Kershaw P, Guichard F, Setiabudi D. A Late Quaternary palaeoecological record from the Banda Sea, Indonesia: Patterns of vegetation, climate and biomass burning in Indonesia and northern Australia. Palaeogeogr. Palaeoclimatol. Palaeoecol. 2000; 155: 135-153. doi: 10.1016/S0031-0182(99)00098-X.

60. Han Y, An Z, Marlon JR, Bradley RS, Zhan C, Arimoto R, et al. Asian inland wildfires driven by glacial-interglacial climate change. Proc. Natl. Acad. Sci. USA. 2020; 117(10): 5184-5189. doi: 10.1073/pnas.1822035117.

61. Rickly PS, Guo H, Campuzano-Jost P, Jimenez JL, Wolfe GM, Bennett R, et al. Emission factors and evolution of SO_2 measured from biomass burning in wildfires and agricultural fires. Atmos. Chem. Phys. 2022; 22: 15603–15620. doi.org/10.5194/acp-22-15603-2022.

62. Duarte E, Salgueiro V, Costa MJ, Lucio PS, Potes M, Bortoli D, Salgado R. 2023. Fire-pollutant-atmosphere components and its impact on mortality in Portugal during wildfire seasons. GeoHealth, 2023; 7: e2023GH000802. doi. org/10.1029/2023GH000802.

63. Senf F, Heinold B, Kubin A, Müller J, Schrödner R, Tegen I. How the extreme 2019–2020 Australian wildfires affected global circulation and adjustments. XXVIII General Assembly of the International Union of Geodesy and Geophysics (IUGG) 2023. doi.org/10.57757/IUGG23-0795

64. Mansergas A, Anglada J. The gas-phase hydrogen-bonded complex between ozone and hydroperoxyl radical. A theoretical study. J. Phys. Chem. 2007; A: 111. 976-81. 10.1021/jp066211t.

65. Witze A. Rare ozone hole opens over Arctic - and it's big. Nature 2020; 580 (7801):18-19.

66. Barnes EA, Screen JA. The impact of arctic warming on the midlatitude jet-stream: Can it? Has it? Will it? WIREs Clim Change 2015; 6: 277–286. doi: 10.1002/wcc.337.

67. Beilman DW, Massa C, Nichols JE, Elison Timm O, Kallstrom R and Dunbar-Co S. Dynamic Holocene Vegetation and North Pacific Hydroclimate Recorded in a Mountain Peatland, Moloka‘i, Hawai‘i. Front. Earth Sci. 2019; 7: 188. doi: 10.3389/feart.2019.00188.

68. Chen SF, Yu B, Chen W, Wu RV. A review of atmosphere-ocean forcings outside the Tropical Pacific on the El Niño-southern oscillation occurrence. Atmosph. 2018; 9: 439. doi.org/10.3390/atmos9110439.

69. Chylek P, Folland C, Klett JD, Wang M, Hengartner N, Lesins G, Dubey MK. Annual mean Arctic Amplification 1970–2020: Observed and simulated by CMIP6 climate models. Geophys. Res. Let. 2022; 49: e2022GL099371. doi. org/10.1029/2022GL099371

70. Ballantyne AP, Andres R, Houghton R, Stocker BD, Wanninkhof R, Anderegg W, Cooper LA, DeGrandpre M, Tans PP, Miller JB, Alden C, White JWC. Audit of the global carbon budget: estimate errors and their impact on uptake uncertainty. Biogeosc. 2015;12: 2565-2584. doi.org/10.5194/bg-12-2565-2015.

2009 71. Hammer Ø, Harper D, Ryan PD. PAST-Paleontological statistics software package for
2010 education and data analysis. Paleontol. Electron. 2001; 4: 1–9.
2011 72. Tans P, Keeling CD. NOAA
2012 https://gml.noaa.gov/webdata/ccgg/trends/co2/co2_mm_mlo.txt (last accessed 15 2 2024).
2013 73. Carbon brief (https://www.carbonbrief.org/global-co2-emissions-have-been-flat-for-a-
2014 decade-new-datareveals/).
2015 74. Gasser T, Crepin L, Quilcaille Y, Houghton RA, Ciais P, Obersteiner M. Historical CO_2
2016 emissions from land use and land cover change and their uncertainty. Biogeosc. 2020; 17:
2017 4075–410. doi: org/10.5194/bg-17-4075-2020.
2018 75. Winkler K, Fuchs R, Rounsevell M, Herold M. Global land use changes are four times
2019 greater than previously estimated. Nature Communications. 2021; 12: 10.1038/s41467-
2020 021-22702-2.
2021 76. Bennington V, Gloege L, McKinley GA. Variability in the Global Ocean Carbon Sink
2022 From 1959 to 2020 by Correcting Models with Observations. Geophys. Res. Lett, 2020;
2023 49, e2022GL098632, doi.org/10.1029/2022GL098632.
2024 77. Griffiths PT, Murray LT, Zeng G, Shin YM, Abraham NL, Archibald AT, et al.
2025 Tropospheric ozone in CMIP6 simulations. Atmos. Chem. Phys. 2021; 21: 4187–4218
2026 .Available: https://doi.org/10.5194/acp-21-4187-2021.
2027 78. Hakkarainen J, Ialongo I, Maksyutov S, Crisp D. Analysis of Four Years of Global X CO_2
2028 Anomalies as seen by orbiting carbon observatory-2. Remote Sens. 2019a; 11: 850.
2029 Available: https://doi.org/10.3390/rs11070850
2030 79. NOAA/GML: Trends in Atmospheric Carbon Dioxide, NOAA Global Monitoring
2031 Laboratory, https://gml.noaa.gov/ccgg/trends/gl_gr.html (last access: 23 August 2024).
2032 80. Peter R, Kuttippurath J, Chakraborty K, et al. A high concentration CO_2 pool over the
2033 Indo-Pacific Warm Pool. Sci. Rep. 2023; 13: 4314. doi.org/10.1038/s41598-023-31468-0

2034 81. Hakkarainen J, Ialongo I, Maksyutov S, Crisp D. Supplementary materials: analysis of four
2035 years of global X CO_2 anomalies as seen by orbiting carbon observatory-2. Remote Sens.
2036 2019b; 11: 850.
2037 82. Thomsen V. 2000. Le Châtelier's Principle in the Sciences. Journal of Chemical Education
2038 - J Chem. Educ. 2000; 77: 173. doi.10.1021/ed077
2039 83. Verma S, Yadava P, Lal D, Mall R, Kumar H, Payra S. Role of Lightning NOx in ozone
2040 formation: A Review. Pure and Applied Geophysics. 2021; 178. 10.1007/s00024-021-
2041 02710-5.
2042 84. Cox R, Ammann M, Crowley j, Herrmann H, Jenkin M, Mcneill VF, Mellouki A, Troe J,
2043 Wallington T. Evaluated kinetic and photochemical data for atmospheric chemistry:
2044 Volume VII – Criegee intermediates 2020; doi.org/10.5194/acp-2020-472.
2045 85. Bisht JSH, Machida T, Chandra N, Tsuboi K, Patra PK, Umezawa T, et al. Seasonal
2046 variations of SF6, CO_2, CH_4, and N_2O in the UT/LS region due to emissions, transport, and
2047 chemistry. J. Geoph. Res. Atmos. 2021; 126, e2020JD033541. doi.
2048 org/10.1029/2020JD03354.
2049 86. Farrar JT, Weller RA. Intraseasonal variability near 10°N in the eastern tropical Pacific
2050 Ocean. *J. Geophys. Res.* 2006; 111: C05015. doi:10.1029/2005JC002989.
2051 87. Jia H, Li S, Wu L, Li S, Sharma VK, Yan B. Cytotoxic Free Radicals on Air-Borne Soot
2052 Particles Generated by Burning Wood or Low-Maturity Coals. *Environ. Sci. Technol.*
2053 2020; 54 (9): 5608–5618. doi.org/10.1021/acs.est.9b06395
2054 88. Yu P, Owen T, Bardeen C, Zhu Y, Rosenlof K, Portmann R, et al. Black carbon lofts
2055 wildfire smoke high into the stratosphere to form a persistent plume. Science. 2019; 365:
2056 587-590. doi: 10.1126/science.aax1748.
2057 89. Haarig M, Ansmann A, Baars H, Jimenez C, Veselovskii I, Engelmann R., Althausen D.
2058 Depolarization and lidar ratios at 355, 532, and 1064 nm and microphysical properties of

2059 aged tropospheric and stratospheric Canadian wildfire smoke, Atmos. Chem. Phys. 2018;
2060 18, 11847–11861, /doi.org/10.5194/acp-18-11847-2018.
2061 90. Ditas J, Ma N, Zhang, Y, Assmann D, Neumaier M, Riede H, et al. Strong impact of
2062 wildfires on the abundance and aging of black carbon in the lowermost stratosphere.
2063 PNAS. 2018; 115. 201806868. doi: 10.1073/pnas.1806868115.
2064 91. Peterson D, Fromm M, McRae R, Campbell J, Hyer E, Taha Get al. Australia's Black
2065 Summer pyrocumulonimbus super outbreak reveals potential for increasingly extreme
2066 stratospheric smoke events. npj Climate and Atmos. Sc.. 2021; 4. doi: 10.1038/s41612-
2067 021-00192-9.
2068 92. Bush RT, McInerney FA. 2013. Leaf wax n-alkane distributions in and across modern
2069 plants: Implications for paleoecology and chemotaxonomy. Org. Geochem. 2013; 79: 65-
2070 73. doi.org/10.1016/j.orggeochem.2014.12.003
2071 93. Balzade Z, Sharif F, Anbaran S. Extending Alkenes, Value Chain to Functionalized
2072 Polyolefins. Alkenes - Recent Advances, New Perspectives and Applications, 2021.
2073 doi.org/10.5772/intechopen.99078.
2074 94. Schumann U, Bugliaro L, Dörnbrack A, Baumann R, Voigt C. Aviation contrail cirrus and
2075 radiative forcing over Europe during 6 months of COVID-19. Geoph. Res. Let., 2021; 48,
2076 e2021GL092771. doi. org/10.1029/2021GL092771
2077 95. Zhu J, Penner JE. Indirect effects of secondary organic aerosol on cirrus clouds. J.
2078 Gesophys. Res. Atmos. 2020; 125: e2019JD032233. doi: 10.1029/2019JD032233
2079 96. Engineering toolbox. https://www.engineeringtoolbox.com/gasses-solubility-water-
2080 d_1148.html (down loaded Mars 2024)
2081 97. Hawkins E. 'Warming stripes' (May 22, 2018). Available: http://www.climate-lab-
2082 book.ac.uk/2018/warming-stripes/.

98. Yulin AV, Lis N, Egorova E. Interannual and seasonal variability of arctic sea ice extent according to satellite observations. Russian Arctic 2019; 7: 26-35. doi: 10.24411/2658-4255-2019-10073.

99. Ouyang Z, Qi D, Chen L, Takahashi T, Zhong W, DeGrandpre M, et al. Sea-ice loss amplifies summertime decadal CO_2 increase in the western Arctic Ocean. Nat. Clim. Chang. 2020; **10**: 678–684. doi.org/10.1038/s41558-020-0784-2.

100. Alobaydy, O. Impacts of Cement Production on the Environment with Practical Solutions: A critical review. J. Res. Technol. Eng. 2024; 5 (2), 2024, 12-275.

101. Gomez-Leal I, Pallé E, Selsis F. Photometric variability of the disk-integrated thermal emission of the earth. Astroph. J. 2012; 752: 28. Doi: 10.1088/0004-637X/752/1/28.

102. Tatarchenko VA, 2010. Infrared characteristic radiation of water condensation and freezing in connection with atmospheric phenomena. Earth-Sci. Rev. 2010; 10: 24-28.

103. Ming A, Winton VHL, Keeble J, Abraham NL, Dalvi MC, Griffiths P, et al. Stratospheric ozone changes from explosive tropical volcanoes: Modelling and ice core constraints. J. Geophys. Res. 2020*;* 125: e2019JD032290. doi.org/10.1029/2019JD032290.

104. Ni J, Liu S. & Lang X, He Z, Yang G. Sulphur hexafluoride in the marine atmosphere and surface seawater of the Western Pacific and Eastern Indian Ocean. Environmental Pollution. 335. 2023; 122266. doi. 10.1016/j.envpol.2023.122266.

105. Simmonds PG, Rigby M. Manning AJ, Park S, Stanley KM, McCulloch A, et al. The increasing atmospheric burden of the greenhouse gas sulphur hexafluoride (SF_6). Atmos. Chem. Phys. 2020; 20: 7271–7290. doi.org/10.5194/acp-20-7271-2020.

106. Caesar, L., Rahmstorf, S., Robinson, A., Feulner, G., Saba, V., 2018. Observed fingerprint of a weakening Atlantic Ocean overturning circulation. Nature. 556. 10.1038/s41586-018-0006-5.

2107 107. Liu W, Duarte Cavalcante Pinto D, Fedorov A, Zhu J. The impacts of a weakened Atlantic
2108 Meridional Overturning Circulation on ENSO in a warmer climate. Geoph. Res. Let.,
2109 2023; 50: e2023GL103025. doi: org/10.1029/2023GL103025.
2110 108. Maslin MA, Brierley, CM. The role of orbital forcing in the Early Middle Pleistocene
2111 Transition. Quaternary International. 2015; 389. doi: 10.1016/j.quaint.2015.01.047.
2112 109. Petit JR. Jouzel J, Raynaud D, Barkov NI, Barnola JM, Basile I, et al. Climate and
2113 atmospheric history of the past 420,000 years from the Vostok ice core, Antarctica. Nature
2114 1999; 399 (6735): 429-436.
2115 110. Liang Y, Stamatis C, Fortner E, Wernis R, Rooy P, Majluf F, et al. Emissions of organic
2116 compounds from western US wildfires and their near-fire transformations. Atmosph.
2117 Chem. and Phys; 2022: 22. 9877-9893. 10.5194/acp-22-9877-2022.
2118 111. Patočka V, Šrámek O, Tosi N. Minimum heat flow from the core and thermal evolution of
2119 the Earth. Phys. Earth Planet. Inter. 2020; 305: 106457. doi: 10.1016/j.pepi.2020.106457
2120 112. Santer B, Sausen R, Wigley T, Boyle JS, Achutarao K, Doutriaux C, Hansen JE, Meehl G,
2121 Roeckner, E, Ruedy R, Schmidt G, Taylor KE. Behaviour of Tropopause Height and
2122 Atmospheric Temperature in Models, Reanalyses and Observations: Decadal Changes. J.
2123 Geophys. Res. 2003;108(D1): 4002. doi:10.1029/2002JD002258
2124 113. Boylan P, Helmig D, Park J. Atmospheric measurement techniques open access
2125 characterization and mitigation of water vapour effects in the measurement of ozone by
2126 chemiluminescence with nitric oxide. Atmos. Meas. Tech. 2014; 7: 1231–1244.
2127 doi:10.5194/amt-7-1231-2014.
2128 114. Zhang J, Wei Y, Fang Z. Ozone Pollution: A major health hazard worldwide. Front.
2129 Immunol. 2019. doi: 10:2518.

115. Xiao X, Haberle SG, Shen J, Xue B, Burrows M, Wang S. Postglacial fire history and interactions with vegetation and climate in southwestern Yunnan Province of China. Clim. Past. 2017; 13: 613–627. doi.org/10.5194/cp-13-613-2017.

116. Ohneiser K, Ansmann A, Witthuhn J, Hartwig D, Chudnovsky A, Walter G, Senf F. Self-lofting of wildfire smoke in the troposphere and stratosphere: simulations and space lidar observations. Atmos. Chem. Phys. 2002; 23: 2901-2925. doi. 10.5194/acp-23-2901-2023.

117. Sun J, Tian B, Chen Z. Effect of ozone addition and ozonolysis reaction on the detonation properties of C2H4/O2/Ar mixtures. Proc. Combustion Inst. 2023; 39: 27977-2806. doi.org/10.1016/j.proci.2022.09.029 1540-7489

118. Bednarz EW, Hosseini, R, Chipperfield M. Atmospheric impact of chlorinated very short-lived substances over the recent past -Part 2: Impacts of ozone. Atmos. Chem. Phys. 2023; 23: 13701-13711. Doi.org/10.5194/apc-23-1301-2023.

119. Williams R, Hegglin M, Kerridge B, Jöckel P, Latter B, Plummer D. Characterising the seasonal and geographical variability in tropospheric ozone, stratospheric influence and recent changes. Atmosph.Chem. and Phys. 2019; 19: 3589-3620. doi: 10.5194/acp-19-3589-2019.

120. Ellis R, Palmer M. Modulation of ice ages via precession and dust-albedo feedbacks. Geosc. Front. 2016; 7: 891-909.

121. Berger A, Yin Q. Astronomical theory and orbital forcing. The Sage handbook of environmental change. In: Matthews JA, editor. SAGE Publications LTD, 2012. pp. 403-423.

122. Viaggi P. Quantitative impact of astronomical and sun-related cycles on the Pleistocene climate system from Antarctica records. Quat..Sci. Ad. 2021; 4: 100037. doi.org/10.1016/j.qsa.2021.100037.

123. Brown S, Crosweller S, Sparks S, Cottrell E, Deligne N, Ortiz N, Hobbs L, Kiyosugi K, Loughlin S, Siebert L, Takarada S. Characterisation of the Quaternary eruption record: analysis of the large magnitude explosive volcanic eruptions (LaMEVE) database. J. Appl. Volcanol. 2014; 3: 5 http://www.appliedvolc.com/content/3/1/5

124. Gorkavyi N, Rault D, Newman P, Da Silva A, Dudorov A. New stratospheric dust belt due to the Chelyabinsk bolide. Geophys. Res. Lett. 2013; 40. Doi: 10.1002/grl.50788.

125. Brown P, Spalding R, Revelle D, *et al.* The flux of small near-Earth objects colliding with the Earth. *Nature* 2002; 420: 294-296. https://doi.org/10.1038/nature01238

126. Zhu D, Ciais P, Chang J, Krinner G, Peng S, Viovy N, Penuelas J, Zimov S. The large mean body size of mammalian herbivores explains the productivity paradox during the Last Glacial Maximum. Nat. Ecol. Evol. 2018; 2(4): 640–649. doi: 10.1038/s41559-018-0481-y.

127. Remsberg EE. Methane as a diagnostic tracer of changes in the Brewer–Dobson circulation of the stratosphere. Atmos. Chem. Phys. 2015; 15: 3739–3754.

128. Andersen BG, Borns HW. The Ice Age world. An introduction to Quaternary history and research with emphasis on North America and northern Europe during the last 2.5 million years: Oslo-Copenhagen-Stockholm, Scandinavian University Press; 1994.

129. Stephens D, Meuleners M, Van Loon H, Lamond M, Telcik N. Differences in atmospheric circulation between the development of weak and strong warm events in the southern oscillation. J.of Climate. 2007; 20: 2191-2209. 10.1175/JCLI4131.1.

130. Paradiz B, Dilara P, Umlauf G, Bajsic I, Butala V. Dioxin emissions from coal combustion in domestic stove: formation in the chimney and chlorine content influence. Thermal science. 2015; 296 (19): 295-304.

131. Hossain S, Bari, S. Effect of Different Working Fluids on Shell and Tube Heat Exchanger to Recover Heat from Exhaust of An Automotive Diesel Engine. World Renewable Energy Congress 2011; 764-771. 10.3384/ecp11057764.

132. Papapetrou M, Kosmadakis G, Cipollina A, La Commare U, Micale G. Industrial waste heat: estimation of the technically available resource in the EU per industrial sector, temperature level and country. Appl. Therm. Eng. 2018; 138: 207–216.

133. Cartapanis O, Bianchi D, Jaccard SL, Galbraith ED. Global pulses of organic carbon burial in deep-sea sediments during glacial maxima. Nat. Comm. 2016; 7: 1-7.

134. Davies JH, Davies DR. Earth's surface heat flux. Solid Earth. 2010; 1: 5–24.

135. Minton DA, Malhotra R. Assessing the massive young sun hypothesis to solve the warm young Earth puzzle Ap J. 2007; 660: 1700. doi:10.1086/514331.

136. Spalding C, Fischer WW, Laughlin G. An orbital window into the ancient sun's mass. Astrophys. J. L. 2018; 869 (1), L19. doi:10.3847/2041-8213/ aaf219

137. Wei W, Chen S, Wang Y, Cheng L, Wang X, Cheng, S. The impacts of VOCs on $PM_{2.5}$ increasing via their chemical losses estimates: A case study in a typical industrial city of China. Atmos. Env. 2022; 273: 118978. doi.org/10.1016/j.atmos env.2022.118978.

138. Shaddick G, Thomas ML, Mudu P, Ruggeri G, Gumy S. Half the world's population are exposed to increasing air pollution. NPJ Clim. Atmos. Sci. 2020; 3 (1) :1–5. doi:10.1038/s41612-020-0124-2.

139. Bates NR, Johnson RJ. Forty years of ocean acidification observations (1983–2023) in the Sargasso Sea at the Bermuda Atlantic Time-series Study site. Front. Mar. Sci. 2023; 10:1289931. doi: 10.3389/fmars.2023.1289931.

140. Dore J, Lukas R, Sadler D, Church M, Karl D (2009). Physical and biogeochemical modulation of ocean acidification in the Central North Pacific. PNAS. 2009; 106: 12235-40. 10.1073/pnas.0906044106.

141. Kuok Ho, DT (2019). Are We Already in a Climate Crisis? Glob J Civil Environ Eng. 1. 2019; 1: 25-32.

142. Xie H, Wang F, Wang Y, Liu T, Wu Y, Liang B. CO_2 mineralization of natural wollastonite into porous silica and CaCO3 powders promoted via membrane electrolysis. Environmental Earth Sciences. 2018; 77. doi.10.1007/s12665-018-7330-9.

143. Calil P, Richards K. Transient upwelling hot spots in the oligotrophic North Pacific. J. Geophys. Res. (Oceans). 2010; 115. doi.10.1029/2009JC005360.

144. Polonskii A, Serebrennikov A. Intensification of Atlantic and Pacific Large-Scale Upwelling under Recent Climate Conditions. Doklady Earth Sciences. 2020; 492: 480-484. doi.10.1134/S1028334X20060161.

145. Ohba T, Nakagawa M. Minerals in Volcanic Ash. Non-Magmatic Minerals. 2002; 2: 6.

146. Kanji Z, Ladino L, Wex H, Boose Y, Burkert-Kohn M, Cziczo D, Krämer M, 2017. Overview of Ice Nucleating Particles. Meteorol. Monogr. 2017; 58: 10.1175/AMSMONOGRAPHS-D-16-0006.1.

147. Pering TP, McGonigle AJS, Tamburello G, Aiuppa A , Bitetto M, Rubino C, Wilkes TC. A Novel and Inexpensive Method for Measuring Volcanic Plume Water Fluxes at High Temporal Resolution. Remote Sens. 2017; 9: 146.

148. De Giacomo A, Dell'Aglio M, Salajková,'Z, Vaníčková E, Mele D, Dellino P. Real-time analysis of the fine particles in volcanic plumes: A pilot study of Laser Induced Breakdown Spectroscopy with Calibration-Free approach (CF-LIBS), J. Volcanol. Geoth. Res. 2022; 432, 107675, doi.org/10.1016/j.jvolgeores.2022.107675

149. Durant AJ, Shaw RA, WI R, Mi Y, Ernst GGJ. Ice nucleation and overseeding of ice in volcanic clouds. J. Geophys. Res. 2008; 113: D09206. doi:10.1029/2007JD009064.

2225 150. Vestreng V, Gunnar M, Fagerli H, Reis S, Tarrason L.. Twenty-five years of continuous
2226 sulphur dioxide reduction in Europe. Atmospheric Chem. and Phys. 2007; 7. 3663-3681.
2227 doi: 10.5194/acpd-7-5099-2007.
2228 151. Western LM, Redington A, Manning A, Henne S, Graziosi F, Weston Let al. CFC-11
2229 emissions are declining as expected in Western Europe. Atmos. Chem. Phys. 2023; 22(14):
2230 9601–9616. doi.org/10.5194/acp-22-9601-2022.
2231 152. Surl L, Roberts T, Bekki S. Observation and modelling of ozone-destructive halogen
2232 chemistry in a passively degassing volcanic plume. Atmos. Chem. Phys. 2021; 21: 12413-
2233 12441. doi.org/10.5194/acp-21-12413-2021
2234 153. Lu QB. Critical review on radiative forcing and climate models for global climate change
2235 since 1970. Atmosphere 2023; 14: 1232. doi.org/10.3390/ atmos1408123.
2236 154. Holzworth R, Brundell J, McCarthy M, Jacobson A, Rodger C, Anderson T. Lightning in
2237 the Arctic. Geophysical Research Letters. 2021; 48. doi: 10.1029/2020GL091366.
2238 155. Sun M, Liu D, Qie X, Mansell E, Yair Y, & Fierro A, et al . Aerosol effects on
2239 electrification and lightning discharges in a multicell thunderstorm simulated by the WRF-
2240 ELEC model. Atmos. Chem. Phys. 2021; 2: 14141-14158. 10.5194/acp-21-14141-2021.
2241 156. Zhang Z, Wang L, Xue N, Du Z. Spatiotemporal analysis of active fires in the Arctic
2242 region during 2001–2019 and a fire risk assessment model. Fire. 2021; 4(3): 57.
2243 https://doi.org/10.3390/fire4030057.
2244 157. Herrmann M, Schöne M, Borger C, Warnach S, Wagner T, Platt U, Gutheil E. Ozone
2245 depletion events in the arctic spring of 2019: a new modelling approach to bromine
2246 emissions, Atmos. Chem. Phys. 2022; 22: 13495–13526. doi.org/10.5194/acp-22-13495-
2247 2022.
2248 158. Hardacre C. Palmer P, Engström K, Rounsevell M, Murray-Rust, D. Probabilistic
2249 estimation of future emissions of isoprene and surface oxidant chemistry associated with

land-use change in response to growing food needs. Atmospheric Chemistry and Physics. 2013: 13. doi 10.5194/acp-13-5451-2013.

159. Basu S, Mackey KRM. Phytoplankton as key Mediators of the Biological Carbon Pump: Their response to a Changing Climate. Sustainability. 2018; 10: 869. doi: 10.3390/su10030869.

160. Tricka CG, Brian DB, Cochlan WP, Wells ML, Trainer VL, Pickell LD. Iron enrichment stimulates toxic diatom production in high-nitrate, low-chlorophyll areas PNAS 2010; 107: 13: 5887-5892. doi:10.1073/pnas.0910579107

161. Van Waveren IM, Visscher H, 1994. Analysis of the composition and selective preservation of organic matter in surficial deep–sea sediments from a high–productivity area (Banda Sea, Indonesia). Palaeogeogr. Palaeoclimatol. Palaeoecol. 1994; 112: 85-111.

162. Honjo S. Coccoliths: Production, transportation and sedimentation. Mar. Micropal. 1976; 1: 65-79. doi:10.1016/0377-8398(76)90005-0

163. Wells M, Trainer V, Smayda T, Karlson B, Trick C, Kudela R, Ishikawa A, Bernard S, Wulff A, Anderson D, Cochlan W. Harmful algal blooms and climate change: Learning from the past and present to forecast the future. Harmful Algae 2015; 49: 68-93. doi: 10.1016/j.hal.2015.07.009

164. Radach G, Pätsch J. Variability of continental riverine freshwater and nutrient inputs into the North Sea for the years 1977–2000 and its consequences for the assessment of eutrophication. Estuaries and Coasts. 2007; 30 (1) : 66–81.

165. Copernicus ECMWF project (https://lnkd.in/eFghYMJ9),

166. Souza CM Jr. Z. Shimbo J, Rosa MR, Parente LL, A. Alencar A, Rudorff BFT, Hasenack H, Matsumoto M, G. Ferreira L, Souza-Filho PWM, et al. Reconstructing three decades of land use and land cover changes in Brazilian biomes with landsat archive and earth engine. Remote Sensing. 2020; 12(17): 2735. //doi.org/10.3390/rs12172735.

167. Chiaka J, Zhen L. Land Use, environmental, and food consumption patterns in Sub-Saharan Africa, 2000–2015: A Review. Sustainability. 2021: 13. 8200. doi:10.3390/su13158200.

168. Slot M, Winter K. The effects of rising temperature on the ecophysiology of tropical forest trees. In: Guillermo Goldstein G, Santiago LS, editors. Tropical Tree Physiology; Adaptations and Responses in a Changing Environment: New York, Springer International Publishing. 2016. p. 385-412. doi: 10.1007/978-3-319-27422-5_18

169. Makita N, Kosugi Y, Sakabe A, Kanazawa A, Ohkubo S, Tani M. Seasonal and diurnal patterns of soil respiration in an evergreen coniferous forest: Evidence from six years of observation with automatic chambers. PLOS ONE 13(2): e0192622. doi.org/10.1371/journal. pone.0192622

170. Langematz U. Stratospheric ozone: down and up through the Anthropocene. ChemTexts. 219; 5. 10.1007/s40828-019-0082-7.

171. Lu O. Observation of large and all-season ozone losses over the tropics. AIP Advances. 2022; 12. 075006. doi. 10.1063/5.0094629.

172. Condamine FL , Silvestro D, Koppelhus EB, Antonelli A. The rise of angiosperms pushed conifers to decline during global cooling PNAS. 2020; 117 (46) 28867-28875. doi 10.1073/pnas.2005571117

173. Sternai P, Caricchi L, Pasquero C, Garzanti E, van Hinsbergen D, Castelltort S. Magmatic Forcing of Cenozoic Climate?. J. Geoph. Res.: Solid Earth. 2020; 125. doi. 10.1029/2018JB016460.

Figure captions

Fig 1. Examples of erroneous historical validation of the CO_2 driven climate model for system earth. Visualization of the table of Foote [2] where her error margin is highlighted as two

colours because she measured temperature after 2 or 3 minutes. Some experiments were shorter than other ones and this analysis gives the rates of change for identical duration and identical measuring intervals. It is not possible to evaluate how damp her damp air was. Moreover, it seems difficult to obtain 100% pure carbonic acid gas as it is very unstable.

Fig 2. Details of the Keeling illustrating two ways to calculate the yearly atmospheric growth (G_{ATM}). (a) Method used herein : $G_{ATM} = ML_{YI} - ML_{YD}$. (b) method used by the WCRP $G_{ATM} = \Delta C / \Delta t$.

Fig 3. Visualization of the difference in timing and yearly amplitude between the atmospheric CO_2 concentrations in different geographical localities for the randomly chosen 1992-1996 period. (a) Mauna Loa (red line), (b) the South Pole (black line). The data are from NOAA [79] (Appendix 5).

Fig 4. Polynomial function drawn through the monthly atmospheric CO_2 concentrations as recorded by NOAA on the South Pole between 1980 and 2022 [79]. This function serves to establish the average seasonal amplitude in atmospheric CO_2 emission of the south pole by subtracting the monthly average from the mean determined by the function y = 8.784*x^2E-07 + 102*x + 331.9.

Fig 5. Box plots allowing for the comparison of six potential methods to calculate the atmospheric increase in CO_2 concentration. (a) Here 1y: method used herein ($G_{ATM} = ML_{YI} - ML_{YD}$) for one year; (b) Here 3 y: method used here in for the average of 3 years; (c) May 1 y: method used by the WCRP ($G_{ATM} = \Delta C / \Delta t$), from May to May of the former year; (d) Sept. 1y: method used by the WCRP ($G_{ATM} = \Delta C / \Delta t$), from September to September from the former year; (e) May 3y: method used by the WCRP ($G_{ATM} = \Delta C / \Delta t$), from May to May of three years before; (d) Sept. 3y: method used by the WCRP ($G_{ATM} = \Delta C / \Delta t$), from September to September from the three years before. Black dashed rectangle: largest spread; blue dashed rectangle: largest interquartile; red dashed rectangle: lowest and highest medians.

Fig 6. Superimposed box and jitter plots for equation (2). G_{ATM} calculated as IE-$S_{TOT,}$ as $G_{ATM\text{-}Here}$ (= ML_{YI}-ML_{YD}) for one and three year, measured as $G_{ATM\text{-}WCRP} = \Delta C/\Delta t$, for the month of May and September for one and three years, respectively; the difference X between the six calculations methods for G_{ATM} based on the measurements at Mauna Loa and G_{ATM} calculated as IE-$S_{TOT;}$ red dashes line: Median of G_{ATM} as calculated here for one year.

Fig 7. **Box plots illustrating that X, the imbalance in the GCE, is positive and reflects the difference between seasonal ocean CO_2 emission and seasonal CO_2 uptake.** ML_{YI}: yearly atmospheric increase in CO_2 (Fig 2), ML_{YD} yearly atmospheric decrease in CO_2 (Fig 2), IE: Total of the industrial emission (E_{FOS} + E_{LUC}), S_{TOT}: total of the CO_2 sinks (S_{OCEAN} + S_{LAND}), O_{SE}: seasonal ocean emission, O_{SU} :seasonal ocean CO_2 uptake, G_{ATM}: $G_{ATM\text{-}Here}$ 1y.

Fig 8. Counterintuitive relation between atmospheric CO_2 growth (G_{ATM}) and land CO_2 sinks and sources. A. Correlation between atmospheric growth (G_{ATM}) and land use change emission in CO_2 (E_{LUC}), B. Correlation between atmospheric growth (G_{ATM}) and CO_2 land sinks (S_{LAND}), C. Correlation between atmospheric growth (G_{ATM}) and the surface area of land use change (S_{LUC}).

Fig 9. Ocean CO_2 uptake and emission. A. Duration of ocean CO_2 uptake (red) and CO_2 emission (black) compared, B. Yearly ocean CO_2 uptake (black) and yearly ocean CO_2 emission (red) compared, C. Monthly ocean CO_2 uptake (black) and monthly ocean CO_2 emission (red) compared.

Fig 10. Comparison between the trend in monthly increase in CO_2 emission and increase in CO_2 uptake over time. Here we see that monthly emission increases faster than monthly uptake.

Fig 11. Analysis of how the emission season became longer than the uptake season, for 60 years, each time considering 2 decades. A. transition from emission to uptake moves to a later period, B. transition from uptake to emission moves to an earlier period.

Fig 12. Details of the 6 functions that determine the uptake and emission of CO_2 by the northern Pacific Ocean and their sum ($\sum_{1\text{-}6}$). (1) Ocean CO_2 uptake following from an increase in ocean water solubility due to ocean cooling related to seasonal ice melt (U_{SIM}), (2) increase in ocean CO_2 uptake following from an increase in ocean water solubility due to ocean cooling related to seasonal melt driven by the short lived GHG (O_3) (U_{SLGHG}), (3) ocean CO_2 uptake through biological draw down (U_{BDD}), (4) ocean CO_2 emission following from a decrease in ocean water solubility due to seasonal ocean warming (E_{SOW}), (5) increase in ocean CO_2 emission following from a decrease in ocean water solubility due to ocean warming related to seasonal tropospheric heat anomaly stemming from the short lived GHG (O_3) accumulation in the Arctic (E_{SLGHG}), (6) Purple: CO_2 emission from cumulative ocean heat uptake throughout the year because of ozone depletion in the stratosphere, (E_{SOD}), (7) Apple green: monthly sum of all these functions (Sum 1-6).

Fig 13. Comparing the monthly reconstruction of the Northern Pacific Carbon Equation (NPCE) based on the assumption it is pollutant driven, and the monthly atmospheric CO2 concentrations recorded by NOAA at Mauna Loa.

A. Function (black) expressing the reconstructed pollutant driven North Pacific CO_2 emission behaviour ((((E_{SOD} + E_{SLGHG} + E_{SOW}) - (U_{SLGHG} + U_{BDD} + U_{SM})) + 320 ppm)) compared to (red) the monthly recording of the CO_2 concentration at Moana Loa as placed online by the NOAA [72]. B. The regression analysis comparing both functions. Details of the functions are given in Appendix 10. The various components of the NPCE are explained further below.

Fig 14. Ocean CO2 Sinks (S_{OCEAN}) and yearly northern Pacific G_{ATM} compared.

Regression analysis comparing the ocean sinks (S_{OCEAN}) [76] and yearly atmospheric growth G_{ATM} as measured at Mauna Loa.

Fig 15. Sawtooth pattern projected on the four last climate cycles. Blue lines: temperature anomaly (Δ t in C^{o}), green lines: CO_2 atmospheric concentration (in ppm), red lines: dust concentration(in ppm).

Fig 16. Comparison between the four last climate cycles and the Milankovitch cycles. Green: CO_2, blue: temperature, red: dust, red shading: high obliquity, blue shading: low obliquity.

Fig 17. Trend analyses between land sinks (S_{LAND}) and land use change CO_2 emission (E_{LUC}) or surface of land use change (S_{LUC}).

APPENDICES

Appendix 1 Intro The table of Foote serving for Fig 1

Appendix 2 Intro Table of Arrhenius analysed

Appendix 3 M&M Explaining how G ATM was calculated in here (Serving for Fig 2)

Appendix 4 M&M G ATM from ppm to Gt C and the duration of emission and uptake in month

Appendix 5 M&M Monthly average atmospheric CO_2 concentration as measured by on the South Pole compared to ML and the regression analysis smoothing the curve.

Appendix 6 M&M Calculation of the average seasonnal amplitude in the southern hemisphere

Appendix 7 M&M Sink and source of CO2 as found in literature plus pollutants and surface of land use change

Appendix 8 M&M Regression analysis with the informartion for the Tables 1 and 4 on top.

Appendix 9 M&M Six calculation methods for atmospheric growth compared.

Appendix 10 M&M Reconstruction of the Keeling explained.

Appendix 11 M&M Average duration of a day length Northern Hemisphere.

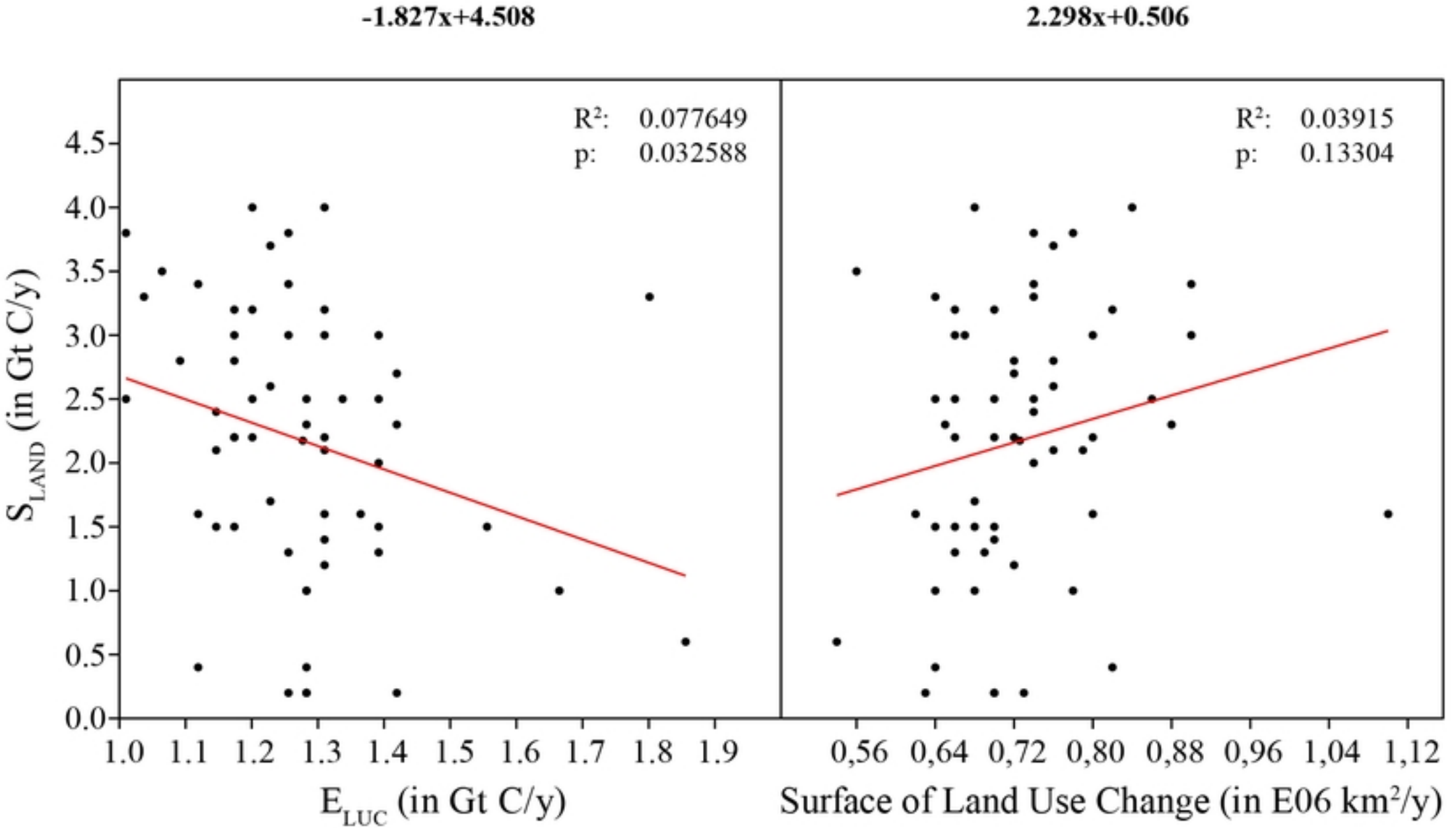
-1.827x+4.508
2.298x+0.506
R²: 0.077649
p: 0.032588
R²: 0.03915
p: 0.13304
S_LAND (in Gt C/y)
E_LUC (in Gt C/y)
Surface of Land Use Change (in E06 km²/y)
0.0
0.5
1.0
1.5
2.0
2.5
3.0
3.5
4.0
4.5
1.0 1.1 1.2 1.3 1.4 1.5 1.6 1.7 1.8 1.9
0,56 0,64 0,72 0,80 0,88 0,96 1,04 1,12

Fig 17

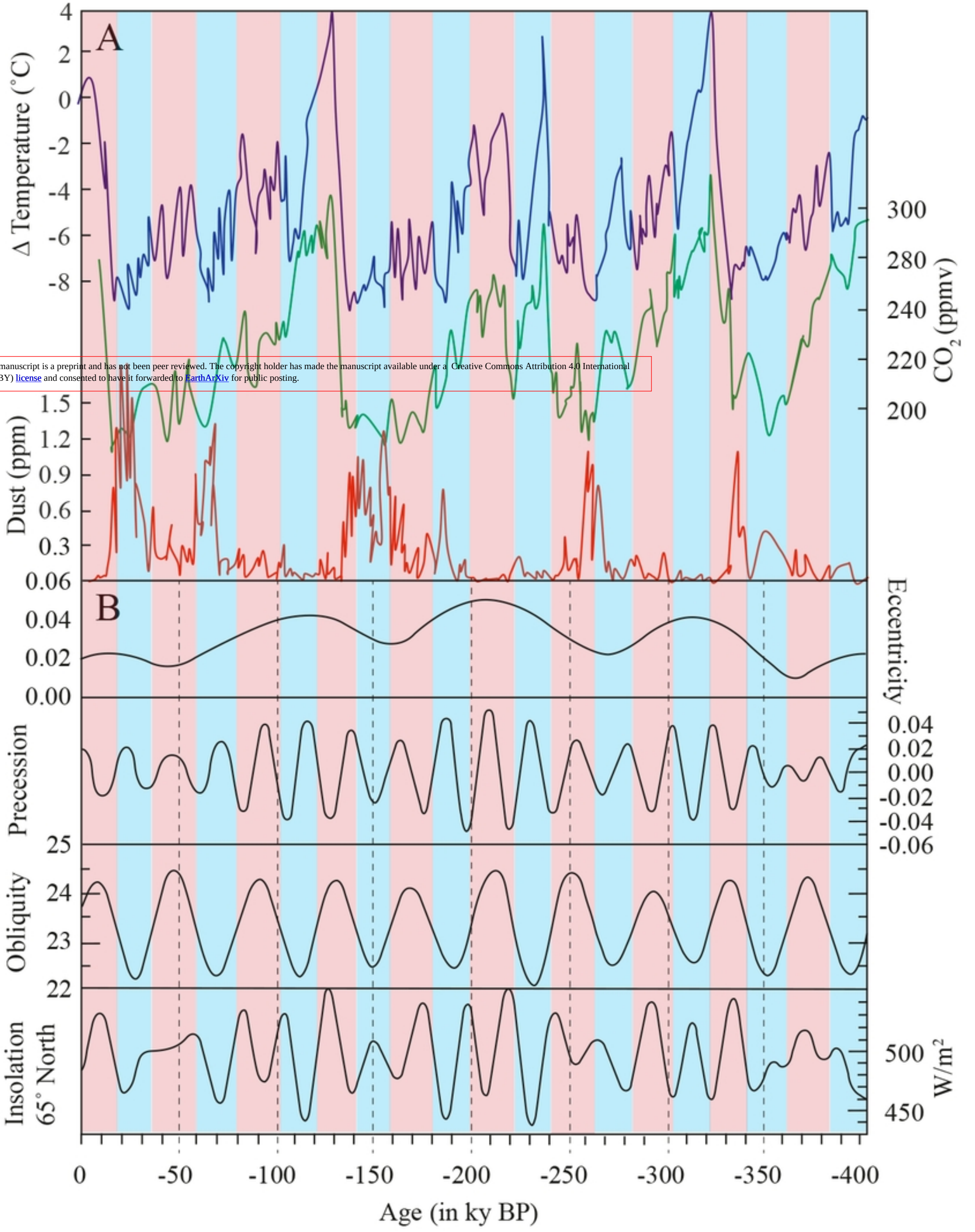

Fig 16

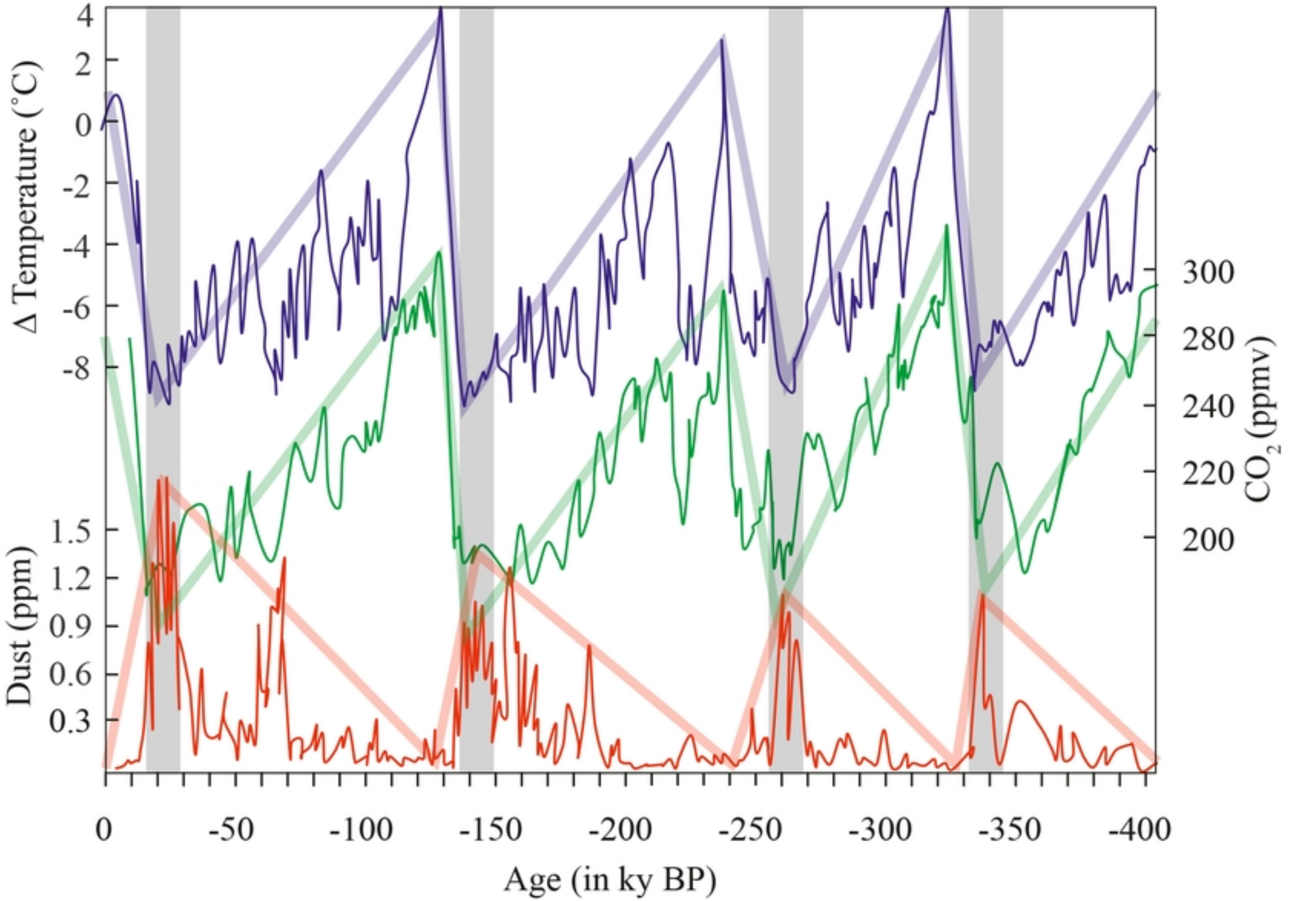
Δ Temperature (°C)
4
2
0
-2
-4
-6
-8
Dust (ppm)
1.5
1.2
0.9
0.6
0.3
CO_2 (ppmv)
300
280
240
220
200
0
-50
-100
-150
-200
-250
-300
-350
-400
Age (in ky BP)

Fig 15

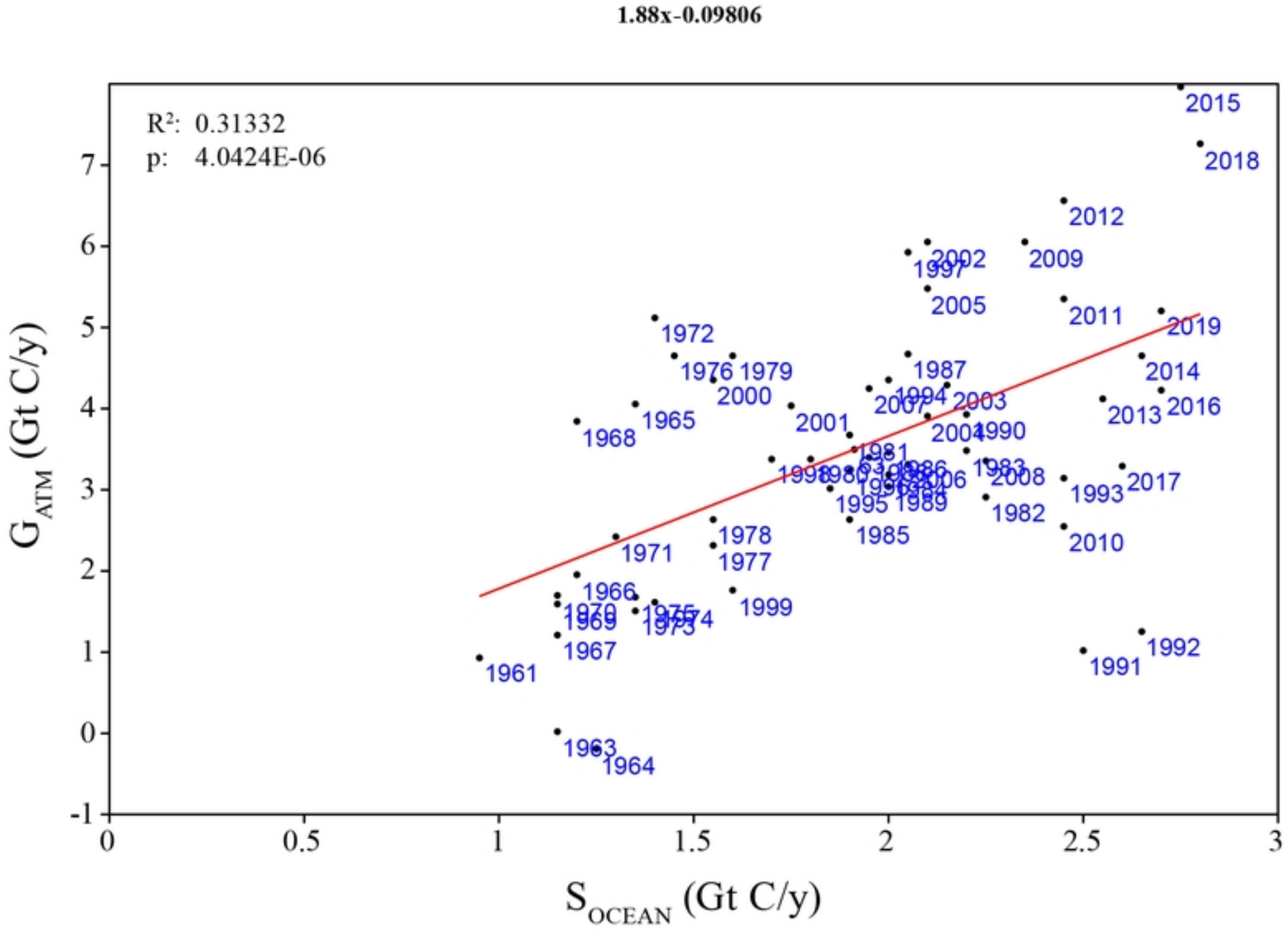
1.88x-0.09806
R²: 0.31332
p: 4.0424E-06
G_ATM (Gt C/y)
S_OCEAN (Gt C/y)
2015
2018
2012
2002
2009
1997
2005
2011
2019
1972
1976
1979
1987
2014
2000
1994
2007
2003
2013
2016
1965
2001
1968
2004
1990
1981
1983
2008
2017
1993
1995
1989
1982
1978
1985
2010
1971
1977
1966
1999
1969
1973
1967
1992
1961
1991
1963
1964

Fig 14

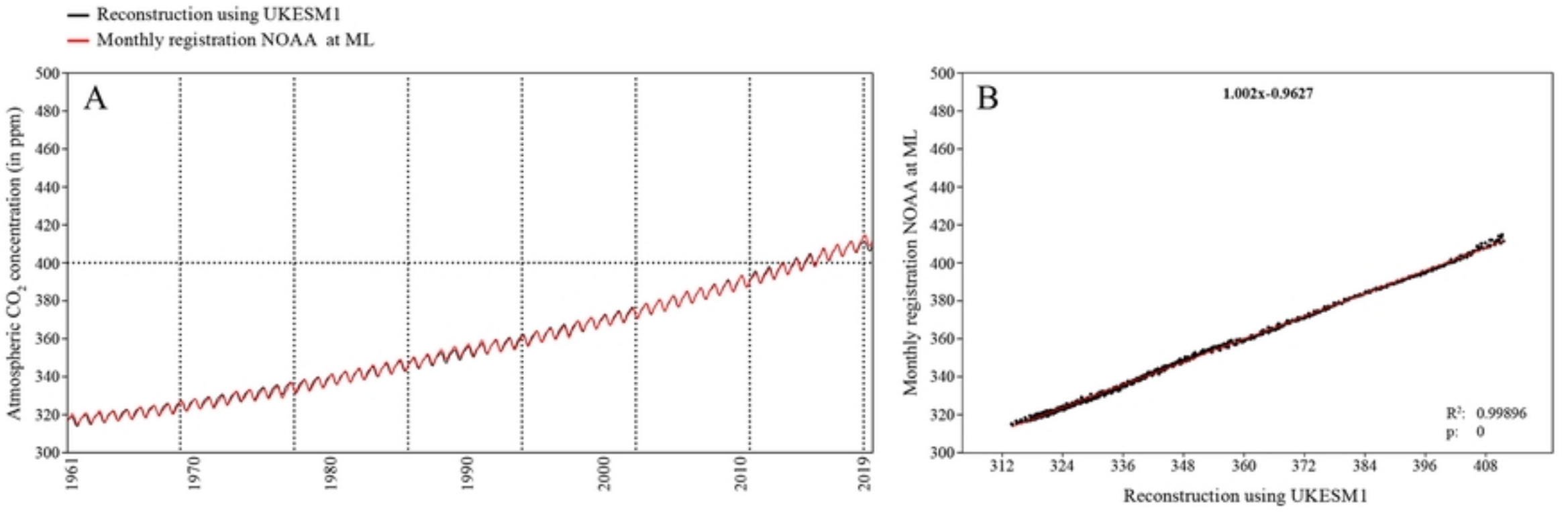
Reconstruction using UKESM1
Monthly registration NOAA at ML
A
Atmospheric CO_2 concentration (in ppm)
500
480
460
440
420
400
380
360
340
320
300
1961
1970
1980
1990
2000
2010
2019
B
1.002x-0.9627
Monthly registration NOAA at ML
R^2: 0.99896
p: 0
312
324
336
348
360
372
384
396
408
Reconstruction using UKESM1

Fig13

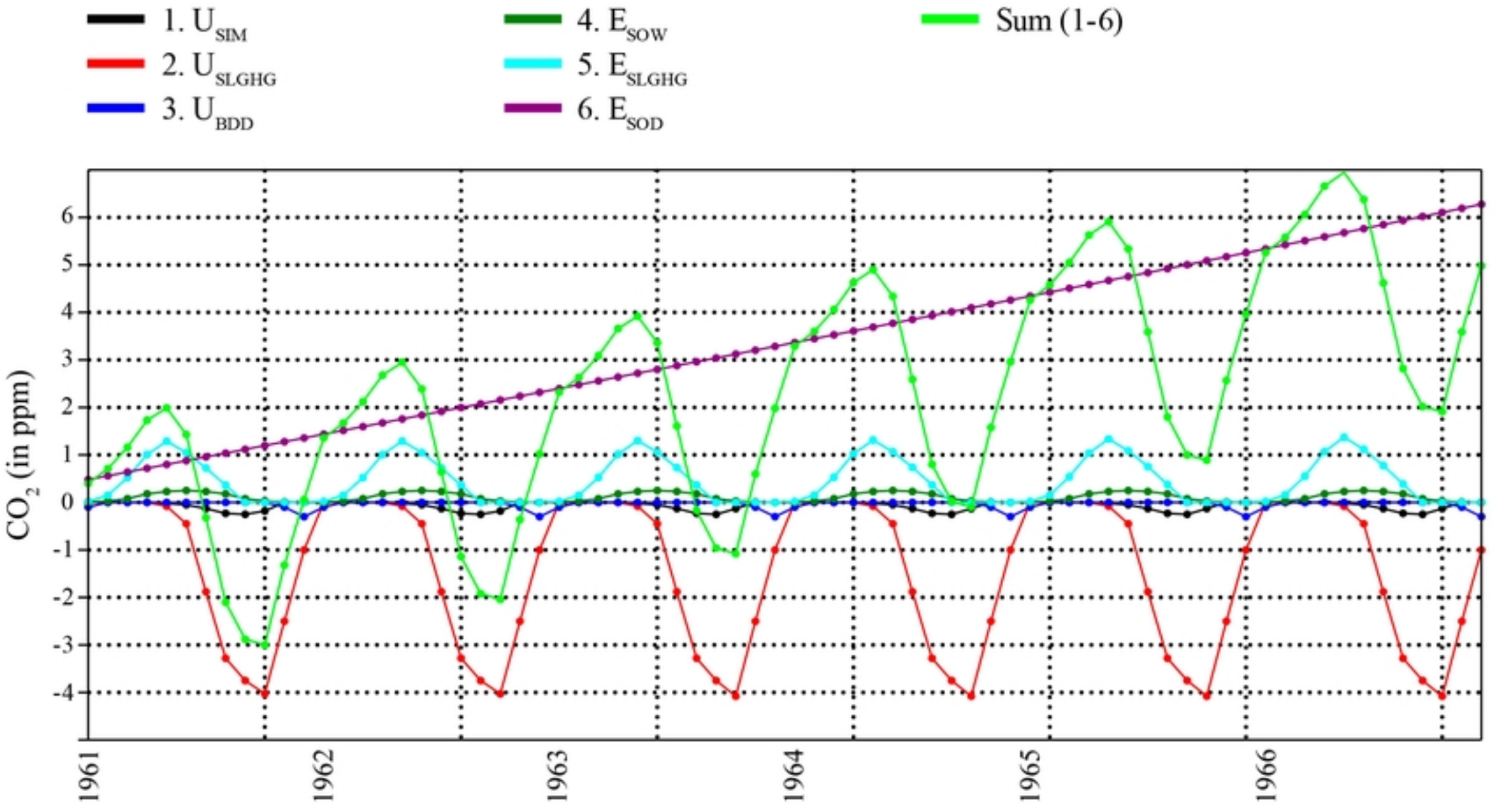
1. U_{SIM}
2. U_{SLGHG}
3. U_{BDD}
4. E_{SOW}
5. E_{SLGHG}
6. E_{SOD}
Sum (1-6)
CO_2 (in ppm)
6
5
4
3
2
1
0
-1
-2
-3
-4
1961
1962
1963
1964
1965
1966

Fig 12

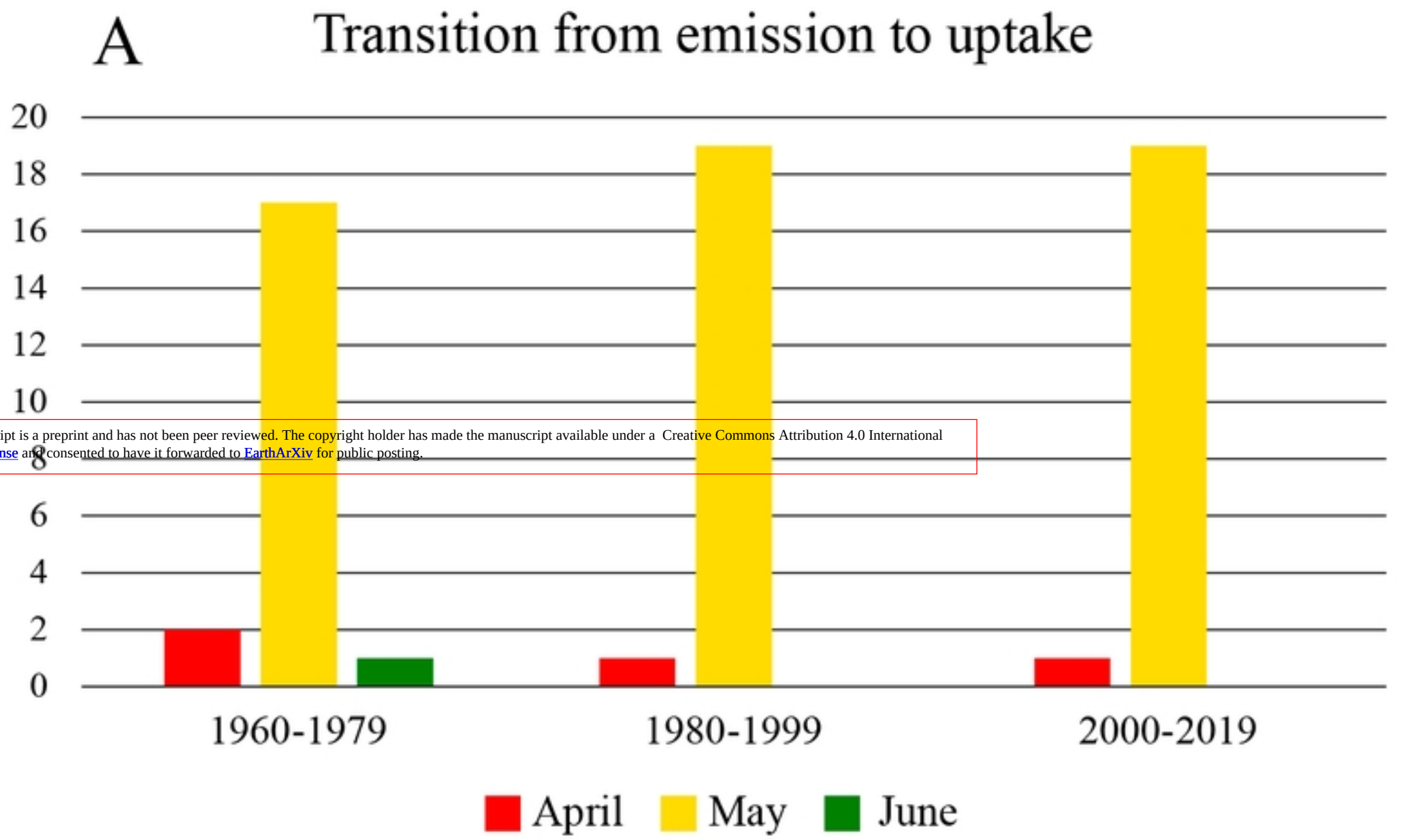

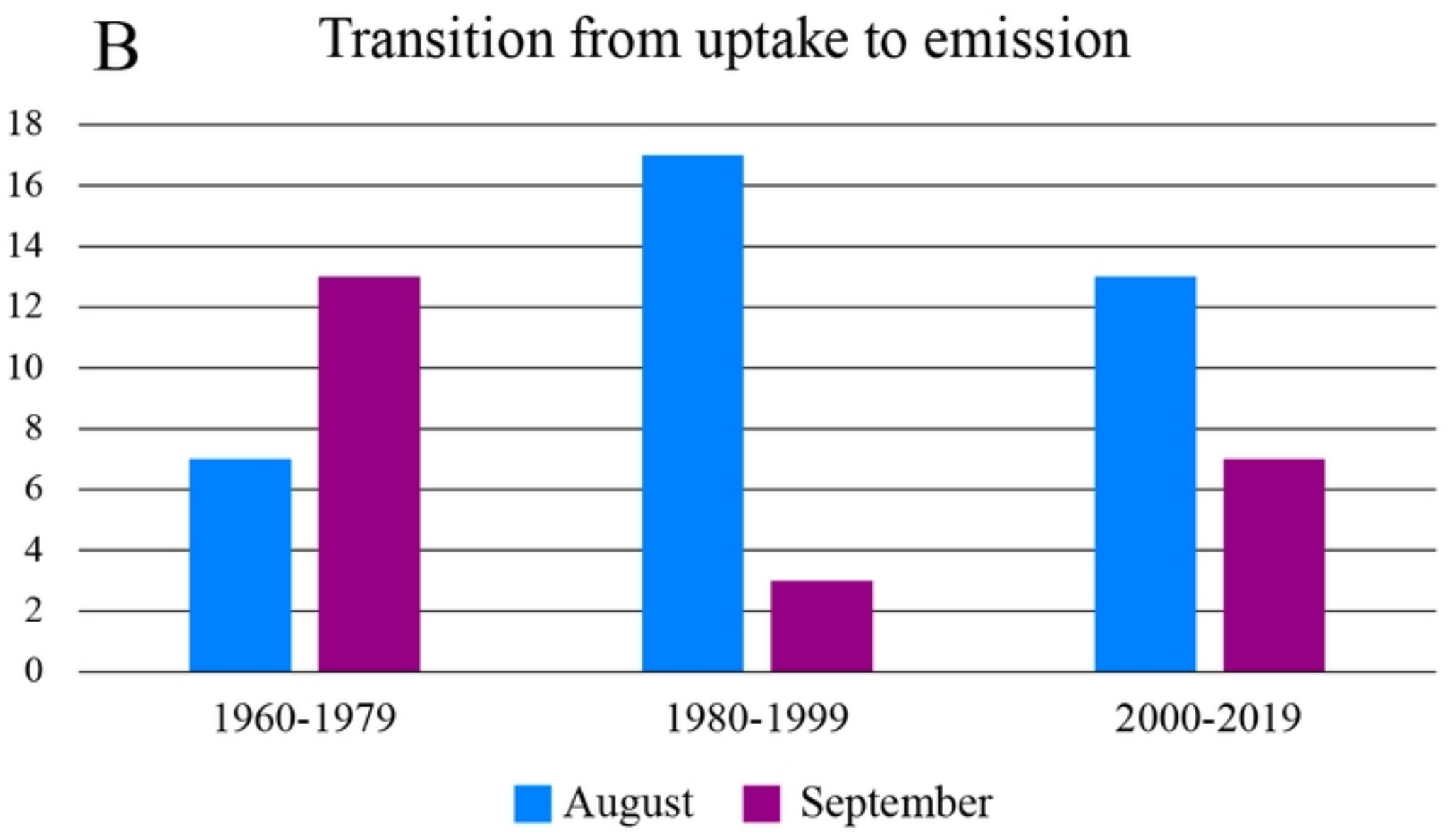

Fig 11

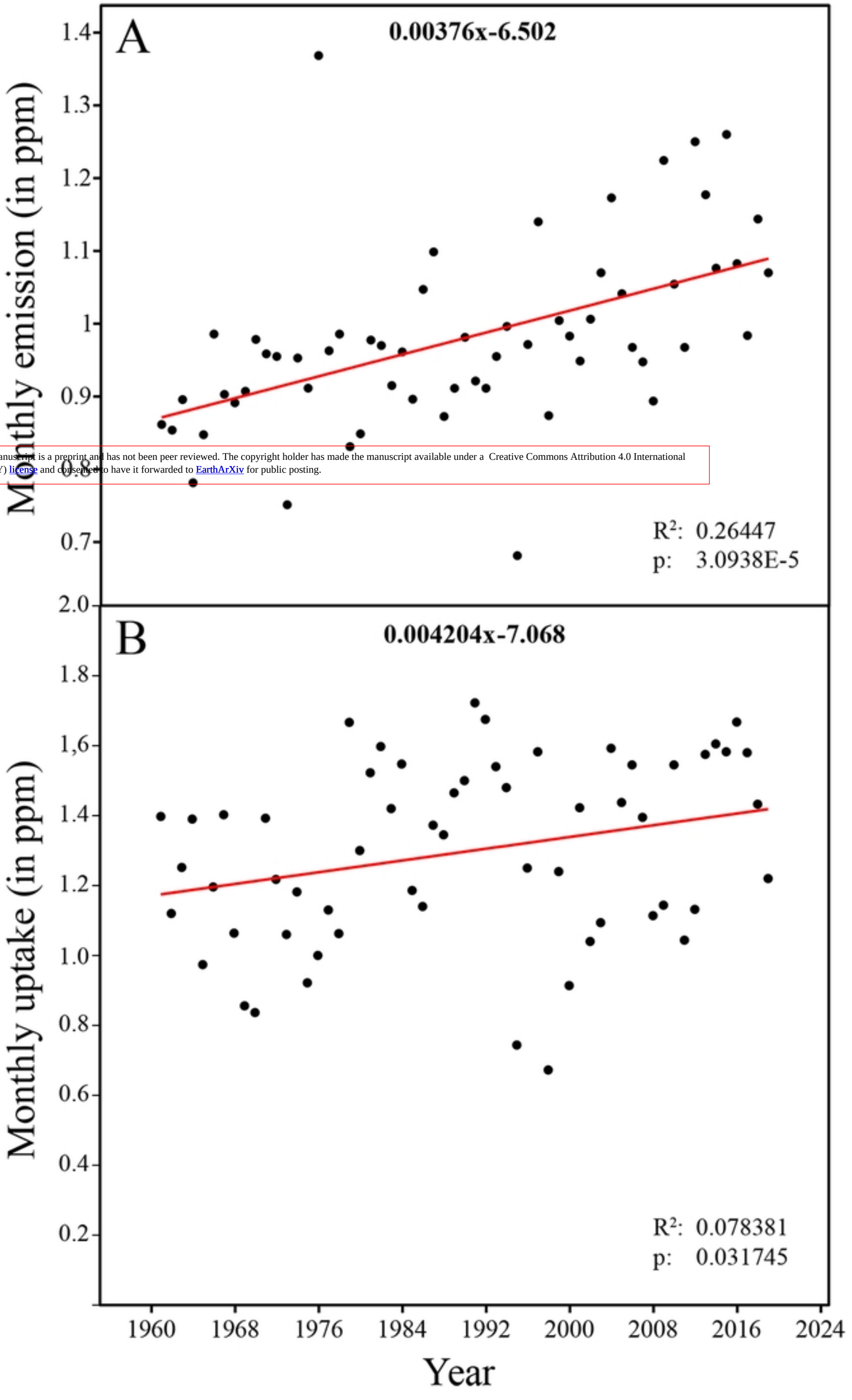

Fig 10

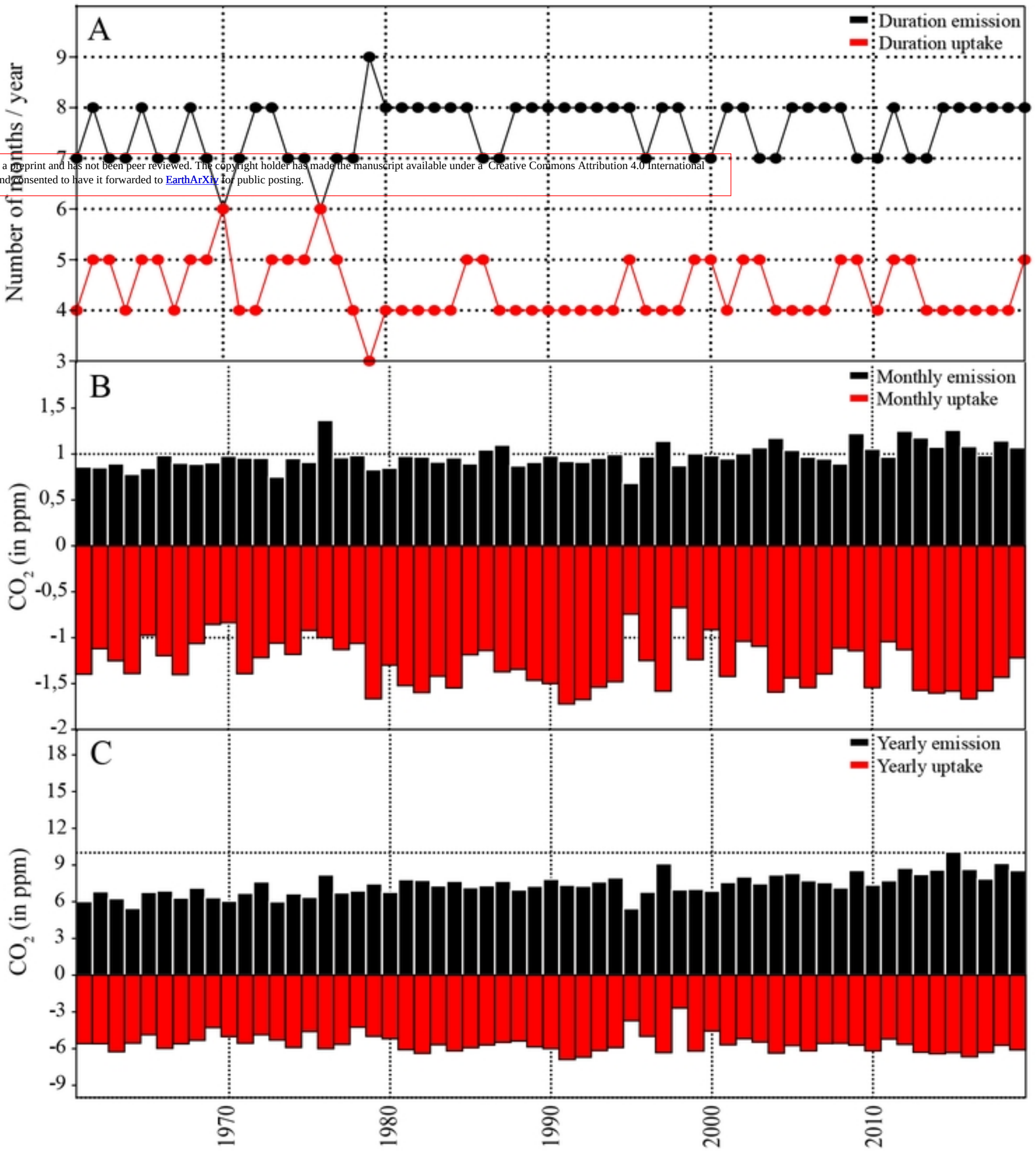

Fig 9

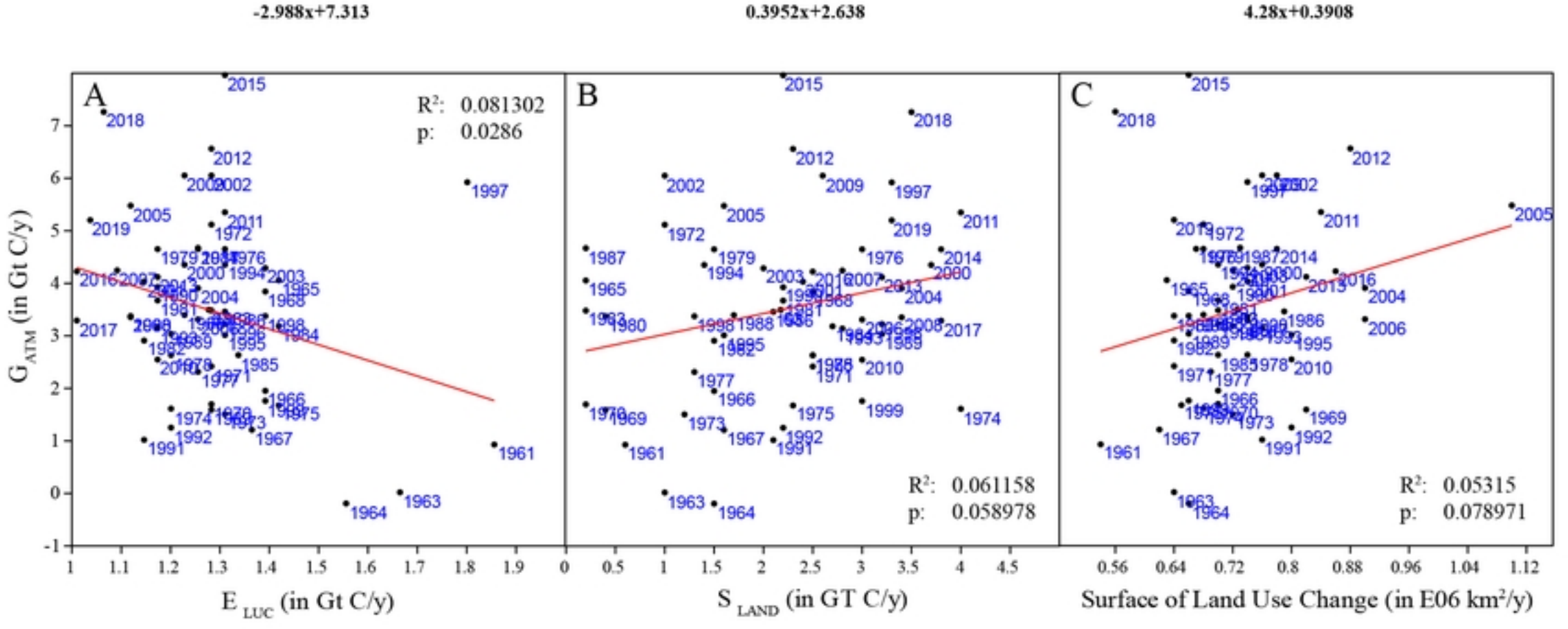
-2.988x+7.313
0.3952x+2.638
4.28x+0.3908
A
B
C
R²: 0.081302
p: 0.0286
R²: 0.061158
p: 0.058978
R²: 0.05315
p: 0.078971
G ATM (in Gt C/y)
E LUC (in Gt C/y)
S LAND (in GT C/y)
Surface of Land Use Change (in E06 km²/y)

Fig 8

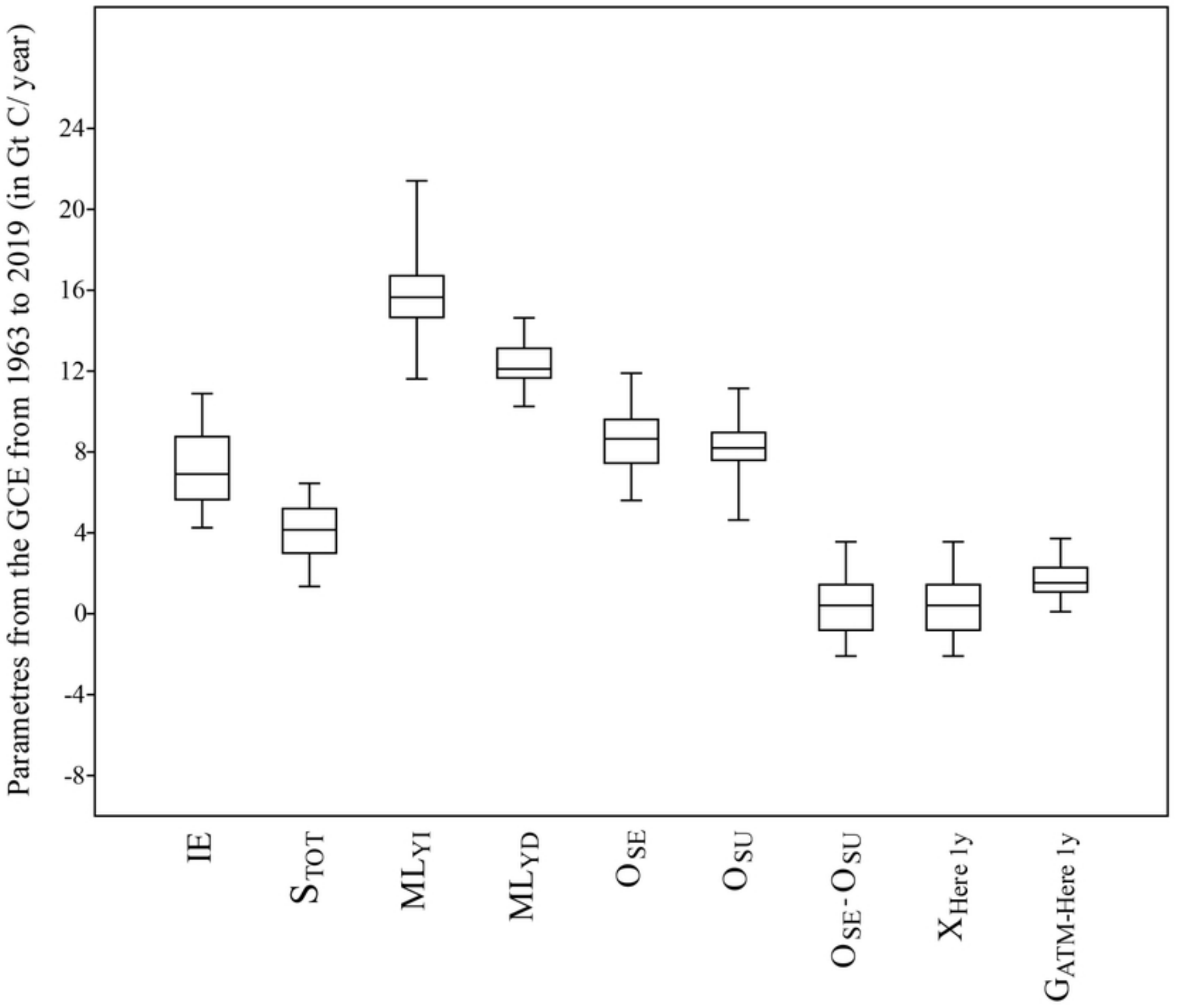

Fig 7

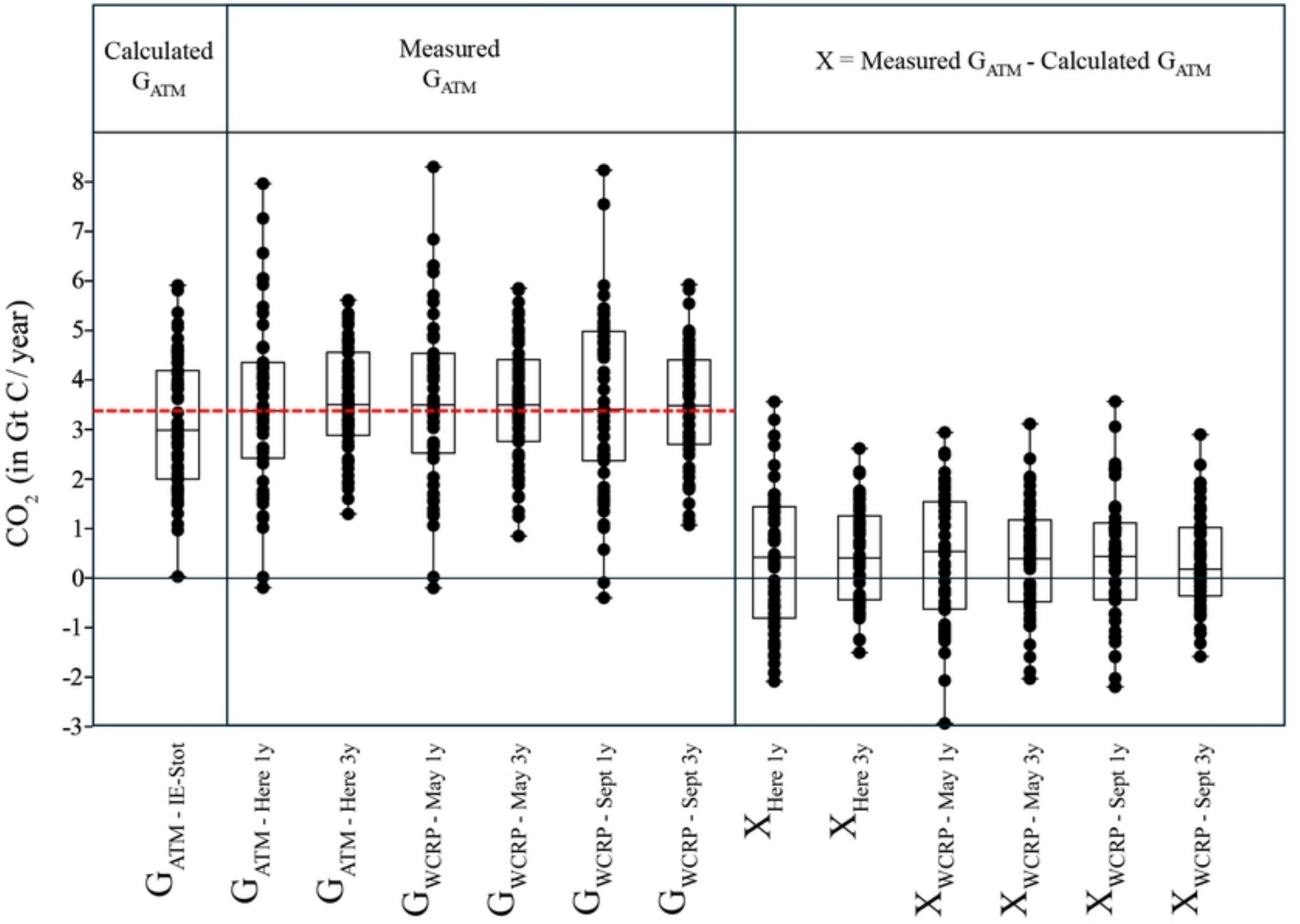
Calculated G_{ATM}
Measured G_{ATM}
X = Measured G_{ATM} - Calculated G_{ATM}
CO_2 (in Gt C/ year)
8
7
6
5
4
3
2
1
0
-1
-2
-3
G_{ATM} - IE-Stot
G_{ATM} - Here 1y
G_{ATM} - Here 3y
G_{WCRP} - May 1y
G_{WCRP} - May 3y
G_{WCRP} - Sept 1y
G_{WCRP} - Sept 3y
$X_{Here\ 1y}$
$X_{Here\ 3y}$
X_{WCRP} - May 1y
X_{WCRP} - May 3y
X_{WCRP} - Sept 1y
X_{WCRP} - Sept 3y

Fig 6

Fig 5

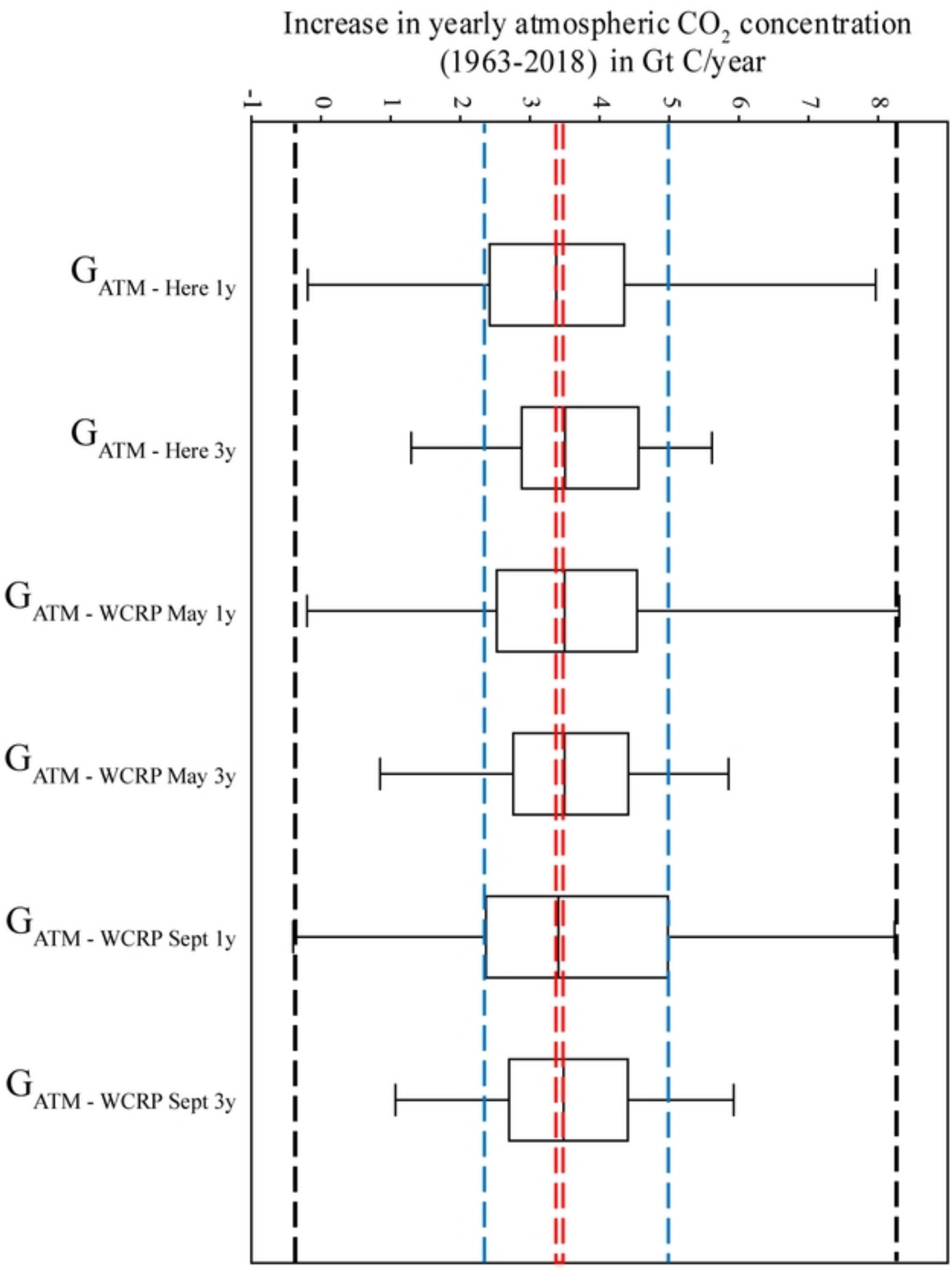
Increase in yearly atmospheric CO_2 concentration (1963-2018) in Gt C/year
-1
0
1
2
3
4
5
6
7
8
$G_{ATM - Here\ 1y}$
$G_{ATM - Here\ 3y}$
$G_{ATM - WCRP\ May\ 1y}$
$G_{ATM - WCRP\ May\ 3y}$
$G_{ATM - WCRP\ Sept\ 1y}$
$G_{ATM - WCRP\ Sept\ 3y}$

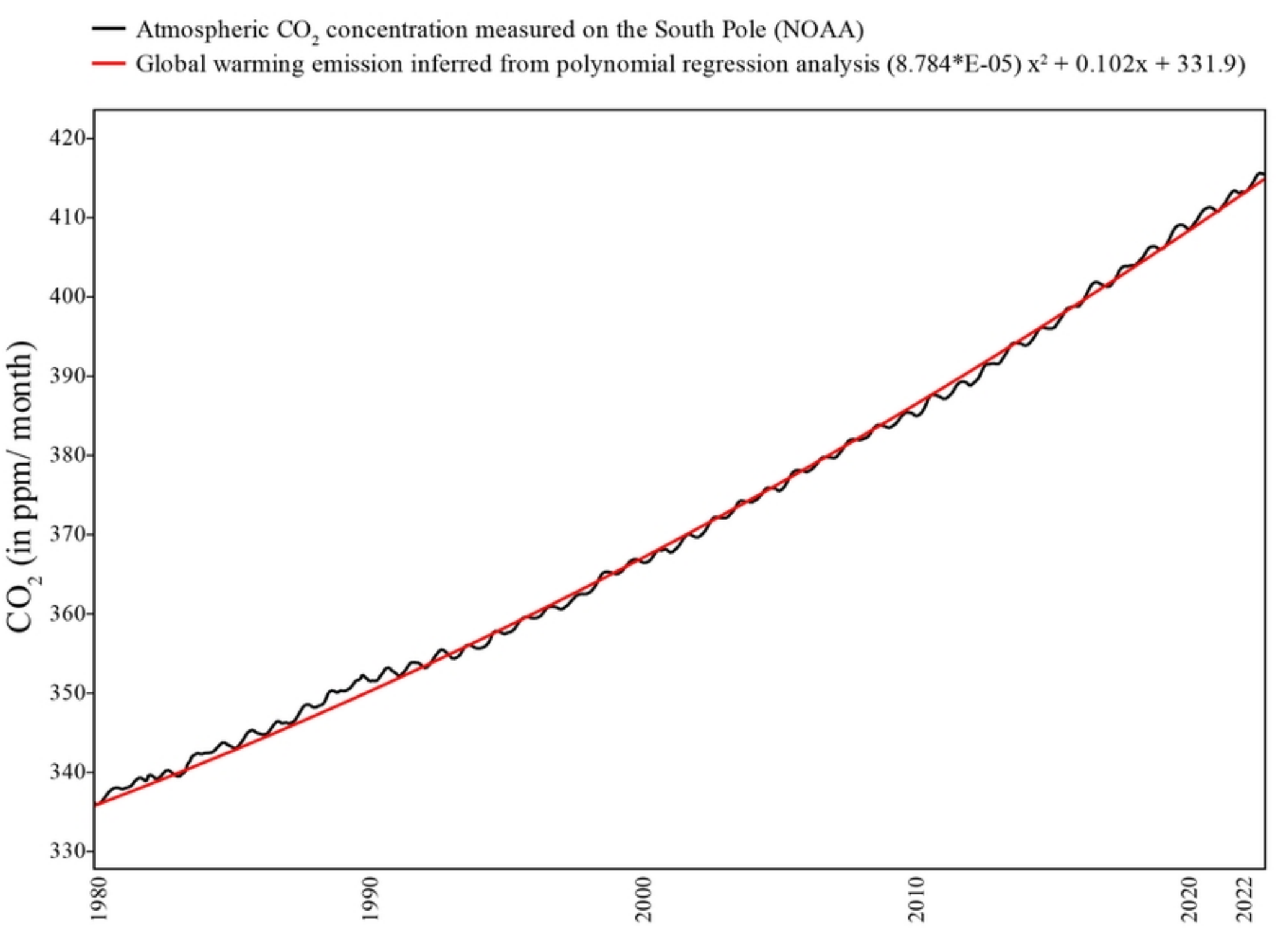
Atmospheric CO_2 concentration measured on the South Pole (NOAA)
Global warming emission inferred from polynomial regression analysis (8.784*E-05) x^2 + 0.102x + 331.9)
CO_2 (in ppm/ month)
420
410
400
390
380
370
360
350
340
330
1980
1990
2000
2010
2020
2022

Fig 4

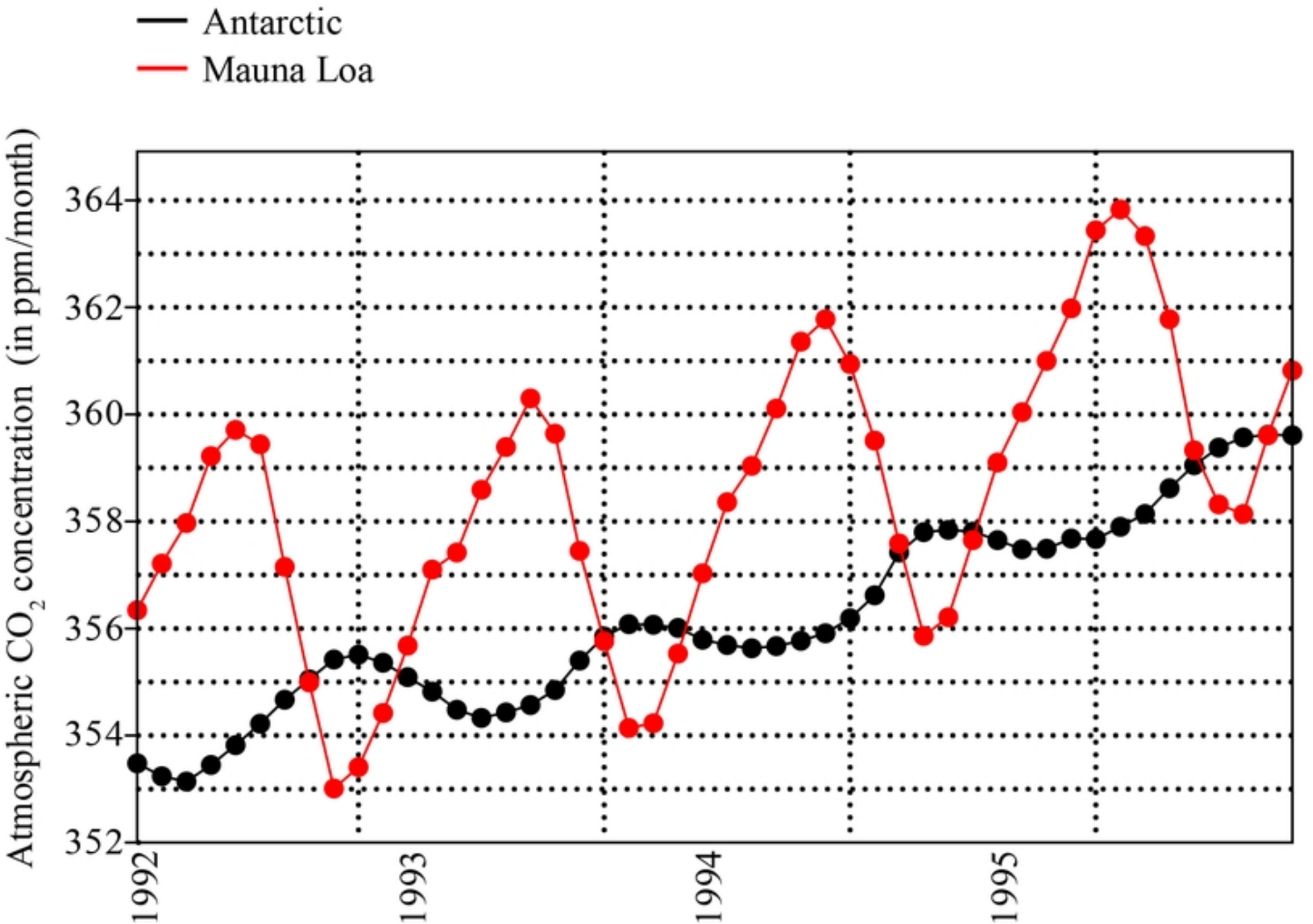
Antarctic
Mauna Loa
Atmospheric CO_2 concentration (in ppm/month)
364
362
360
358
356
354
352
1992
1993
1994
1995

Fig 3

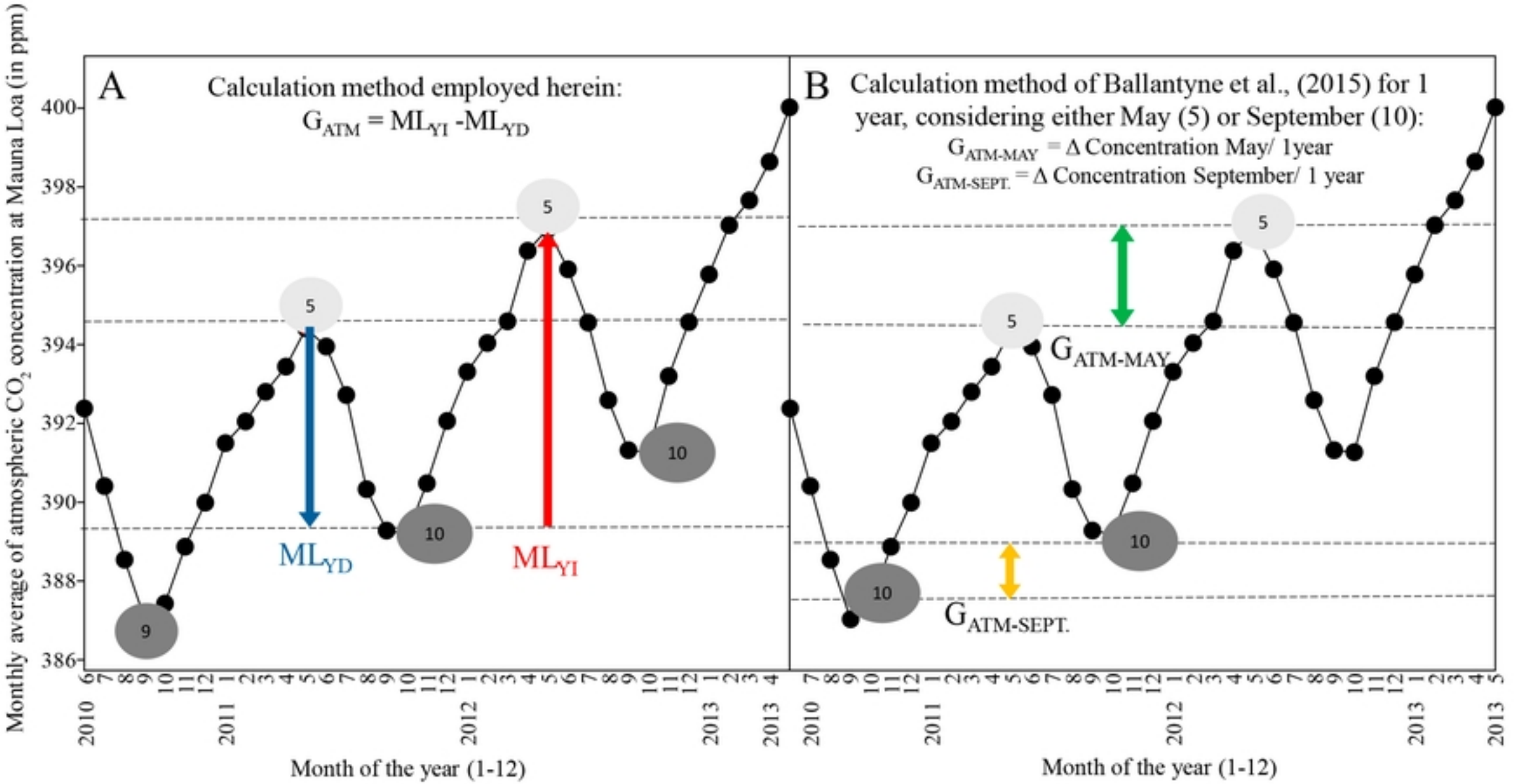
A
Calculation method employed herein:
$G_{ATM} = ML_{YI} - ML_{YD}$
B
Calculation method of Ballantyne et al., (2015) for 1 year, considering either May (5) or September (10):
$G_{ATM-MAY}$ = Δ Concentration May/ 1year
$G_{ATM-SEPT.}$ = Δ Concentration September/ 1 year
Monthly average of atmospheric CO_2 concentration at Mauna Loa (in ppm)
ML_{YD}
ML_{YI}
$G_{ATM-MAY}$
$G_{ATM-SEPT.}$
Month of the year (1-12)
Month of the year (1-12)

Fig 2

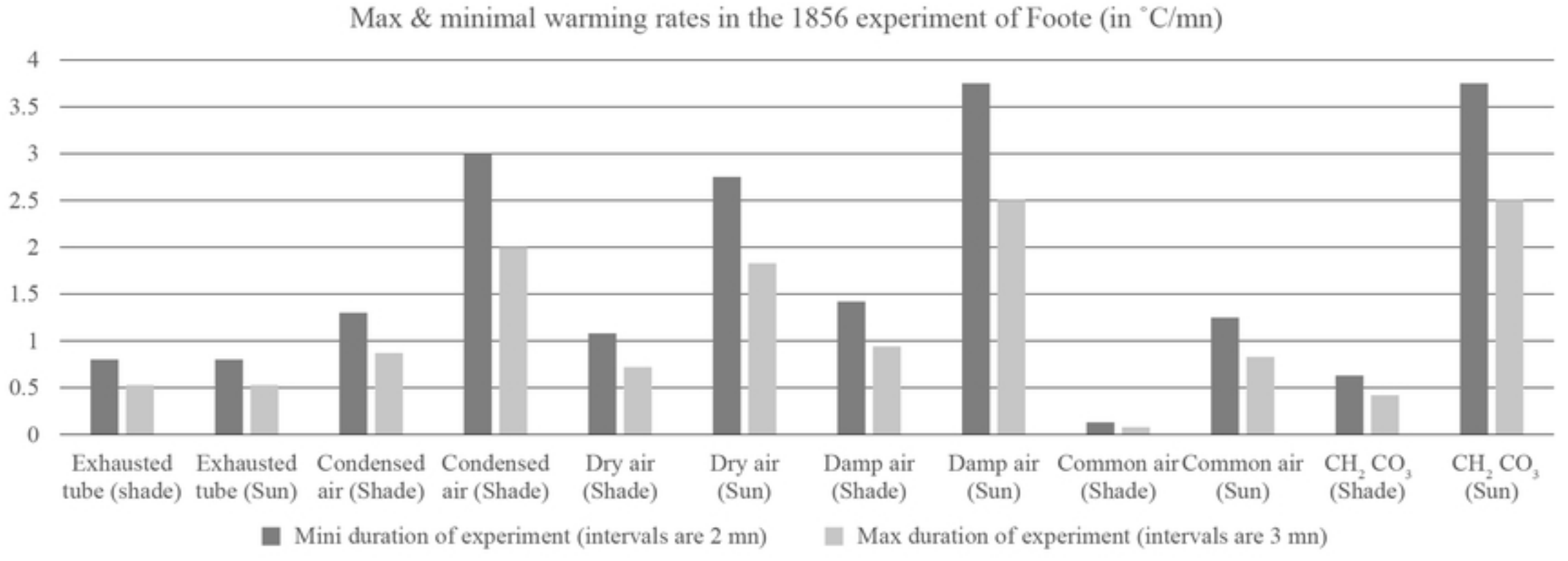
Max & minimal warming rates in the 1856 experiment of Foote (in ˚C/mn)
4
3.5
3
2.5
2
1.5
1
0.5
0
Exhausted tube (shade)
Exhausted tube (Sun)
Condensed air (Shade)
Condensed air (Shade)
Dry air (Shade)
Dry air (Sun)
Damp air (Shade)
Damp air (Sun)
Common air (Shade)
Common air (Sun)
$CH_2 CO_3$ (Shade)
$CH_2 CO_3$ (Sun)
Mini duration of experiment (intervals are 2 mn)
Max duration of experiment (intervals are 3 mn)

Fig 1